To my beloved mother

and sister Betool

- o - o - o - o -

Proportional Analysis of Composite Polycrystalline Specimens by Electron Diffraction.

A Thesis submitted for the Degree of

DOCTOR OF PHILOSOPHY

in

The University of Aston in Birmingham

by

W.A.A. AL-BERMANI

B.Sc, M.Sc.

Department of Physics

1980

PROPORTIONAL ANALYSIS OF COMPOSITE POLYCRYSTALLINE SPECIMENS BY ELECTRON DIFFRACTION

A thesis submitted for the degree of doctor of philosophy in the department of physics, University of Aston in Birmingham

By

W. A. A. AL-BERMANI

1980

SUMMARY

Selected area electron diffraction patterns have been obtained from vacuum-evaporated thin films of aluminium, copper, nickel and silver both single and in combinations of aluminium-copper, aluminium-nickel and silver-copper.

The relative integrated intensities of the diffraction patterns from both single and composite specimens were measured by microdensitometry. Selected pairs of maxima were taken from both single-specimen patterns and composite-specimen patterns in order to deduce whether their relative intensity ratios were consistent with the kinematic or with the dynamic theories of electron diffraction.

For single specimens, it was found that both kinematic and dynamic conditions can occur, but the kinematic condition dominated.

For the composite specimens, it was shown that the expression relating the intensity ratios (I_1'/I_2') to the thickness ratios (t_1/t_2) and the fraction of electrons diffracted into I_1' and I_2', (k_1'/k_2') namely

$$I_1'/I_2' = (k_1'/k_2').(t_1/t_2)$$

could be used to determine (t_1/t_2), provided (i) that k_1' and k_2' were given by the kinematic theory of electron diffraction, (ii) the crystallite size was less than the extinction distance and (iii) the average interplanar spacing of the two diffraction maxima was greater than about 1.4A° (for aluminium-copper) and about 2.0A° (for aluminium-nickel).

Key words

Electron Diffraction, Relative Intensities, Thicknesses Ratio, Composite Specimen.

A C K N O W L E D G E M E N T

The author would like to state his gratitude and appreciation to his supervisor Dr T.F.J. Quinn for his continuous guidance and help through the project which contributed greatly to the fulfillment of the work.

He would also like to acknowledge the financial support which was received from the Ministry of Education of the Republic of Iraq throughout the project.

Thanks are also due to the staff of the Physics Department at the University of Aston, and in particular to Mr R.L. Keen and Mr G.V. Cochrane.

Finally, the author wishes to thank Miss K. Atanaskovic for typing the thesis.

C O N T E N T S

.....

.....

.....

....

LIST OF SYMBOLS

d	Interplanar spacing, (A^{o}).
D	Debye-Waller factor,
f_e	Atomic scattering factor, (A^{o}).
F_e	Structure factor, (A^{o}).
I_o	Incident intensity, (Number of electrons per area per time).
I_{hkl}	Diffracted intensity, (Number of electrons per area per time).
K	Total number of electrons scattered through all angles by all processes.
ℓ	Silt length, (cm).
L	Camera length, (cm).
m	Mass of the material, (gm).
M_a	Atomic mass.
P	Multiplicity.
R	Ring radius, (cm).
t	Thickness of specimen, (A^{o}).
T	Temperature, (K^{o}).
v_o	Unit cell volume, $(A^{o})^3$.
δ_e	Elastic cross section, $(A)^2$.
δ_i	Inelastic cross section, $(A^{o})^2$.
Δ	Extinction distance, (A^{o}).
ε	Crystallite size, (A^{o}).
θ	Bragg angle, (degree).
Θ	Characteristic temperature, (K^{o}).
λ	Wavelength, (A^{o}).
λ_e	Elastic mean free path, (A^{o}).
λ_i	Inelastic mean free path, (A^{o}).
λ_T	Total mean free path, (A^{o}).
ρ	Density of the material, (gm per cm^3).

LIST OF FIGURES

LIST OF TABLES

- CHAPTER ONE -

1.1 Electron Diffraction

The subject of electron diffraction originated experimentally by Davisson and Germer [1] and by Thomson and Reid [2], in order to verify de Broglies hypothesis regarding the wave nature of the electron, and they found a good qualitative agreement with the theory. Thomson [3-5] through a series of experiments on the diffraction of cathode rays, proved de Broglies hypothesis by comparing his results with x-ray diffraction. Since then electron diffraction has been developed into a method for determining the constitution of matter, especially when thin layers are being investigated. Most of the electron diffraction experiments carried out so far have only involved measurement of the geometry of the diffraction rings and spots, and from this the identity of the diffracting constituents and their relative orientation have been determined [6].

There are two possible approaches to calculate the intensity of an electron diffraction maximum from a crystalline specimen. These are the kinematic theory and the dynamic theory of electron diffraction.

The kinematic theory assumed that only a negligible fraction of an incident electron beam is scattered by a crystal. This means that we can assume that every atom in the crystal receives an incident wave of the same amplitude.

The dynamic theory, takes into account the fact that the

reflected beam is itself reflected by the same planes of atom into the direction of the original beam. The dynamic theory also takes into account the reduction in intensity of the primary beam as it passes through the crystal by the loss of the reflected beam [7].

1.2 Previous Work.

Very few attempts have been made to obtain a quantitative analysis of the proportions of the constituents of a composite specimen from measurements of the diffracted electrons. This must be due to the complexities involved in using electron diffraction techniques in any really quantitative manner, such as whether or not one uses the kinematic theory of electron diffraction (which relates to a situation in which an electron is elastically scattered only once whilst it is with a region of single crystal) or the dynamic theory (which assumes several elastic collisions whilst passing through this region). Other problems are:- 1. Specimen texture, (whether the specimen is laminar, columnar, a mixture or a powder), 2. The effects of preferred orientation, 3. The extent of amorphous material in the specimen (e.g. grain boundaries), 4. Difference in crystallite size between the components of the composite specimen [6].

Experiment had been performed previously with little success using lead as one of the sandwich materials [8]. In 1974 (Quinn and Dawe) [9] showed for composite specimen of copper and aluminium there to be a linear relationship between

the ratio of diffracted electron intensity from the layers of copper and aluminium, and the ratio of the thickness of these layers, although an unexpected experimental constant of proportionality was found. These findings were based on a limited number of observation and it was assumed that the diffraction was taking place under the condition of kinematic theory. Later (Quinn and Boxley 1976) involving a larger range of thickness ratio and electron energy found that both the kinematic and dynamic theories needed to be considered, and it was found that by plotting electron intensity ratio against thickness ratio, two straight lines could be drawn corresponding to the two theories [10]. Further studies were made by (Quinn and Liddicoat, Quinn and Ansell 1977). They found that the crystallite size is important and should be taken into account. Investigation of crystallite size from dark field electron micrographs showed the size to be variable, which was consistent with nonlinearity in the intensity ratio versus thickness ratio plots [11-12].

The aim of the project is to determine the thickness ratio of the two films constituent of the composite specimen, through a theoretical relationship between the ratio of the relative integrated intensities of the diffraction rings formed by the composite specimen, and the thickness ratio of the two films constituent of the composite specimen. This relationship was described by the following equation.

$$(I'_{hkl})_1/(I'_{hkl})_2 = (k'_{hkl})_1/(k'_{hkl})_2 \cdot (t_1/t_2) \qquad (1.1)$$

where (I'_{hkl}) and $(I'_{hkl})_2$ are the relative integrated intensities of the diffraction rings produced by materials (1) and (2) of the composite specimen.

t_1 and t_2 are the respective thicknesses of materials (1) and (2). $(k'_{hkl})_1$ and $(k'_{hkl})_2$ are the fractions of electrons scattered through angles (θ_1) and (θ_2) per unit length of films (1) and (2).

Single and composite specimens of aluminium-copper, aluminium-nickel and silver-copper were prepared by thermal evaporation, firstly for those of high melting point material and then the other component directly onto carbon-coated electron microscope grids. Diffraction patterns were obtained using electron microscopes in the selected area electron diffraction mode of operation with different electron voltages. The micrographs obtained were then analysed using a microdensitometer, and the ratio of relative integrated intensities found for various pairs of diffracted rings. The thickness of the individual films were measured using a multiple beam interferometer and therefore the thickness ratio could be determined. The crystallite size of the specimens were determined using dark field technique.

For single specimens, (n) has been determined by using equation (2.22). By plotting (n) against the total number of scattering, it was found that for some materials there was a transition from kinematic theory to dynamic theory as the total scattering number increases. For the other materials only the kinematic theory was operating.

For composite specimens, (n) has been found for each individual specimen at different voltages. For aluminium-

copper combination it was found that thickness ratio in equation (1.1) can be predicted provided (i) that (k'_1) and (k'_2) are given by kinematic theory of electron diffraction (ii) the crystallite size is less than the extinction distance and (iii) the average interplanar spacing of the two diffraction maxima is greater than about 1.4A°. For aluminium-nickel combination, the average interplanar spacing of the two diffraction maxima is greater than about 2.00A°.

- CHAPTER TWO -

THEORY

A polycrystalline material consists of a very large number of randomly oriented crystals. When an electron beam is diffracted by such a material concentric rings are formed. The following is a presentation of the kinematic and dynamic theories which both deal with the electron diffraction through polycrystalline film. The case is shown for both single and double laminae specimens.

2.1 The scattering of electrons passing through a polycrystalline film.

Consider the lamina of polycrystalline material illustrated in figure (2.1). Let (I_o) be the intensity of an incident electron beam perpendicular to the face of the lamina. Let us assume that the intensity transmitted (I_T) is given by the exponential decay law.

$$I_T = I_o \exp(-Kt) \qquad (2.1)$$

where K is the total number of electrons scattered through all angles by all processes per unit length of path through the specimen.

Now consider a thin sheet of thickness dx positioned at a distance (x) from entry face of the lamina as shown in figure (2.1). It follows from the above equation that the intensity at the sheet is $I_x = I_o \exp(-Kx)$.

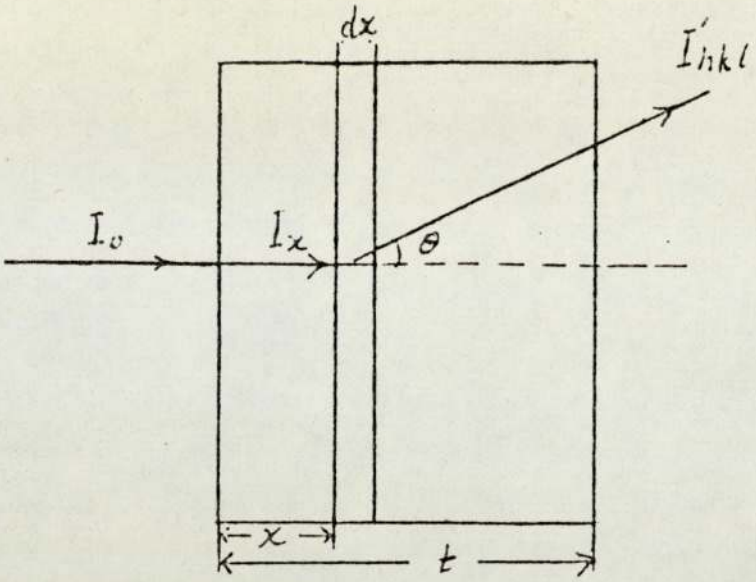

Fig. (2.1) Diffraction through a single lamina.

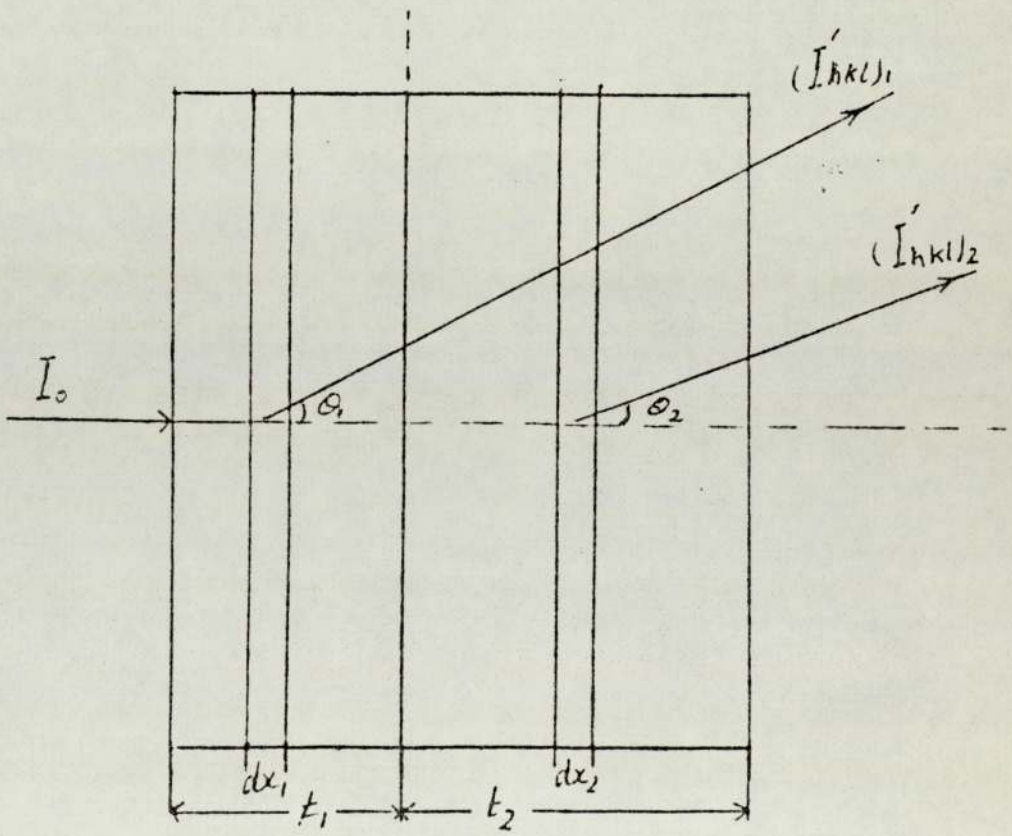

Fig. (2.2) Diffraction through two laminae.

Let K'_{hkl} be the fraction of electrons diffracted into an angle (θ) per unit length of specimen. If dI''_{hkl} is the intensity of the beam diffracted into an angle (θ) by passing through the thin sheet, then we have the following relationship.

$$dI''_{hkl} = k'_{hkl} I_x dx \qquad (2.2)$$

$$dI''_{hkl} = k'_{hkl} I_o \exp(-Kx)dx \qquad (2.3)$$

Allowance must be made for the attenuation by scattering of the diffracted beam before arriving at an expression for the intensity of the beam emerging from the specimen after being diffracted through an angle θ by passing through the thin sheet. If the angle θ is very small (which is the case in electron diffraction), then the distance travelled by the diffracted beam before emerging from the other face of the specimen is (t-x). Therefore the emergent diffracted intensity dI'_{hkl} is given by:

$$dI'_{hkl} = dI''_{hkl} \exp[-K(t-x)] \qquad (2.4)$$

Substituting for dI''_{hkl} from equation (2.3) into equation (2.4) gives:

$$dI'_{hkl} = k'_{hkl} I_o \exp(-Kt)dx \qquad (2.5)$$

Integrating the last equation between the limits x = O

to x = t gives the total intensity of electrons diffracted through an angle θ as:

$$I'_{hkl} = k'_{hkl} I_o t \exp(-Kt) \qquad (2.6)$$

2.2 The scattering of electrons passing through a double laminae.

Now consider a specimen consisting of two laminae in the form illustrated in figure (2.2), one of thickness t_1 and the other of thickness t_2. Let the subscripts (1) and (2) denote the association of a particular parameter to lamina (1) and lamina (2) respectively.

The total intensity of the beam leaving lamina (1) after being diffracted through an angle θ_1 is given by equation (2.6). However before the beam leaves the specimen as a whole, it suffers further attenuation by the factor $\exp(-K_2 t_2)$ when passing through lamina (2). The intensity of the beam leaving the specimen after being diffracted through an angle θ_1 by passing through lamina 1, $(I'_{hkl})_1$, is therefore given by:

$$(I'_{hkl})_1 = (k'_{hkl})_1 I_o t_1 \exp[-(K_1 t_1 + K_2 t_2)] \qquad (2.7)$$

The total intensity of the beam leaving lamina (2) after being diffracted through an angle θ_2 by passing through material (2), $(I'_{hkl})_2$, is given by:

$$(I'_{hkl})_2 = (k'_{hkl})_2 I'_o t_2 \exp(-K_2 t_2) \qquad (2.8)$$

where I'_o is the intensity of the incident beam at the inter-

face of the two laminae and is given by:

$$I'_o = I_o \exp(-K_1 t_1) \qquad (2.9)$$

Substituting for I'_o from equation (2.9) into equation (2.8), an expression is obtained for the total intensity of the beam leaving the specimen after passing through lamina (2), so that:

$$(I'_{hkl})_2 = (k'_{hkl})_2 \, I_o t_2 \exp[-(K_1 t_1 + K_2 t_2)] \qquad (2.10)$$

Dividing equation (2.7) by equation (2.10), an expression is obtained for the relative intensities of a diffraction ring formed by material (1) and a diffraction ring formed by material (2), namely:

$$\frac{(I'_{hkl})_1}{(I'_{hkl})_2} = \frac{(k'_{hkl})_1}{(k'_{hkl})_2} \cdot \frac{t_1}{t_2} \qquad (2.11)$$

2.3 The intensity of scattered electrons by a polycrystalline specimen.

An atom scatters electrons inelastically and elastically. Inelastically due to the interaction of the incident electrons with atomic electrons and elastically due to the interaction of the incident electrons with atomic nucleus.

Electrons, because of their wave nature, are diffracted by crystals to give diffraction patterns of which the shapes are determined by the structures and dimensions of the crystals. There are two possible approaches to calculating

the intensity of an electron diffraction maximum from a crystalline specimen. There are the kinematic theory and the dynamic theory of electron diffraction.

The kinematic theory of diffraction assumes that the incident electrons are elastically scattered by an atom and leave the crystal without further interaction. This assumption is not strictly correct since one should take into account the diminution by the amount which gets diffracted on the way through the crystal as well as the diminution by inelastic scattering [7].

The dynamic theory of electron diffraction operates when there is a sufficient thickness of crystal to create a dynamic equilibrium between the primary and diffracted beams. This theory takes into account the fact that the reflected beam is itself reflected by the same planes of atoms into the direction of the original beam. The dynamic theory also takes into account the reduction in intensity of the primary beam as it passes through the crystal by the loss of the reflected beam [12] and [7].

2.4 The relative integrated intensity for the kinematic theory of diffraction.

For a beam of electrons incident on a polycrystalline material, the intensity of the electron beam diffracted by a particular set of atomic planes into a complete ring, I'_{hkl}, would be [7].

$$\frac{I'_{hkl}}{I_o} = \frac{[(F_e)_{hkl}]^2 . \lambda^2 . t . d_{hkl}}{2v_o^2} \qquad (2.12)$$

Where (I_o) is the incident intensity, $(F_e)_{hkl}$ is the structure factor for electron of the material for the atomic planes given by Miller indices hkl, (λ) is the wavelength of the electron beam, (t) is the thickness of the specimen, (v_o) is the volume of the unit cell, and (d_{hkl}) is the spacing between the sets of atomic planes given by Miller indices which are producing the diffracted ring.

The above expression should be modified to allow for thermal vibration of the atoms (the Debye-Waller temperature factor), the probability of a particular plane (hkl) being available for diffraction (the multiplicity factor, P_{hkl}), the attenuation of the beam by scattering process exp(-Kt), and finally to allow for the fact that one normally measures across the profile of the diffraction ring with a slit placed tangentially to the ring. Such a slit will admit a fraction $(\ell/2\pi R)$ of the electrons diffracted into complete ring of radius (R), (where ℓ is the slit length). But (R) is related to (d_{hkl}) through the following equation.

$$R\, d_{hkl} = \lambda L \qquad (2.13)$$

Hence $\ell/2\pi R = \ell\, d_{hkl}/2\pi L\lambda$, where (L) is the camera length.

Therefore equation (2.12) becomes

$$\left(\frac{I_{hkl}}{I_o}\right) = \frac{\lambda\left[(F_e)_{hkl}\right]^2 e^{-2D_{hkl}}.t.\ell.d_{hkl}^2.P_{hkl}.\exp(-Kt)}{4\pi L\ v_o^2} \qquad (2.14)$$

where (I_{hkl}) is the diffracted intensity per unit length of a diffraction ring, $(e^{-2D}hkl)$ is Debye-Waller temperature factor.

For a given camera length (L), and a given slit length (ℓ), the relative integrated intensity could be written as:

$$\frac{I_{hkl}}{I_o} = \frac{\left[(F_e)_{hkl}\right]^2.e^{-2D_{hkl}}.\lambda.t.d_{hkl}^2.P_{hkl}.\exp(-Kt)}{4\pi\ v_o^2} \qquad (2.15)$$

where (I_{hkl}/I_o) is the relative integrated intensity for the kinematic theory.

2.5 The relative integrated intensity for the dynamic theory of diffraction.

Here, (I'_{hkl}) for a complete ring is given by the following equation [7].

$$\frac{I'_{hkl}}{I_o} = \frac{(F_e)_{hkl}.\lambda.d_{hkl}.t}{4\ v_o\varepsilon} \qquad (2.16)$$

Where (ε) is the crystallite size of the material, the other symbols have the same meaning as before.

In order to modify equation (2.16) to account for thermal vibration, multiplicity, attenuation factor and the

method of measuring intensities, one has to multiply by e^{-D}, P_{hkl}, $\exp(-Kt)$ and $\ell d_{hkl}/2\pi\lambda L$ thus obtaining the following equation:

$$\left(\frac{I_{hkl}}{I_o}\right) = \frac{(F_e)_{hkl} \cdot e^{-D_{hkl}} \cdot t \cdot \ell \cdot d^2_{hkl} \cdot P_{hkl} \cdot \exp(-Kt)}{8\pi\, v_o L \varepsilon} \qquad (2.17)$$

Hence the full expression for the relative integrated intensity for the dynamic theory is:

$$\frac{I_{hkl}}{I_o} = \frac{(F_e)_{hkl} \cdot e^{-D_{hkl}} \cdot t \cdot d^2_{hkl} \cdot P_{hkl} \cdot \exp(-Kt)}{8\pi\, v_o \varepsilon} \qquad (2.18)$$

2.6 Theoretical comparison of the relative integrated intensity between the kinematic and dynamic theories of diffraction.

By comparison of equations (2.15) and (2.18) one may deduce a relationship between the relative integrated intensity for the kinematic theory and the relative integrated intensity for the dynamic theory.

$$\frac{(I_{hkl}/I_o)Kin}{(I_{hkl}/I_o)Dyn} = \frac{2(F_e)_{hkl} \cdot e^{-D_{hkl}} \cdot \lambda \cdot \varepsilon}{v_o} \qquad (2.19)$$

From equation (2.19) one can see that at a certain value of crystallite size (ε) namely $\varepsilon = (v_o/2\,(F_e)_{hkl} \cdot e^{-D_{hkl}} \cdot \lambda)$ the relative integrated intensity for both kinematic and dynamic theories will have the same value. For (t) smaller than (ε), one could assume that the kinematic theory gives

a good approximation to the dynamic theory. A more basic criterion is that (ε) should not be greater than the extinction distance (Δ) for using the kinematic theory where:

$$\Delta = \frac{\pi V_o}{(F_e)_{hkl} \lambda e^{-D_{hkl}}} \qquad (2.20)$$

It can be seen that (Δ) depends inversely upon $(F_e)_{hkl}$ and λ. Consequently, each diffraction ring will have its own associated extinction distance.

The two equations (2.15) and (2.18) for kinematic and dynamic theories can be written in the form:

$$\frac{I_{hkl}}{I_o} = \left[\frac{(F_e)_{hkl} e^{-D_{hkl}}}{V_o}\right]^n \left[\frac{\lambda^{n-1} . t . d_{hkl}^2 \cdot P_{hkl} \cdot e^{-Kt}}{4\pi (2\varepsilon)^{2-n}}\right] \qquad (2.21)$$

where n = 1 for dynamic theory, and

n = 2 for kinematic theory.

For a given crystallite size (ε), a given thickness (t) and a given wavelength (λ), it should be possible to deduce whether a given specimen is diffracting according to the kinematic or dynamic theory by comparing the intensity (I_2) of each maximum with the strongest (I_1), so that:

$$\frac{I_1}{I_2} = \left[\frac{(F_e)_1 e^{-D_1}}{(F_e)_2 e^{-D_2}}\right]^n \left(\frac{d_1^2 P_1}{d_2^2 P_2}\right)$$

and this equation could be written as follows:

$$\log\left(\frac{I_1}{I_2}\cdot\frac{d_2^2 P_2}{d_1^2 P_1}\right) = n \log\left[\frac{(F_e)_1 e^{-D_1}}{(F_e)_2 e^{-D_2}}\right] \qquad (2.22)$$

where the subscript (1) relates to the (hkl) of the strongest line and subscript (2) stands for all the other possible (hkl) maxima in the electron diffraction pattern. A logarithmic plot of equation (2.22) should therefore produce a straight line whose slope has a value equal to (n).

2.7 The theoretical expression of (k'_{hkl}) for both kinematic and dynamic theories.

It was shown in section (2.1) that:

$$I_{hkl}/I_o = k'_{hkl}.t.\exp(-Kt) \qquad (2.6)$$

In deriving this equation, account has been taken of the diminution of the incident beam and diffracted beam by total scattering.

Comparison of equation (2.6) with equation (2.12), suitably modified to allow for multiplicity and for thermal vibration of atoms, gives the kinematic theoretical expression for k'_{hkl}, i.e.:

$$(k'_{hkl})_{KIN.} = \frac{\left[(F_e)_{hkl}\right]^2 . e^{-2D_{hkl}} . \lambda^2 . d_{hkl} . P_{hkl}}{2\, v_o^2} \qquad (2.23)$$

The exponential term in equation (2.6) was ignored since equation (2.12) did not allow for total scattering.

Similarly, by comparing equation (2.6) with equation

(2.16), the dynamic theoretical expression for k'_{hkl} is:

$$(k'_{hkl})_{DYN.} = \frac{(F_e)_{hkl} \cdot \lambda \cdot e^{-D_{hkl}} \cdot d_{hkl} \cdot P_{hkl}}{4 \, v_o \varepsilon} \qquad (2.24)$$

For two laminae, the ratio of the integrated intensities of maxima from each lamina is given by:

$$(I'_{hkl})_1/(I'_{hkl})_2 = \left[(k'_{hkl})_1/(k'_{hkl})_2\right] \cdot (t_1/t_2) \qquad (2.11)$$

If the conditions are those of the kinematic theory, equation (2.11) may be written from equation (2.23) as follows:

$$\frac{(I'_{hkl})_1/(I'_{hkl})_2}{(t_1/t_2)} = \frac{(F_{e1})^2}{(F_{e2})^2} \left(\frac{e^{-2D_1}}{e^{-2D_2}}\right) \left(\frac{d_1}{d_2}\right) \left(\frac{P_1}{P_2}\right) \left(\frac{v_2^2}{v_1^2}\right) \qquad (2.25)$$

However, if the conditions are those of dynamic theory, equation (2.11) may be written from equation (2.24) as follows:

$$\frac{(I'_{hkl})_1/(I'_{hkl})_2}{(t_1/t_2)} = \left(\frac{F_{e1}}{F_{e2}}\right) \left(\frac{e^{-D_1}}{e^{-D_2}}\right) \left(\frac{d_1}{d_2}\right) \left(\frac{P_1}{P_2}\right) \left(\frac{\varepsilon_2}{\varepsilon_1}\right) \left(\frac{v_2}{v_1}\right) \qquad (2.26)$$

In these last two equations (2.25) and (2.26), the subscripts (1) and (2) stand for material (1) and material (2) respectively in a two component sandwich.

If the two materials have approximately the same

crystallite size, one can use equations (2.25) and (2.26) to test for which theory is operating by determining the slopes of experimentally measured $(I'_{hkl})_1/(I'_{hkl})_2$ versus (t_1/t_2) graphs and then plotting the logarithm of these slopes times (d_1P_1/d_2P_2) versus the logarithm of $(F_{e1}e^{-D}1\ v_2)/(F_{e1}e^{-D}2\ v_2)$.

The slope of the resulting graph should be equal to (2) for kinematic theory and (1) for dynamic theory.

If one could be sure which theory operates, one can use equations (2.25) and (2.26) to deduce the thickness ratio from measurement of $(I'_{hkl})_1/(I'_{hkl})_2$ and calculation of other parameters.

Equations (2.25) and (2.26) may be written in the form:

$$\frac{(I'_{hkl})_1/(I'_{hkl})_2}{t_1/t_2} = \left[\frac{F_{e1}e^{-D_1}\ v_2}{F_{e2}e^{-D_2}\ v_1}\right]^n \left[\frac{d_1P_1\varepsilon_2^{\,2-n}}{d_2P_2\varepsilon_1^{\,2-n}}\right] \qquad (2.27)$$

- CHAPTER THREE -

EXPERIMENTAL DETAILS

Single and composite specimens have been prepared by thermal evaporation directly on a carbon-coated microscope grid. A diffraction pattern for both kinds of specimen has been obtained at different voltages using electron microscopes. The film thickness has been measured by using an interferometer. To measure the relative integrated intensity all the diffraction patterns have been traced by the microdensitometer. Dark field technique was used for obtaining the crystallite size.

3.1 The preparation of carbon-coated electron microscope grids.

A thin amorphous film of carbon was evaporated onto a piece of flat mica by passing a large electric current through two carbon electrodes mounted in an evaporator, which was maintained at 10^{-5} torr throughout the evaporation.

After the evaporation was completed air was let into the system and the mica with the carbon-coating removed. The mica was then placed carefully in a dish of distilled water with the carbon film on the top, whereupon the film lifted off the mica and floated to the surface of the water. The mica was then removed from the water and in its place was put a number of copper electron microscope grids which

were resting on a small piece of metal guaze. The water was then allowed to flow out of the dish by turning a tap located beneath the dish. Then the floating carbon film was lowered onto the copper grids as the level of the water dropped. When the carbon film was in contact with the grids they were allowed to dry.

The amorphous carbon films on the copper grids enabled metal films to be supported, whilst not disturbing the electron microscope diffraction patterns significantly.

3.2 The evaporation techniques

In order to calculate the approximate mass (m) of metal of density (ρ) needed to deposite a certain thickness (t) at distance (ℓ) from the filament. A spherical evaporation from a point source was assumed. This is described by the following equation.

$$t = \frac{m}{4\pi \rho \ell^2} \qquad (3.1)$$

By varying the mass of the metal and the distance from the filament, the thickness of the resulting film could be made approximately to any required value.

To produce the films in the required state the metal was deposited by thermal evaporation on the carbon-coated electron microscope grids so that the film could be inserted into the microscope for examination.

Films of different thickness were made from the same mass of metal by placing the grids on a ladder. The steps

of this ladder were mov able. These steps were positioned so that there was an unobstructed path from the filament to the grids on the steps.

It was necessary to use different filaments for the two metals to avoid contamination from any residual metal left on the filament from previous evaporation.

The metal with high melting point was laid before the one with low melting point. The reason was that the temperature of the low melting point on sublimation onto the high melting point metal film surface was not high enough to melt the film and so cause alloying of the two metals.

Six carbon-coated copper grids and a glass slide were placed on each of the five steps on the ladder. The purpose of the slide was to provide a film the thickness of which could be measured. It was necessary to have a very definite step to the edge of the film on the glass slide and to achieve this a razor blade was used.

For the copper and aluminium combination, a known mass of pure copper wire was wound around the tungsten filament and the assembly was covered by a bell-jar. The system was pumped down to 10^{-5} torr. Evaporation of the copper from the filament was carried out in the following way:

The heater current was increased rapidly from zero to a value high enough to cause the filament to become red and almost white hot. After a few seconds at this applied current the copper wire melted forming a drop at the base of the "V" of the filament. The current was then quickly

decreased so that the filament was well below red-heat. On increasing the current again, but this time slowly; the droplet of the copper rose into the angle of the "v" shape due to the effect of the surface tension. The filament could then be returned to white heat. As soon as the droplet had completely evaporated, the heater current was switched off to avoid contamination of the films by the tungsten filament.

The first evaporation having been completed, air was let into the bell-jar which was removed and the inside cleaned. The filament was replaced with one wound with aluminium wire.

It was necessary to change the position of the copper-covered grids so that sandwiches of various thicknesses of copper and aluminium would be obtained. One grid was removed from each step to give a single thickness specimen, also the glass slides coated with a layer of copper were then removed from the ladder and replaced by new ones. One blank carbon-coated grid was also placed on each step so that a single film of aluminium could be obtained for each thickness. The procedure for evaporation of the aluminium was then identical to that used for the evaporation of the copper.

The specimens having been prepared, were placed in a box designed for holding grids, each compartment being labelled so that the different specimens could be identified.

The glass slides were then returned to the evaporator. They were then overlaid with a film of aluminium of about

1000 A° in thickness, so that one can measure the thickness of each film using the multiple beam interferometer.

The arrangement of the grids for both evaporation is shown in figure (3.1).

Figure (3.1a) shows the distribution of the grids for the first evaporation, A, B, C, D and E removed from the ladder after the first evaporation to give the single films of the copper with different thickness.

Figure (3.1b) shows the distribution of the grids for the second evaporation, where the F's grids stands for pure aluminium films.

The same evaporation procedure was carried out for different combinations of materials.

3.3 Measurement of film thickness

The film thickness deposited on the glass slide was measured on a multiple beam interferometer in accordance with manufacturer's instructions [13]. This measurement gives the thickness of the films deposited on the grids.

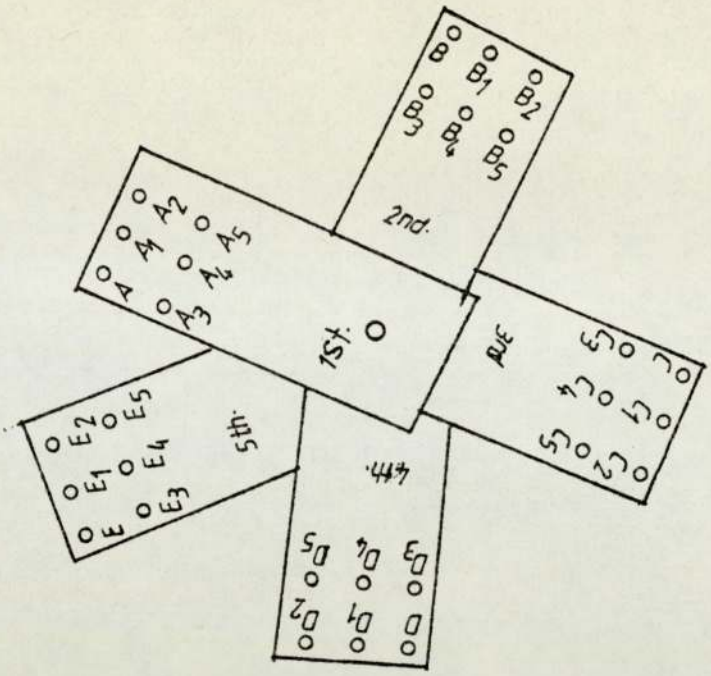

a. Arrangement for first evaporation.

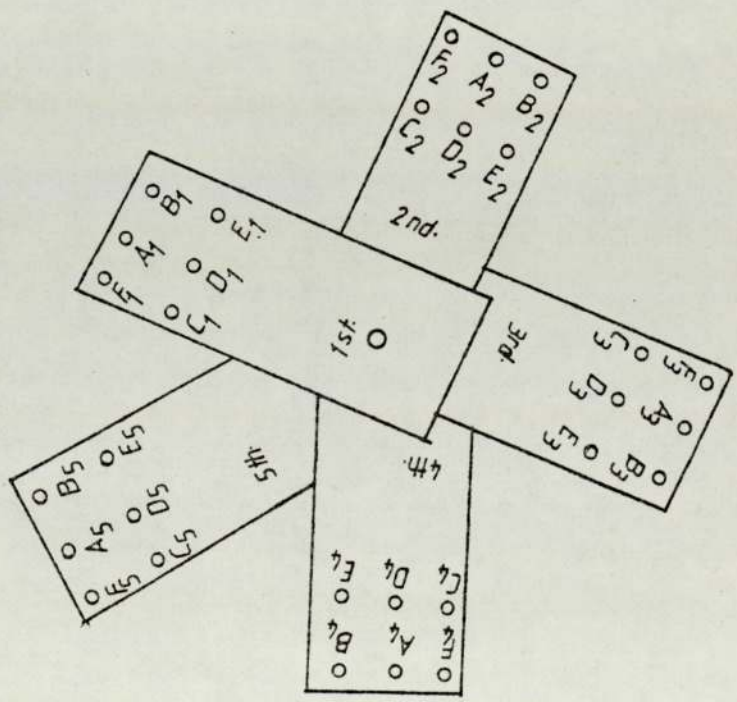

b. Arrangement for second evaporation.

Fig. (3.1) Evaporation Arrangement.

3.4 Diffraction experiment

Diffraction experiments were carried out at different electron accelerating voltages. The experiment were performed on the Philips EM200 Microscope at Aston University and on the EM7 at Birmingham University. Because the investigations were largely concerned with sample thickness, it was important that the region of the specimen being used for diffraction was flat and free from cracks. To obtain a diffraction pattern from such an area, the electron microscopes were used in the selected area mode, as shown in Figure (3.2).

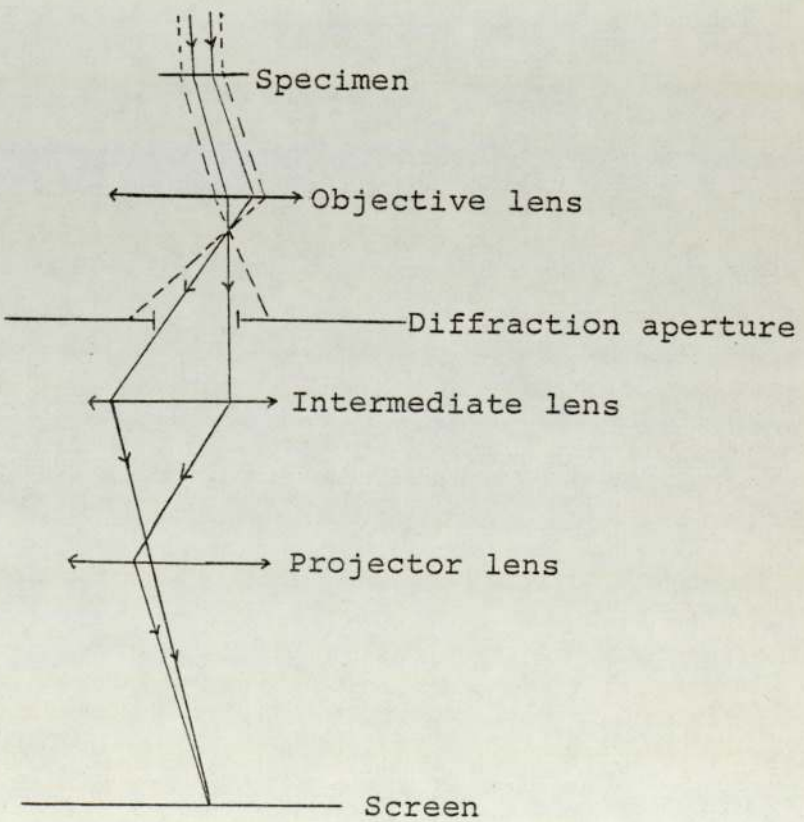

Fig. (3.2) Selected area diffraction.

The diffraction patterns produced consisted of a number of smooth concentric rings as can be seen in the sample plate (3.1). For a number of specimens the rings were not smooth but spotty, thus implying an insufficient number of crystallites in the area under investigation to produce enough crystal plane orientation for a smooth ring. To overcome this, the diffraction aperture was increased in size, so increasing the selected area and hence the number of crystallites.

The diffraction patterns were recorded by removing the microscope screen, so that the electron beam fell directly onto the cut film placed in a camera beneath the former screen position. Photographs were taken of the diffraction patterns of all the specimens at the given accelerating voltage, with exposure time applicable to the brightness of the film. In order that the density of blackening measurement from the micrograph could be compared with those from another, it was assumed that all the cut film plates taken from one batch had the same sensitivity to the electrons.

3.5 The measurement of crystallite size of the specimen using dark field electron microscopy

The crystallite size of all the single films has been obtained using the dark field technique. See sample plate (3.2). Each specimen was placed in the specimen port of the EM200 electron microscope. A dark field from the (111) ring was produced in the following way. A diffraction pattern was

DIFFRACTION PATTERN OF
PURE COPPER.

DIFFRACTION PATTERN OF
PURE ALUMINIUM.

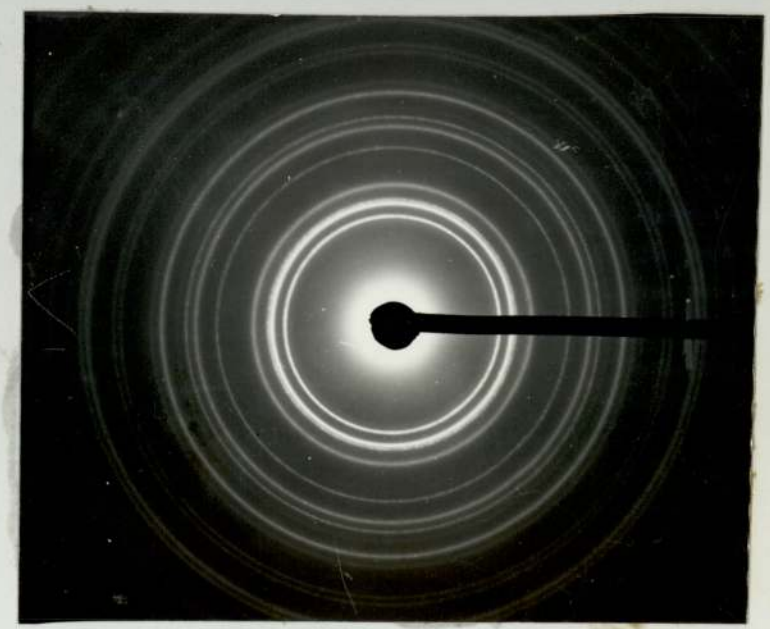

DIFFRACTION PATTERN OF COMPOSITE SPECIMEN
(ALUMINIUM+COPPER).

Plate (3.1); Sample of the diffraction patterns of aluminium-copper combination at 100kv.

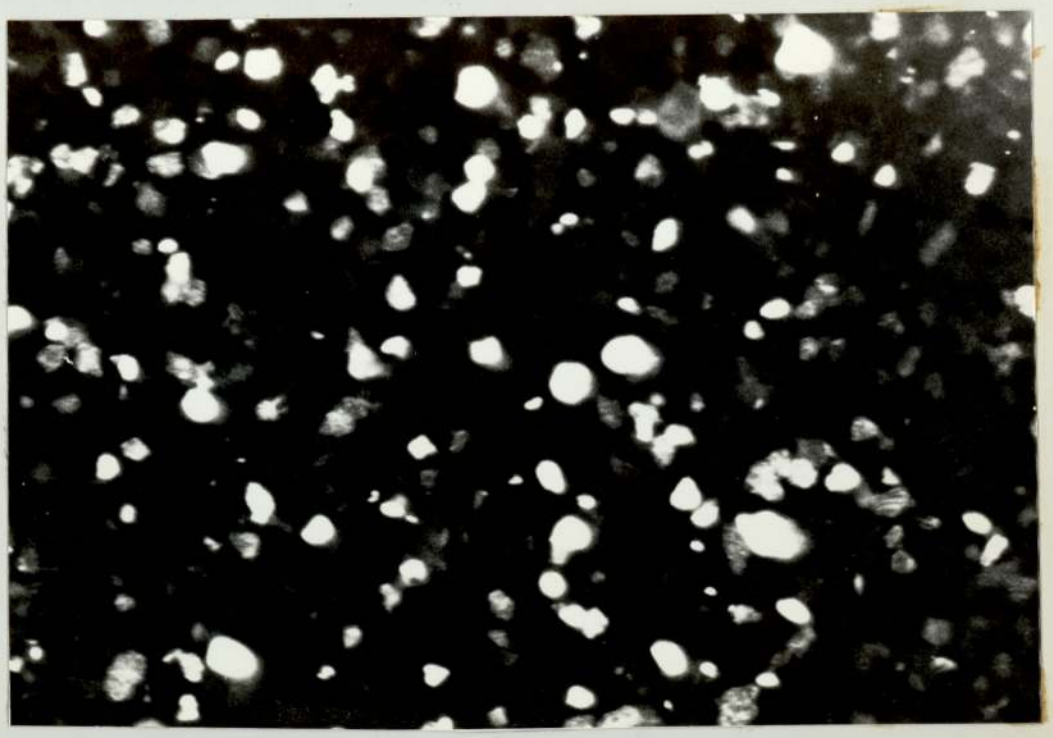

CRYSTALLITE SIZE OF ALUMINIUM (300A^{O})
t = 510A^{O}.

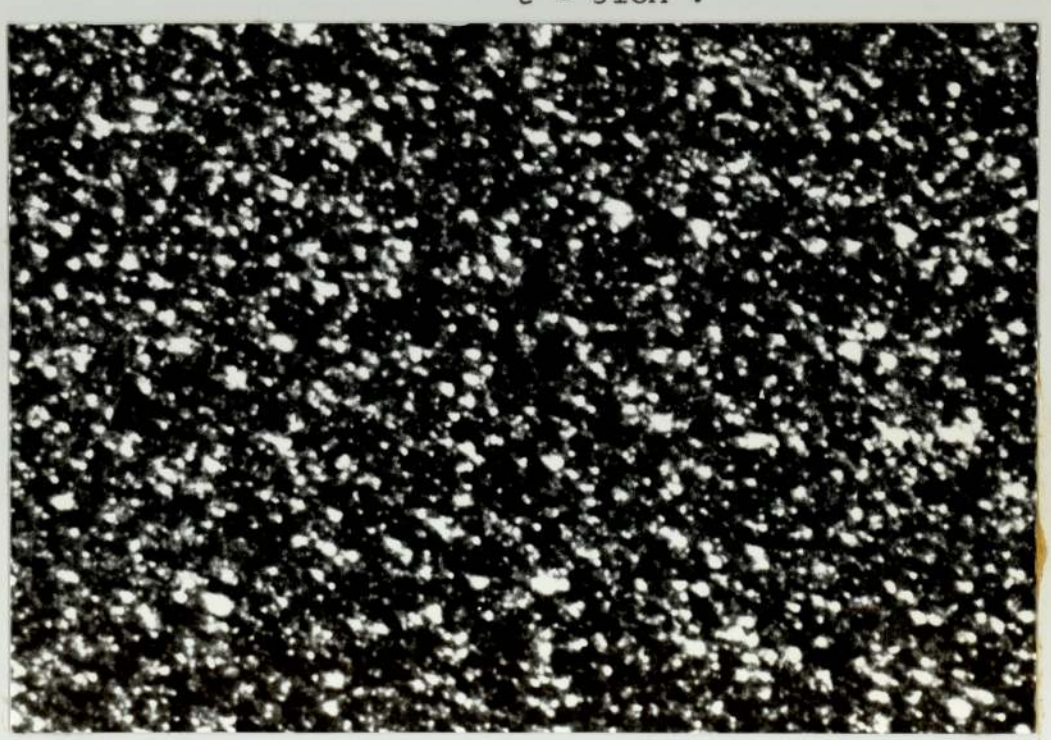

CRYSTALLITE SIZE OF NICKEL (85A^{O})
t = 200A^{O}.

Plate (3.2); Sample of the crystallite size.

formed, then small objective aperture was selected so that only a part of any one ring would be visible at the time. The beam was tilted until a part of the (111) diffraction ring came into view through the small objective aperture. The microscope was then operated in the normal manner and an image of bright crystals set in a dark field being formed. A photograph of this image was then taken.

The crystallite size was determined by measuring the images of the crystallite on the photograph with the aid of a graph paper and a viewer. Several crystallite images were measured on each photograph so that after allowance for the magnification an average value of the crystallite size could be found for each photograph.

3.6 Microdensitometry

Microdensitometer traces were taken [14] of all the diffraction micrographs in order to measure the intensities of the individual diffraction rings as peaks on a rising background. This was done by comparing the intensity of light passing through a standard glass wedge, along which the density of blackening varied from a minimum at one end to a maximum at the other according to a known gradient. Suitable wedges were chosen which would accommodate all the particular intensities required.

At the edge of each micrograph there was a thin strip which had not been exposed, called the clear plate. This was taken as the zero level of the density of blackening of the

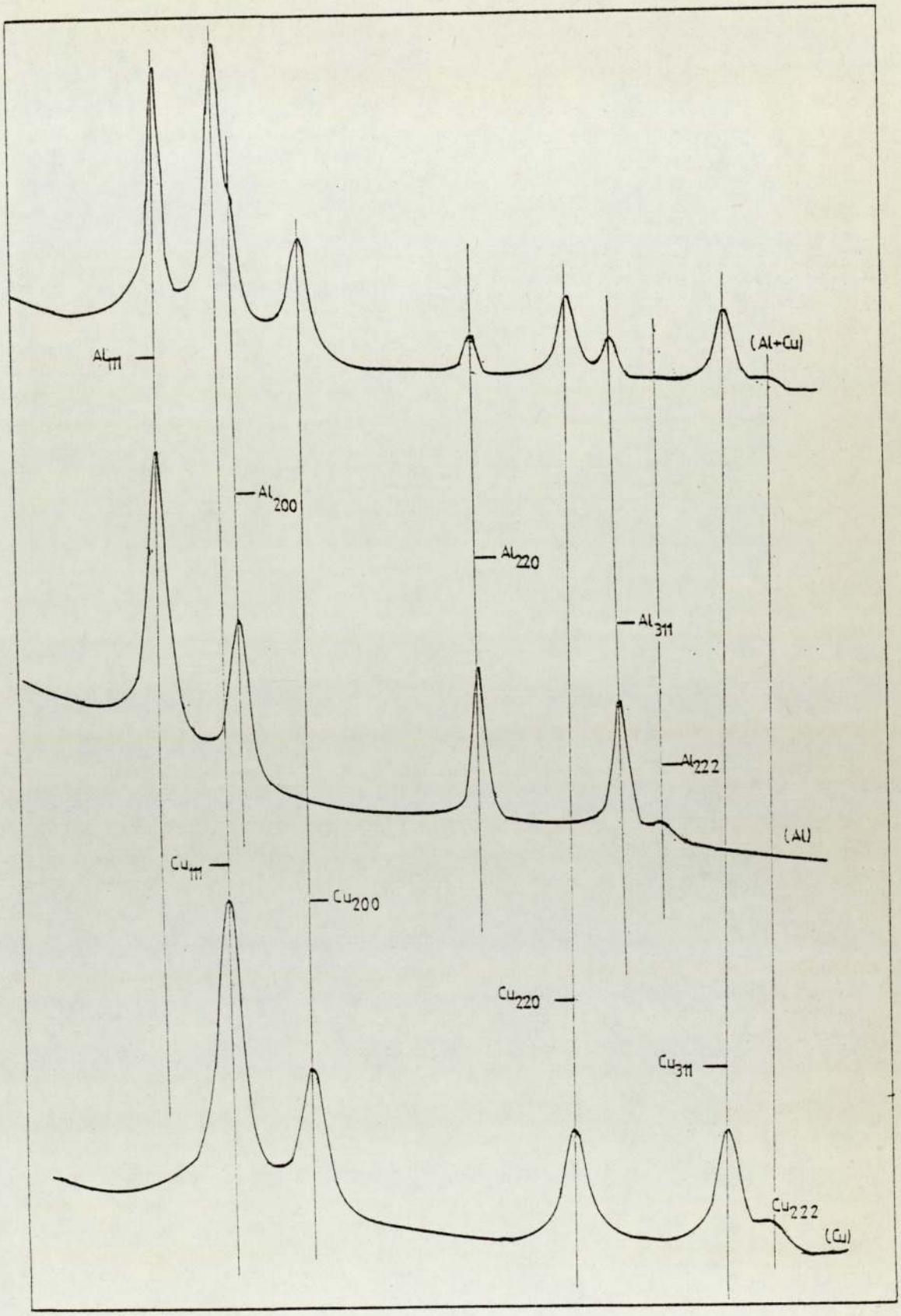

Fig. (3.3) Typical micrographic traces for aluminium and copper.

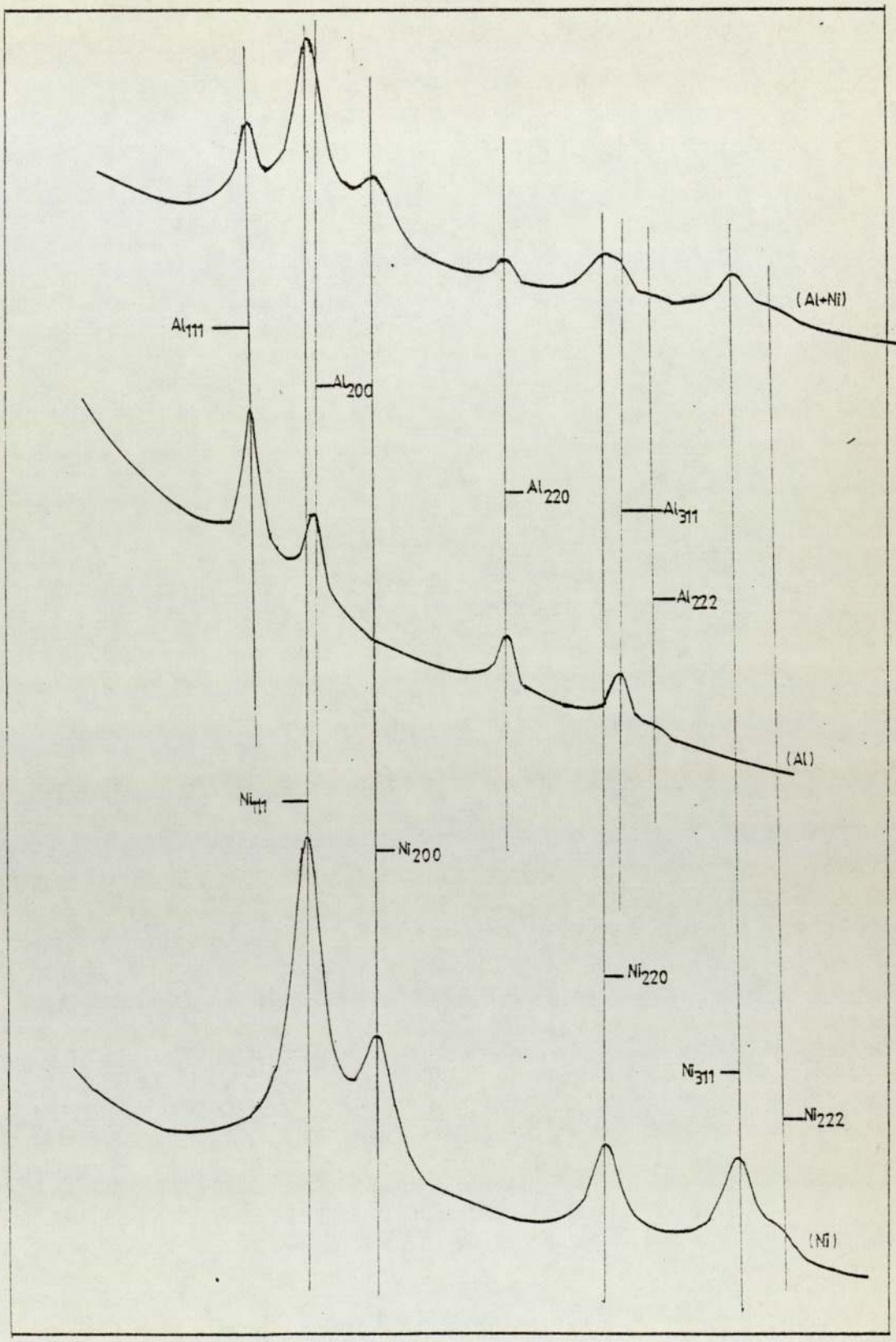

Fig. (3.4) Typical micrographic traces for aluminium and nickle.

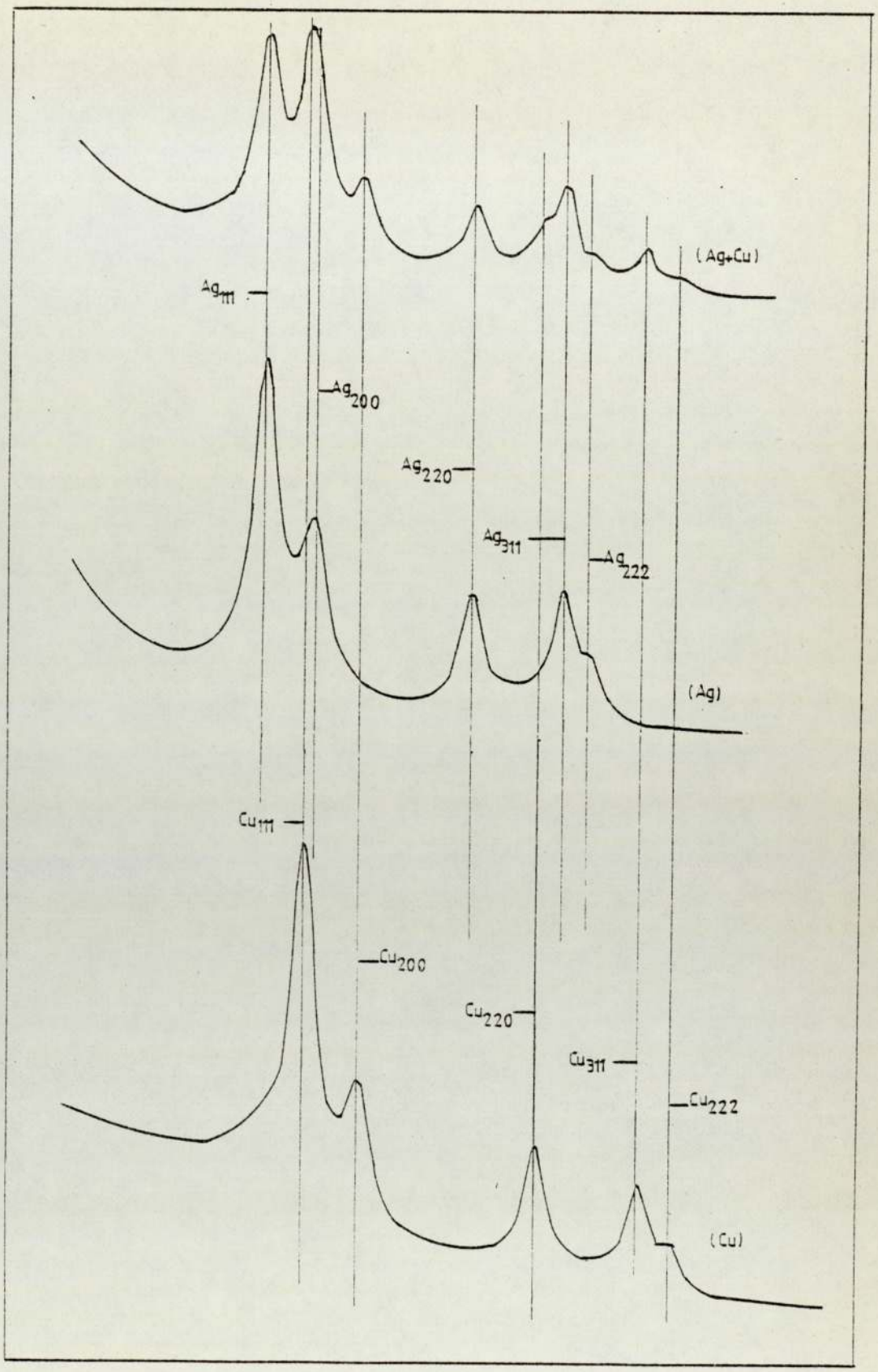

Fig. (3.5) Typical micorgraphic traces for silver and copper.

micrograph.

The density of blackening by electron of the micrograph was therefore known in terms of centimeter. By taking the film free part as zero, and knowing the density per centimeter of the standard wedge, the actual density could be found. Typical microdensitometer traces can be seen in figure (3.3) through (3.5).

3.7 The Calibration Curve

To measure the relative integrated intensities, a calibration curve was needed because the response of the photographic plate was not linear with the intensity of incident electrons. This calibration curve relates the density of blackening to the exposure. The exposure is the product of the intensity of the electron beam falling on the photographic film and the exposure time.

It was assumed that any one batch of film had the same response to the electrons, and each batch was calibrated by first taking photographs of one specimen using different exposure times. Microdensitometer traces were taken of these micrographs and the peaks were identified and selected to give a range of values. Each selected peak value, measured in units of density of blackening was plotted, using logarithm graph paper as the ordinate axis versus the exposure time as the abscissa to give a plot similar to that shown in figure (3.6).

A similar sheet of graph paper was superimposed on the

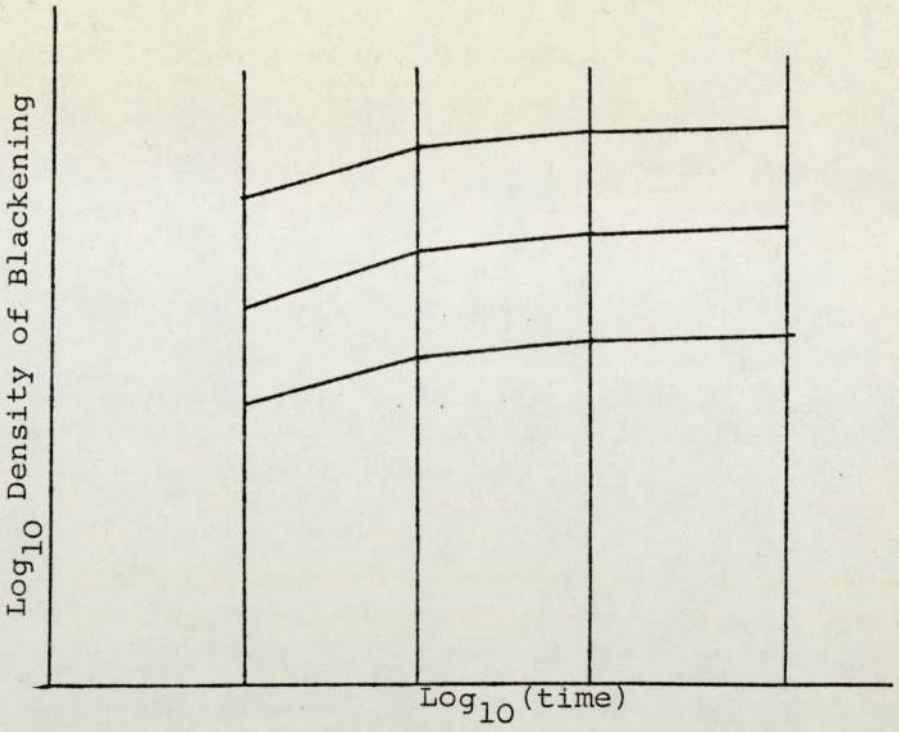

Fig. (3.6) Density of blackening versus exposure time.

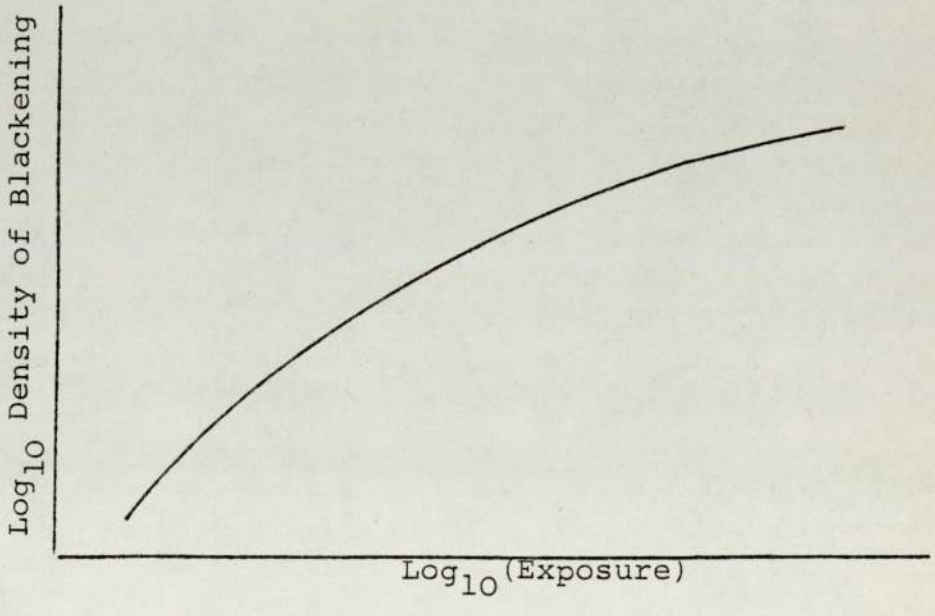

Fig. (3.7) Calibration Curve.

first one and was moved along the abscissa, then the series of points on the first plot were converted to a curve on the second paper. The resultant plot was the calibration curve. See figure (3.7).

3.8 Relative integrated intensities

The background for each microphotometer trace of all specimens was drawn. The values of the densities of blackening at the peaks (D_a), and the background (D_b) were found by multiplying the height in centimeters of the point from the zero level measured on the micrographic trace by the wedge density measured in density per centimeter.

The exposure values (Σ_a) and (Σ_b) corresponding to (D_a) and (D_b) were determined from the calibration curve. The peak exposure (Σ_p) was found from equation (3.2) below

$$\Sigma_p = \Sigma_a - \Sigma_b \qquad (3.2)$$

The half peak exposure (Σ_w) was found from the following equation

$$\Sigma_w = \Sigma_b + \tfrac{1}{2}\Sigma_p \qquad (3.3)$$

This being converted back into density of blackening units (D_w) using the calibration curve. The half peak point (P_w) was then found as follows:-

$$P_w = D_w / \text{wedge density} \qquad (3.4)$$

So that the half peak point could be measured for each peak, a line was then drawn through the half peak point parallel to the slope of the background. A right-angle

triangle was constructed beneath this line, it being used as the hypotenuse and the two other sides being parallel to x and y axes. The half width (w) was then measured as illustrated in figure (3.8).

The relative integrated intensity (R.I.I.) was then given by

$$R.I.I. = \Sigma_p w. \qquad (3.5)$$

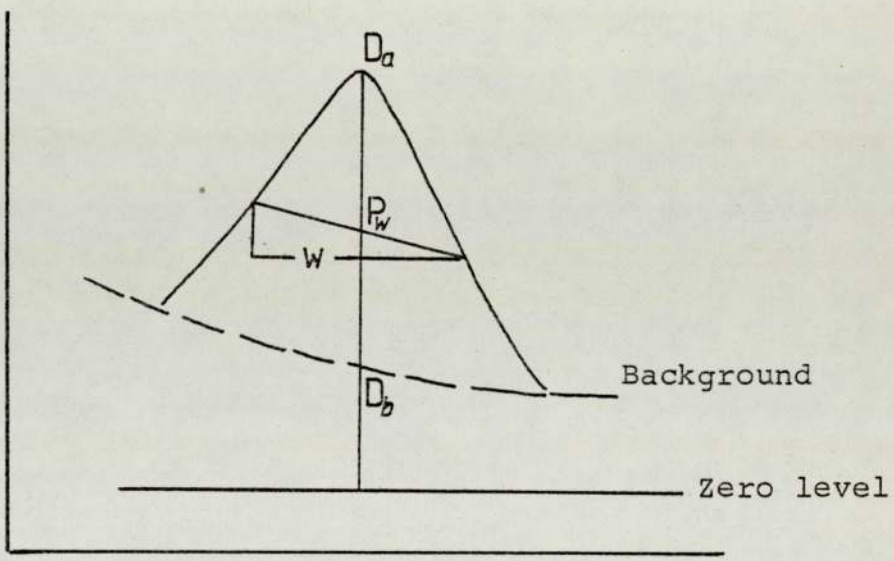

Fig. (3.8) Intensity measurement.

- CHAPTER FOUR -

CALCULATION OF THE BASIC SCATTERING DATA

4.1 The structure factor $[F_{ehkl}(\theta)]$.

The structure factor $[F_{ehkl}(\theta)]$, [15] is given by:-

$$[F_{ehkl}(\theta)] = \sum_{i}^{N} f_i(\theta) \exp[-2\pi i(hu_i+kv_i+lw_i)] \tag{4.1}$$

where u_i, v_i and w_i are the fractional coordinate of atom i, whereas N stands for the number of atoms in the unit cell.

The materials used were face-centred cubic, so that there are four atoms per unit cell at 000, ½½0, 0½½, ½0½.

By using equation (4.1) it could be found that

$$[F_{ehkl}(\theta)] = f_e(\theta) \{1+\exp[-i\pi(k+l)]+\exp[-i\pi(h+l)] +\exp[-i\pi(h+k)] \tag{4.2}$$

Therefore the reflection will occur when hkl are all even or all odd, otherwise $[F_{ehkl}(\theta)] = 0$ and the reflection is absent.

$$[F_{ehkl}(\theta)] = 4f_e(\theta) \tag{4.3}$$

For hkl all even or all odd.

The calculation of the structure factor $[F_{ehkl}(\theta)]$ for all the materials used, was carried out as follows:-

From the data given in table II of reference [16] a graph of $f_e(\theta)$ versus $\frac{1}{2d}$ was drawn for each material as shown in

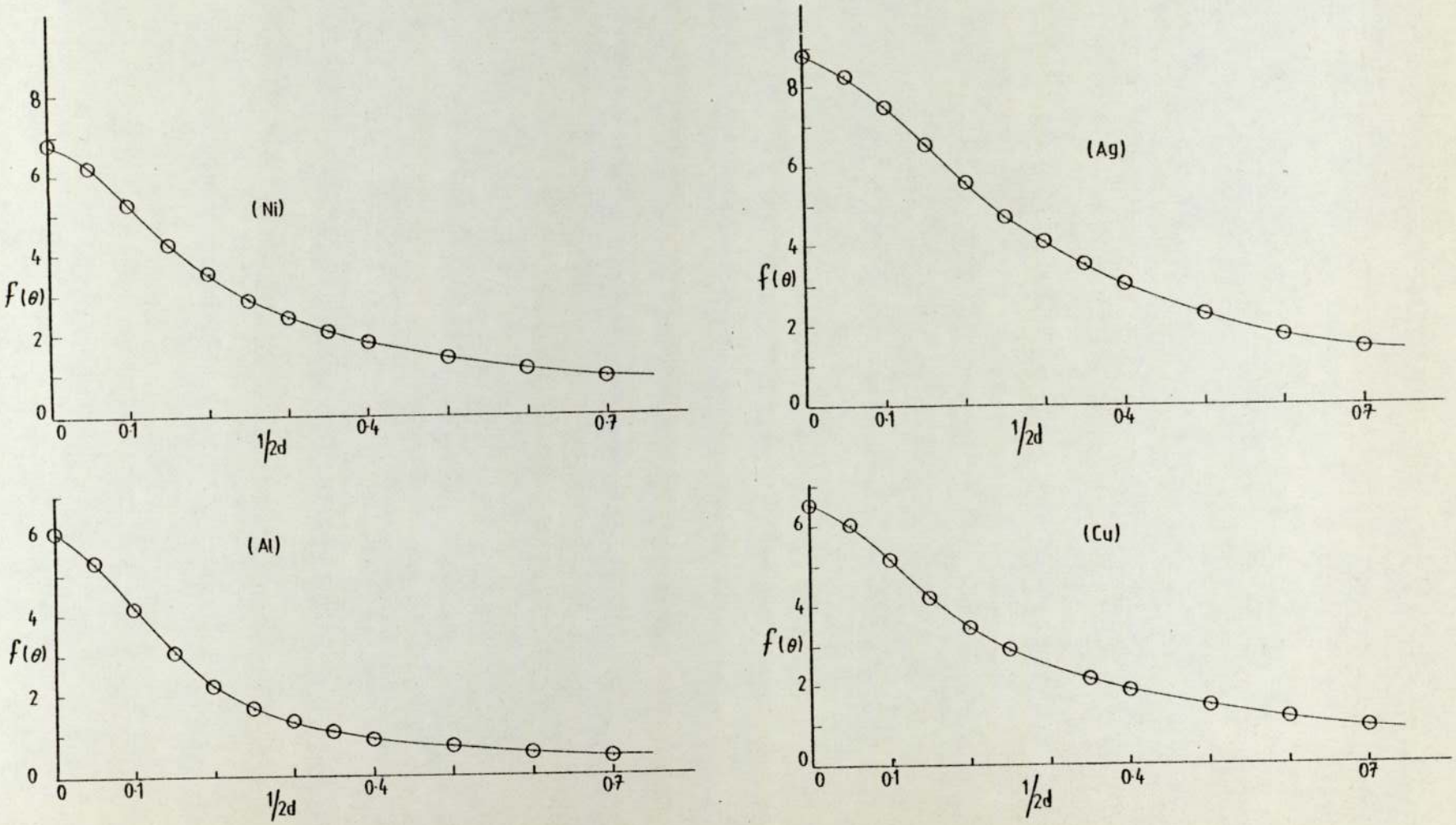

Fig. (4.1) The atomic scattering factor versus half inverse of interplanar spacing.

figure (4.1). Knowing the interplanar spacing (d), $\frac{1}{2d}$ could be calculated, and using the above mentioned graph $f_e(\theta)$ could be determined. Hence using equation (4.3), the structure factor was obtained.

The resulting values of the structure factor for the aluminium, copper, silver and nickel so obtained are shown in table (4.1).

Table (4.1); The structure factor of aluminium, copper, silver and nickel.

	$F_e(\theta)$			
hkl	Al	Cu	Ag	Ni
111	8.56	11.99	21.60	11.80
200	7.06	10.60	19.40	10.32
220	4.48	7.68	14.08	7.40
311	3.62	6.56	11.80	6.10
222	3.46	6.20	11.08	5.90
400	2.84	5.20	9.20	4.88
331	2.50	4.80	8.16	4.28
420	2.40	4.52	7.88	4.16
422	2.16	3.92	6.80	3.80

4.2 Debye-Waller temperature.

All the atoms of crystalline materials are vibrating about their mean position with amplitudes which increase with increase in temperature of the solid. These vibrations will affect the relative coordinates of the atoms and hence the diffraction pattern [17]. It is necessary therefore to take this thermal effect into account. Doing that, we must

calculate the Debye-Waller temperature (e^{-D}), [18].

$$e^{-D} = \exp\left[-B\left(\tfrac{1}{2}d\right)^2\right] \qquad (4.4)$$

and

$$B = \frac{1.14\times10^4}{M_a\,\Theta}\left[\tfrac{1}{4}+\frac{T}{\Theta}\varphi\left(\frac{\Theta}{T}\right)\right] \qquad (4.5)$$

where

Θ is the characteristic temperature, [19]

M_a is the atomic mass,

T is the room temperature and

$\varphi(\frac{\Theta}{T})$ is the Debye function.

Using table (5.2.2B) [18], a graph was drawn between $\varphi(\frac{\Theta}{T})$ versus $(\frac{\Theta}{T})$ - see figure (4.2).

From the graph we can find the value of $\varphi(\frac{\Theta}{T})$ for each particular value of $(\frac{\Theta}{T})$. Then, by substituting the values of all the parameters in equation (4.5) one could determine (B).

After this, e^{-D} can be determined for any particular ring by substitution the value of (B) and the value of (d) for that particular ring in equation (4.4).

Table (4.2) shows the value of Debye-Waller temperature factor e^{-D} for aluminium, copper, silver and nickel for different rings.

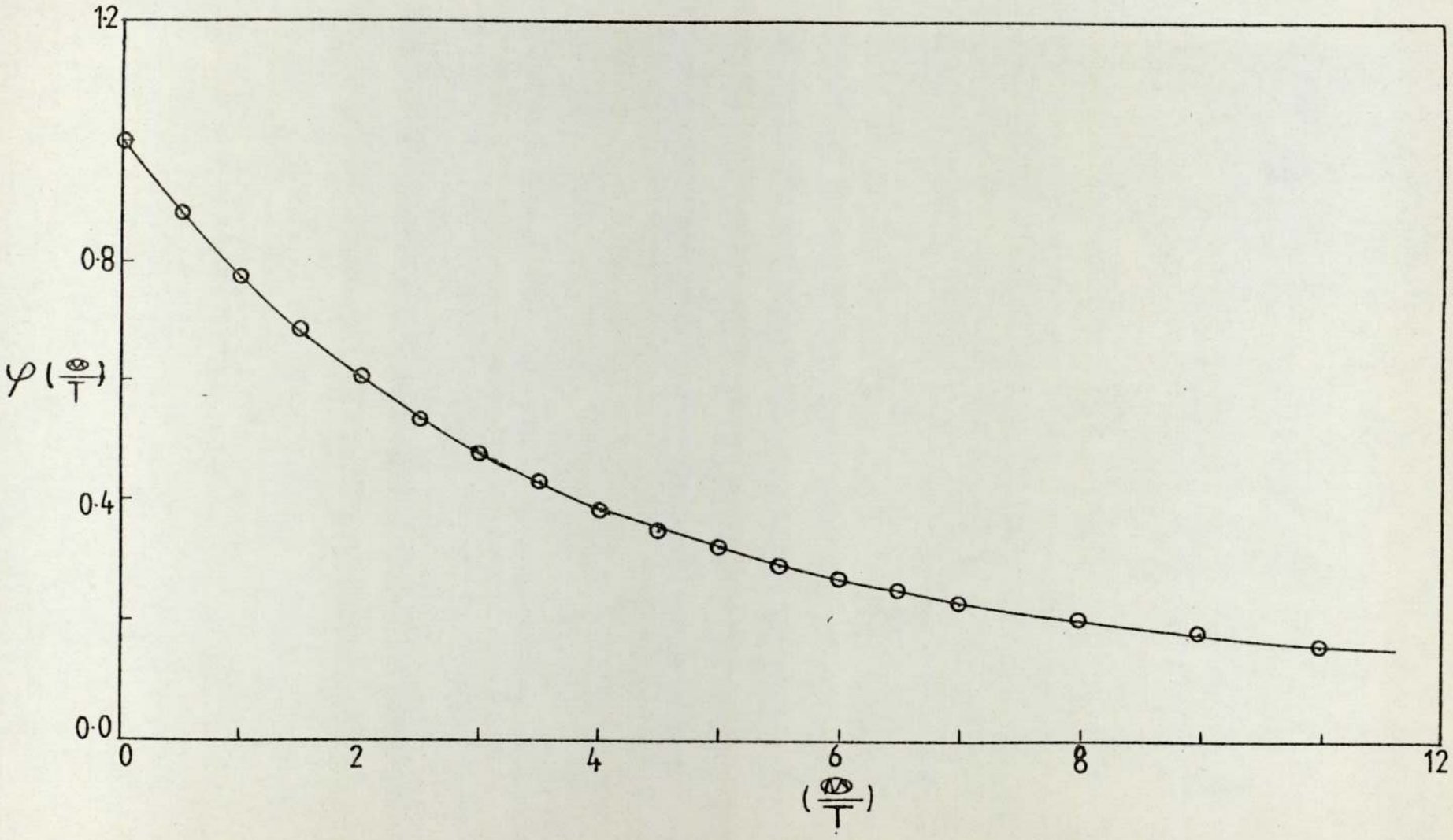

Fig. (4.2) The Debye function versus $(\frac{\Theta}{T})$.

Table (4.2); The Debye-Waller temperature e^{-D} of aluminium, copper, silver and nickel.

	e^{-D}			
hkl	Al	Cu	Ag	Ni
111	0.963	0.970	0.972	0.975
200	0.951	0.960	0.963	0.967
220	0.905	0.921	0.927	0.935
311	0.872	0.893	0.901	0.911
222	0.861	0.884	0.892	0.903
400	0.820	0.850	0.859	0.873
331	0.789	0.822	0.835	0.851
420	0.779	0.813	0.827	0.844
422	0.741	0.781	0.796	0.816

4.3 Other crystallographic data required for evaluation of (k) factor.

Table (4.3) below shows the multiplicity (P) and the interplanar spacing (d) for aluminium, copper, silver and nickel. Also shown in this table are the volume of the unit cell of each material. Note that (d) and (a) (cell dimension) have been taken from powder data diffraction file.

Table (4.3); The interplanar spacing and cell volume for different materials.

		d			
hkl	P	Al	Cu	Ag	Ni
111	8	2.338	2.088	2.359	2.034
200	6	2.024	1.808	2.044	1.762
220	12	1.431	1.278	1.445	1.246
311	24	1.221	1.0900	1.2310	1.0624
222	8	1.1690	1.0436	1.1796	1.0172
400	6	1.0124	0.9038	1.0215	0.8810
331	24	0.9289	0.8293	0.9375	0.8084
420	24	0.9055	0.8083	0.9137	0.7880
422	24	0.8266	0.7379	0.8341	0.7193
Cubic cell volume $a_1^3 (A^o)^3$		66.4010	47.2420	68.2300	43.7560

4.4 Total scattering number.

To calculate the total scattering number (t/λ_T), where (λ_T) is the total mean free path, one needs to find the elastic mean free path (λ_e) and the inelastic mean free path (λ_i) of the electron in the specimen.

4.4.1 Determination of the elastic mean free path (λ_e).

Knowing the atomic number (z) of each material and the accelerating voltage, the graph shown in figure (4.3) was used to obtain $(\rho\lambda_e)$. Hence (λ_e) was calculated for each material and voltage simply by dividing the result by the density (ρ) of the material. The results are listed in table (4.4).

Table (4.4); Calculation of (λ_e) [used in conjunction with figure (4.3)].

kV	$\rho\lambda_e$ (gmcm^{-2}x10^{-5})		λ_e (x10^{-5}cm)			
	Al	Ni,Cu,Ag	Al	Ni	Cu	Ag
80	1.54	1.46	0.570	0.164	0.1630	0.1390
100	1.85	1.74	0.685	0.196	0.1942	0.1660
400	4.20	3.90	1.554	0.438	0.4353	0.3714
500	4.55	4.25	1.684	0.478	0.4743	0.4050
600	4.82	4.55	1.784	0.5112	0.5080	0.4333
800	5.30	5.00	1.962	0.562	0.5580	0.4762
1000	5.50	5.22	2.036	0.587	0.5830	0.4970
Density of material ρ (gmcm^{-3})			2.702	8.900	8.9600	10.5000
Atomic number z			13	28	29	47

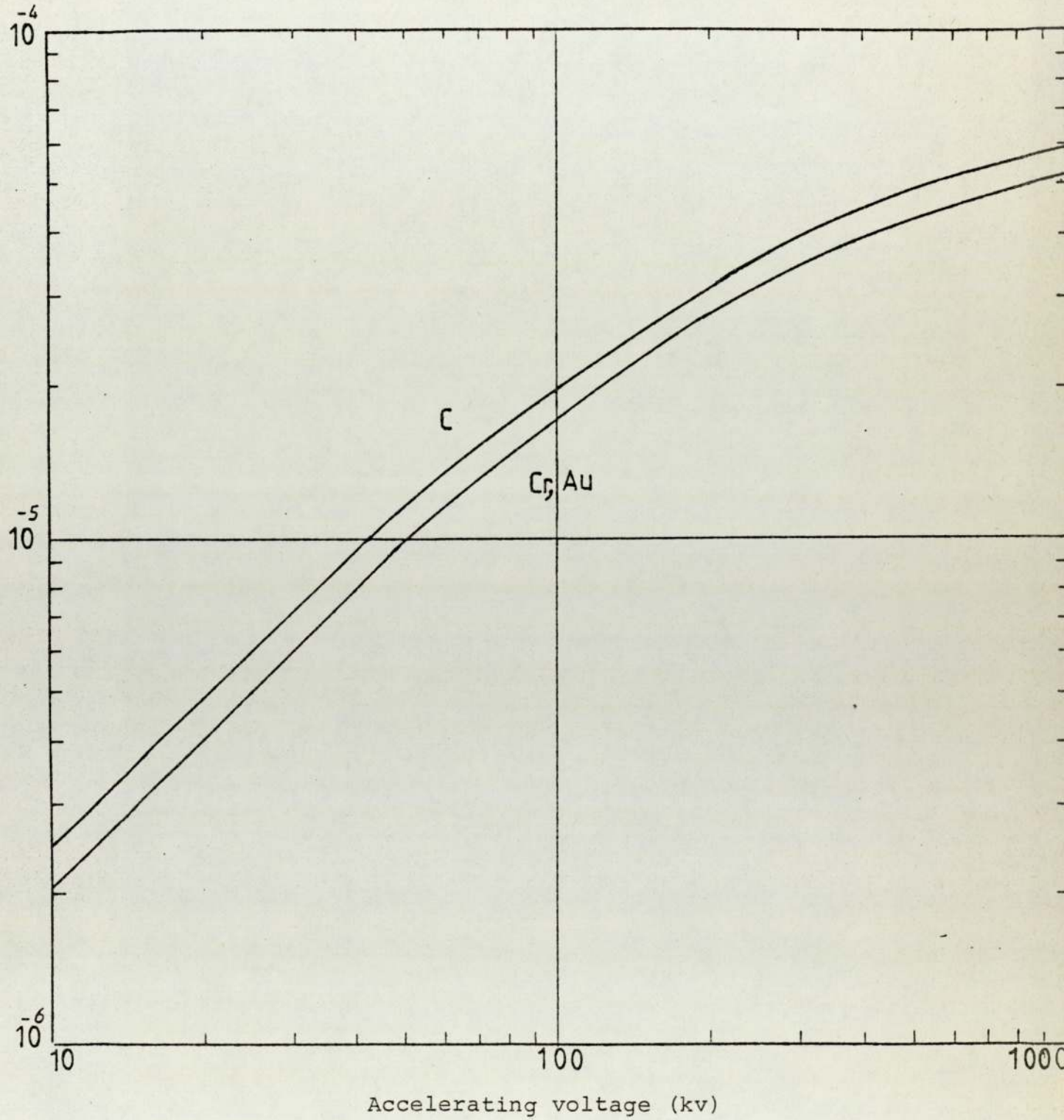

Fig. (4.3) Transparency thickness versus accelerating voltage.[16]

4.4.2 The determination of the inelastic mean free path (λ_i).

In order to calculate (λ_i), figure (4.4) was used |16| from which (σ_i/σ_e) (the inelastic elastic cross section ratio) was obtained for each material according to its atomic number.

Since $\sigma_i/\sigma_e = \lambda_e/\lambda_i$

it follows that

$$\lambda_i = \lambda_e/(\sigma_i/\sigma_e)$$

Hence the inelastic mean free path (λ_i) was obtained for each material and accelerating voltage since (λ_e) has already been found as mentioned before.

Table (4.5); Lists the values of (λ_i) thus obtained.

kV	λ_i ($\times 10^{-5}$ cm)			
	Al	Ni	Cu	Ag
80	0.285	0.1673	0.172	0.228
100	0.343	0.200	0.2044	0.272
400	0.777	0.447	0.458	0.609
500	0.842	0.488	0.499	0.664
600	0.892	0.522	0.535	0.7103
800	0.981	0.5735	0.5874	0.781
1000	1.018	0.599	0.614	0.815
σ_i/σ_e	2.00	0.98	0.95	0.61

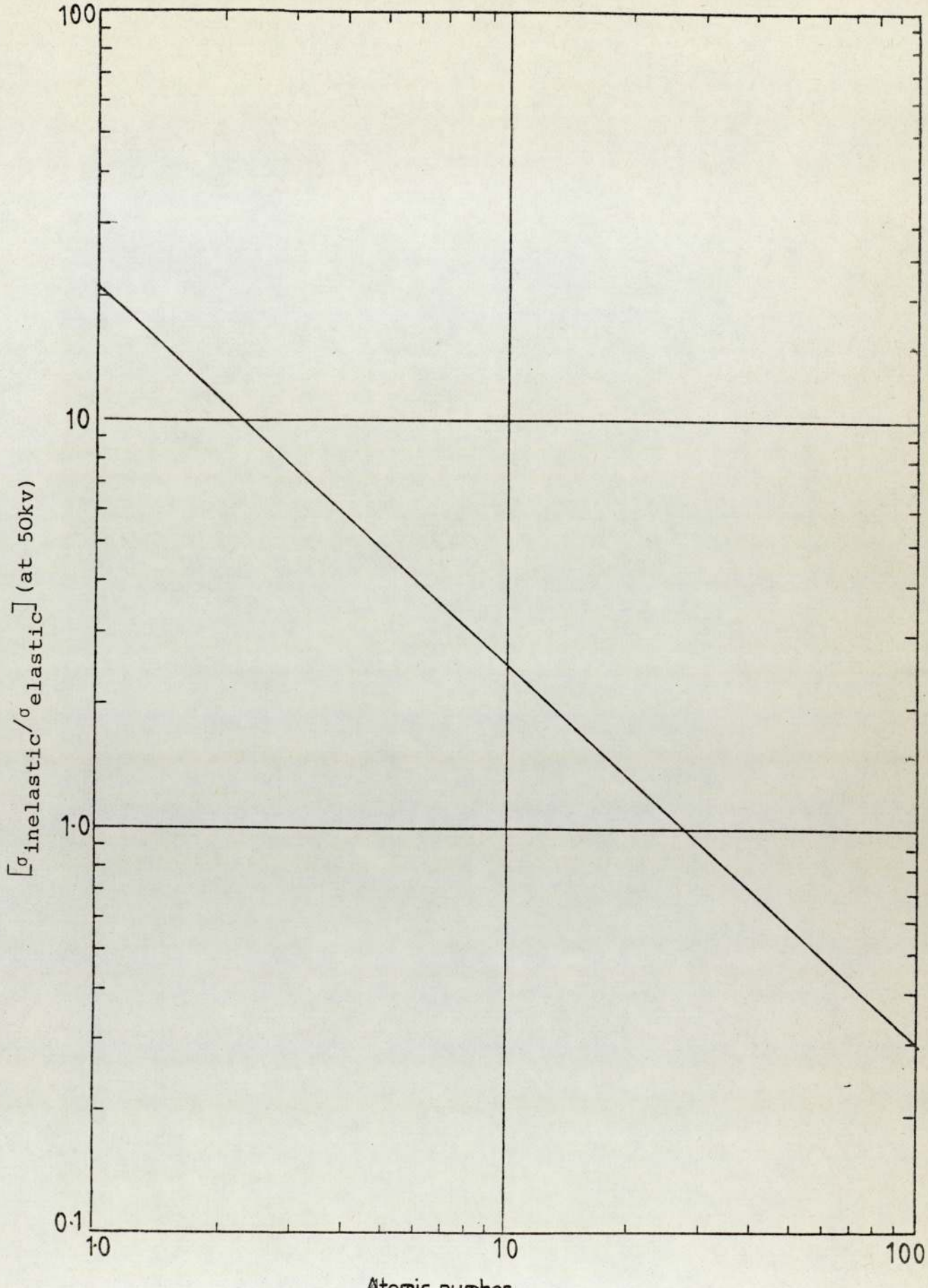

Fig. (4.4) Inelastic to elastic cross section ratio versus the atomic number.

4.4.3 Calculation of total mean free path (λ_T).

Since $1/\lambda_T = 1/\lambda_i + 1/\lambda_e$ and since both (λ_i) and (λ_e) have been obtained, the above equation was therefore used to calculate the total mean free path (λ_T). The results are shown in table (4.6) below.

Table (4.6); The Total Mean Free Path.

	$\lambda_T \times 10^{-5}$ cm			
kv	Al	Ni	Cu	Ag
80	0.190	0.08283	0.0836	0.0863
100	0.2283	0.099	0.0996	0.103
400	0.518	0.221	0.223	0.231
500	0.561	0.2414	0.2432	0.252
600	0.595	0.2582	0.261	0.269
800	0.654	0.284	0.286	0.296
1000	0.679	0.2965	0.299	0.309

Values of the total scattering number (t/λ_T) were then obtained simply by dividing the thickness (t) by (λ_T). The results are shown in tables (4.7), (4.8) and (4.9).

Table (4.7); Total Scattering Number for Single Specimens in (Al+Cu) Combination.

kv	t/λ_T									
	Al_{920}	Al_{720}	Al_{450}	Al_{330}	Al_{300}	Cu_{600}	Cu_{490}	Cu_{400}	Cu_{290}	Cu_{200}
80	4.84	3.79	2.37	1.74	1.58	7.18	5.86	4.78	3.47	2.39
100	4.03	3.15	1.97	1.45	1.314	6.024	4.92	4.02	2.912	2.01
500	1.64	1.28	0.802	0.588	0.535	2.47	2.015	1.645	1.192	0.823
1000	1.35	1.06	0.663	0.486	0.442	2.01	1.64	1.34	0.970	0.67

Table (4.8); Total Scattering Number for Single Specimens in (Ag+Cu) Combination.

kv	t/λ_T									
	Ag_{630}	Ag_{480}	Ag_{360}	Ag_{290}	Ag_{220}	Cu_{880}	Cu_{590}	Cu_{430}	Cu_{330}	Cu_{240}
400	2.73	2.078	1.56	1.255	0.952	3.95	2.65	1.93	1.48	1.08
600	2.342	1.784	1.34	1.08	0.818	3.372	2.261	1.65	1.26	0.919
800	2.13	1.622	1.22	0.98	0.743	3.077	2.063	1.503	1.154	0.839

Table (4.9); Total Scattering Number for Single Specimens in (Al+Ni) Combination.

kv	t/λ_T									
	Al_{810}	Al_{510}	Al_{410}	Al_{350}	Al_{250}	Ni_{660}	Ni_{400}	Ni_{310}	Ni_{200}	Ni_{120}
80	4.26	2.68	2.16	1.84	1.32	7.97	4.83	3.743	2.415	1.45
100	3.55	2.234	1.796	1.533	1.095	6.667	4.04	3.13	2.02	1.212
400	1.564	0.985	0.792	0.676	0.483	2.99	1.81	1.403	0.905	0.543
600	1.36	0.857	0.689	0.588	0.420	2.556	1.55	1.2	0.775	0.465
800	1.24	0.78	0.63	0.535	0.382	2.324	1.41	1.09	0.704	0.4225
1000	1.19	0.751	0.604	0.515	0.368	2.226	1.35	1.046	0.675	0.405

- CHAPTER FIVE -

EXPERIMENTAL RESULTS

5.1 Introduction

In this work three different combinations have been prepared; aluminium and copper, aluminium and nickel, silver and copper and single specimens for each material in each combination. The thickness of the single specimen for all the combinations has been measured using the interferometer. From these measurements, the thickness ratio of each composite specimen have been determined for each combination.

The diffraction patterns for all the specimens, single and composite,have been obtained at different voltages. By using the microdensitometer, the traces of all the diffraction micrographs have been taken in order to measure the intensity of the individual diffraction ring. The intensities of the measurable diffraction rings have been determined as mentioned in Chapter Three for all the single and composite specimens for the three combinations at different voltages. From these measurements, the intensity ratios have been determined.

The experimental results thus obtained are presented in this Chapter.

5.2 Thickness of the Specimens

This section presents three tables which give the thickness of the single and double-layered specimens. It is to be noted that (*) wherever it occurs implies 1, 2, 3, 4 and 5

according to the thickness of the material concerned.

5.2.1 Thickness for Aluminium and Copper.

The following table (5.1) gives the thickness of pure aluminium, pure copper and the total thickness of aluminium and copper in the composite specimen.

Table (5.1)

Specimen & thickness				Total thickness ($t_{Al}+t_{Cu}$), A°				
Al	tA°	Cu	tA°	Al_1+Cu_*	Al_2+Cu_*	Al_3+Cu_*	Al_4+Cu_*	Al_5+Cu_*
Al_1	920	Cu_1	600	1520	1320	1050	930	900
Al_2	720	Cu_2	490	1410	1210	940	820	790
Al_3	450	Cu_3	400	1320	1120	850	730	700
Al_4	330	Cu_4	290	1210	1010	740	620	590
Al_5	300	Cu_5	200	1120	920	650	530	500

5.2.2 Thickness for Aluminium and Nickel.

The following table (5.2) gives the thickness of pure aluminium, pure nickel and the total thickness of aluminium and nickel in the composite specimen.

Table (5.2)

Specimen & thickness				Total thickness ($t_{Al}+Ni$), A°				
Al	tA°	Ni	tA°	Al_1+Ni_*	Al_2+Ni_*	Al_3+Ni_*	Al_4+Ni_*	Al_5+Ni_*
Al_1	810	Ni_1	660	1470	1170	1070	1010	910
Al_2	510	Ni_2	400	1210	910	810	750	650
Al_3	410	Ni_3	310	1120	820	720	660	560
Al_4	350	Ni_4	200	1010	710	610	550	450
Al_5	250	Ni_5	120	930	630	530	470	370

5.2.3 Thickness for Silver and Copper

The following table (5.3) gives the thickness of pure silver, pure copper and the total thickness of silver and copper in the composite specimen.

Table (5.3)

Specimen & thickness				Total thickness ($t_{Ag}+t_{Cu}$), A°				
Ag	tA°	Cu	tA°	Ag_1+Cu_*	Ag_2+Cu_*	Ag_3+Cu_*	Ag_4+Cu_*	Ag_5+Cu_*
Ag_1	630	Cu_1	880	1510	1360	1240	1170	1100
Ag_2	480	Cu_2	590	1220	1070	950	880	810
Ag_3	360	Cu_3	430	1060	910	790	720	650
Ag_4	290	Cu_4	330	960	810	690	620	550
Ag_5	220	Cu_5	240	870	720	600	530	460

5.3 Thickness Ratio

This section presents three tables which give the thickness ratio of aluminium and copper, aluminium and nickel, and, silver and copper.

5.3.1 Thickness Ratio of Aluminium and Copper

The following table (5.4) shows the thickness ratio of aluminium and copper which have different thicknesses as indicated in table (5.1).

Table (5.4)

Al_1/Cu_*	Al_2/Cu_*	Al_3/Cu_*	Al_4/Cu_*	Al_5/Cu_*
1.533	1.200	0.750	0.550	0.500
1.877	1.470	0.918	0.673	0.612
2.300	1.800	1.125	0.825	0.75
3.170	2.480	1.552	1.138	1.034
4.600	3.600	2.250	1.650	1.50

5.3.2 Thickness Ratio of Aluminium and Nickel

The following table (5.5) gives the thickness ratio of aluminium and nickel which have different thicknesses as indicated in table (5.2).

Table (5.5)

Al_1/Ni_*	Al_2/Ni_*	Al_3/Ni_*	Al_4/Ni_*	Al_5/Ni_*
1.227	0.773	0.6212	0.530	0.379
2.025	1.275	1.025	0.875	0.625
2.613	1.645	1.323	1.130	0.806
4.050	2.550	2.050	1.750	1.25
6.750	4.250	3.417	2.917	2.083

5.3.3 Thickness Ratio of Silver and Copper

The following table (5.6) gives the thickness ratio of silver and copper which have different thicknesses as indicated in table (5.3).

Table (5.6)

Ag_1/Cu_*	Ag_2/Cu_*	Ag_3/Cu_*	Ag_4/Cu_*	Ag_5/Cu_*
0.716	0.546	0.409	0.329	0.250
1.068	0.814	0.6102	0.492	0.373
1.465	1.116	0.837	0.674	0.512
1.910	1.455	1.091	0.879	0.667
2.625	2.000	1.500	1.210	0.917

5.4 The Crystallite size of the Specimens

The crystallite size of the specimens have been determined as mentioned in Chapter Three. The following table (5.7) gives the crystallite size for all materials in the three combination.

Table (5.7)

Specimen No.	Al+Cu		Al+Ni		Ag+Cu	
	ε_{Al}	ε_{Cu}	ε_{Al}	ε_{Ni}	ε_{Ag}	ε_{Cu}
1	700	260	440	120	530	290
2	530	340	300	80	640	190
3	400	310	310	100	450	210
4	290	300	230	85	470	180
5	240	230	260	90	490	160

Numbers (1) to (5) mean different thickness of the specimens, from the thickest to the thinnest specimens.

5.5 Relative Integrated Intensity of Single Specimens.

This section presents tables of the intensity ratio of the single specimens in the three combinations, aluminium and copper, aluminium and nickel, and, silver and copper at different voltages.

5.5.1 The Intensity Ratio for Aluminium and Copper in Aluminium and Copper Combination.

In this combination, the measureable diffraction rings for aluminium and for copper were (111), (200), (220) and (311) at 80kv, 100kv, 500kv and 1000kv. Then the intensity ratio was for (111/200), (111/220) and (111/311) for both materials.

The following tables, (5.8) through (5.11) give the intensity ratio for aluminium and for copper at 80kv, 100kv, 500kv and 1000kv respectively.

Table (5.8); Intensity Ratio for Aluminium and for Copper at 80kv.

Specimen	Intensity Ratio		
	I_{111}/I_{200}	I_{111}/I_{220}	I_{111}/I_{311}
Cu_1	2.658	3.838	5.083
Cu_2	2.099	3.658	3.447
Cu_3	2.1005	3.548	3.44
Cu_4	2.2308	4.1498	3.79
Cu_5	2.1457	4.0265	4.3115
Al_1	2.661	4.449	3.213
Al_2	1.880	3.395	3.289
Al_3	2.0499	4.858	4.266
Al_4	2.21	5.19	6.0564

Table (5.9); Intensity Ratio for Aluminium and for Copper at 100kv.

Specimen	Intensity Ratio		
	I_{111}/I_{200}	I_{111}/I_{220}	I_{111}/I_{311}
Cu_1	1.765	5.157	7.012
Cu_2	2.148	3.95	4.153
Cu_3	2.471	4.39	5.01
Cu_4	2.714	4.72	5.55
Cu_5	2.261	4.295	5.64
Al_1	2.65	3.44	3.419
Al_2	2.595	4.78	5.54
Al_3	2.60	4.789	7.44
Al_4	3.74	9.52	11.32

Table (5.10); Intensity Ratio for Aluminium and for Copper at 500kv.

Specimen	Intensity Ratio		
	I_{111}/I_{200}	I_{111}/I_{220}	I_{111}/I_{311}
Cu_1	2.07	4.71	5.025
Cu_2	1.768	3.968	3.336
Cu_3	1.7158	4.21	3.965
Cu_4	2.0336	4.676	4.569
Cu_5	1.6624	4.5726	5.6253
Al_1	1.469	6.331	4.381
Al_2	1.979	6.1538	5.437
Al_3	2.223	5.791	5.747
Al_5	2.272	8.146	7.11

Table (5.11); Intensity Ratio for Aluminium and for Copper at 1000kv.

Specimen	Intensity Ratio		
	I_{111}/I_{200}	I_{111}/I_{220}	I_{111}/I_{311}
Cu_1	2.447	4.1742	5.7186
Cu_2	2.2565	3.6167	4.2316
Cu_3	2.2057	4.1923	3.615
Cu_5	2.1733	5.7287	6.9063
Al_1	1.872	5.593	3.8394
Al_2	3.004	9.762	4.767

5.5.2 The Intensity Ratio for Aluminium and for Nickel in Aluminium and Nickel Combination.

In this combination, the measurable diffraction rings for aluminium and for nickel were (111), (200), (220) and (311) at 80kv, 100kv, 400kv, 500kv and 800kv. Then the intensity ratio was for (111/200), (111/220) and (111/311) for both materials.

The following tables (5.12) through (5.16) give the intensity ratio for aluminium and for nickel at 80kv, 100kv, 400kv, 600kv and 800kv respectively.

Table (5.12); Intensity Ratio for Aluminium and for Nickel at 80kv.

Specimen	Intensity Ratio		
	I_{111}/I_{200}	I_{111}/I_{220}	I_{111}/I_{311}
Al_1	1.603	4.545	4.074
Al_5	2.074	4.167	5.091
Ni_1	2.654	7.261	6.667

Table (5.13); Intensity Ratio for Aluminium and for Nickel at 100kv.

Specimen	Intensity Ratio		
	I_{111}/I_{200}	I_{111}/I_{220}	I_{111}/I_{311}
Al_1	2.117	5.944	6.756
Al_2	2.794	6.326	7.75
Al_3	2.914	6.612	7.00
Al_4	3.108	10.218	9.094
Al_5	1.935	5.389	6.527
Ni_1	2.761	7.635	6.405
Ni_2	2.552	8.862	8.371
Ni_3	3.137	9.277	8.151
Ni_4	3.253	8.39	9.075;
Ni_5	3.0251	8.761	8.312

Table (5.14); Intensity Ratio for Aluminium and for Nickel at 400kv.

Specimen	Intensity Ratio		
	I_{111}/I_{200}	I_{111}/I_{220}	I_{111}/I_{311}
Al_1	2.00	4.47	4.16
Al_2	2.476	4.265	4.222
Al_3	2.89	4.17	4.55
Al_4	1.41	4.615	3.78
Al_5	2.52	5.927	7.927
Ni_1	1.927	4.683	4.338
Ni_2	2.726	6.305	5.774
Ni_3	2.086	5.425	4.567
Ni_4	2.152	6.07	5.15
Ni_5	2.387	5.88	4.86

Table (5.15); Intensity Ratio for Aluminium and for Nickel at 600kv.

Specimen	Intensity Ratio		
	I_{111}/I_{200}	I_{111}/I_{220}	I_{111}/I_{311}
Al_1	1.927	3.977	4.257
Al_2	2.494	4.528	5.448
Al_3	2.47	4.451	6.257
Al_4	2.916	5.811	7.27
Al_5	2.365	4.673	3.2
Ni_1	2.636	5.347	6.00
Ni_2	2.076	5.949	5.57
Ni_3	2.237	5.192	5.757
Ni_4	2.388	5.756	6.197
Ni_5	2.329	6.176	6.262

Table (5.16); Intensity Ratio for Aluminium and for Nickel at 800kv.

Specimen	Intensity Ratio		
	I_{111}/I_{200}	I_{111}/I_{220}	I_{111}/I_{311}
Al_1	1.701	3.943	4.9215
Al_2	1.828	4.856	4.683
Ni_1	2.959	7.803	7.185
Ni_2	3.428	7.605	6.639
Ni_3	3.396	6.528	6.811
Ni_4	2.777	10.829	8.386
Ni_5	2.729	6.969	6.789

5.5.3 The Intensity Ratio for Silver and for Copper in Silver and Copper Combination.

In this combination the measurable diffraction rings for silver and for copper were (111), (200), (220) and (311) at 400kv, 600kv and 800kv. Ring (422) for silver was measurable at 400kv and 600kv, and was measurable for copper at 600kv and 800kv. Then the intensity ratio was for (111/200), (111/220), (111/311) and (111/422).

The following tables (5.17) through (5.19) give the intensity ratio for silver and for copper at 400kv, 600kv and 800kv respectively.

Table (5.17); Intensity Ratio for Silver and for Copper at 400kv.

Specimen	Intensity Ratio			
	I_{111}/I_{200}	I_{111}/I_{220}	I_{111}/I_{311}	I_{111}/I_{422}
Ag_1	1.645	3.499	3.64	24.26
Ag_2	2.389	5.45	3.74	34.26
Ag_3	2.47	4.88	3.489	54.44
Ag_4	2.02	3.6	3.12	64.266
Ag_5	2.18	3.65	3.38	27.32
Cu_1	2.404	3.552	3.959	-
Cu_2	1.927	4.036	3.151	-
Cu_3	2.883	5.948	5.096	-
Cu_4	2.809	5.145	4.65	-
Cu_5	2.98	3.77	4.099	-

Table (5.18); Intensity Ratio for Silver and for Copper at 600kv.

Specimen	Intensity Ratio			
	I_{111}/I_{200}	I_{111}/I_{220}	I_{111}/I_{311}	I_{111}/I_{422}
Ag_1	1.972	4.2187	2.923	23.034
Ag_2	2.4075	6.74	4.535	23.52
Ag_3	1.826	3.513	3.252	23.45
Ag_4	1.146	6.094	2.652	41.413
Ag_5	2.27	4.843	4.25	43.477
Cu_1	2.177	3.9035	3.7118	17.691
Cu_2	2.767	5.0995	5.078	49.653
Cu_3	1.666	4.802	3.243	24.726
Cu_4	2.621	4.147	4.443	42.491

Table (5.19); Intensity Ratio for Silver and for Copper at 800kv.

Specimen	Intensity Ratio			
	I_{111}/I_{200}	I_{111}/I_{220}	I_{111}/I_{311}	I_{111}/I_{422}
Ag_2	1.565	4.213	2.94	-
Ag_3	1.563	4.74	3.44	-
Ag_4	2.179	5.10	4.18	
Cu_1	2.128	4.989	-	29.738
Cu_2	2.1527	4.958	-	22.118
Cu_4	2.3135	7.222	9.562	-

5.6 Relative Integrated Intensity of Double-Layered Specimens.

This section presents tables for the intensity ratio of the two elements in the composite specimen, for aluminium and copper, aluminium and nickel, and, for silver and copper at different voltages.

It is to be noted that (*) signifies 1,2,3,4 and 5 according to the thickness of the material concerned.

5.6.1 The Intensity Ratio of Aluminium and Copper Combination.

In this combination, aluminium and copper were the materials forming the double-layered specimen. The aluminium was on the top of the specimen, and the intensity ratio was aluminium intensity to copper intensity at 80kv, 100kv, 500kv and 100kv. The measurable rings for aluminium were (111), (220) and (311), and for copper were (200), (220) and (311). Then the intensity ratio was for (111/200), (111/220), (111/311) (220/220), (220/311), (311/200), (311/220) and (311/311) for different specimen's thickness.

The following tables (5.20) through (5.23) give the intensity ratio of aluminium-copper specimens at 80kv, 100kv, 500kv and 1000kv respectively, and the thickness ratio of the specimen.

Table (5.20); Intensity and Thickness Ratios of Aluminium-Copper Specimens at 80kv.

Thickness ratios t_{Al}/t_{Cu}	Intensity ratio (I_{Al}/I_{Cu})								
	I_{111}/I_{200}	I_{111}/I_{220}	I_{111}/I_{311}	I_{220}/I_{200}	I_{220}/I_{220}	I_{220}/I_{311}	I_{311}/I_{200}	I_{311}/I_{220}	I_{311}/I_{311}
Al_1/Cu_*									
1.533	0.82	2.18	2.82	0.116	0.307	0.322	0.186	0.4934	0.517
1.877	0.769	1.660	1.58	0.135	0.29	0.277	0.3077	0.664	0.633
2.300	0.794	1.303	1.34	0.176	0.288	0.297	0.376	0.616	0.634
3.170	1.09	1.941	2.46	0.213	0.374	0.474	0.3625	0.650	0.818
4.600	0.95	3.64	2.91	0.2774	1.07	0.8523	0.304	1.166	0.933
Al_2/Cu_*									
1.200	1.200	2.21	2.367	0.093	0.1724	0.1845	0.203	0.375	0.402
1.470	0.802	1.55	1.46	0.10535	0.2033	0.192	0.24	0.462	0.436
1.800	1.11	1.89	2.015	0.1555	0.264	0.2821	0.23	0.384	0.41
2.48	1.108	1.87	2.63	0.2986	0.5045	0.7076	0.4204	0.7104	0.9964
3.600	2.61	3.674	4.085	0.620	0.872	0.9697	0.4689	0.6603	0.734
Al_3/Cu_*									
1.552	3.62	4.43	5.094	0.411	0.5031	0.5786	0.6524	0.7985	0.9184
2.250	1.421	3.596	4.026	0.156	0.3945	0.4418	0.2346	0.594	0.6647
Al_4/Cu_*									
0.673	1.0304	1.88	1.831	0.0773	0.141	0.1373	0.1072	0.1956	0.1905
0.825	1.4965	2.2766	2.644	0.1716	0.2611	0.3032	0.21742	0.331	0.3841
1.138	1.789	2.695	3.049	0.1522	0.22925	0.2594	0.2433	0.3663	0.4144
1.650	1.224	2.489	2.388	0.1839	0.374	0.3588	0.2414	0.4911	0.4711

Table (5.21); Intensity and Thickness Ratios of Aluminium-Copper Specimens at 100kv.

Thickness ratios t_{Al}/t_{Cu}	Intensity ratio (I_{Al}/I_{Cu})								
	I_{111}/I_{200}	I_{111}/I_{220}	I_{111}/I_{311}	I_{220}/I_{200}	I_{220}/I_{220}	I_{220}/I_{311}	I_{311}/I_{200}	I_{311}/I_{220}	I_{311}/I_{311}
Al_1/Cu_*									
1.533	0.696	1.576	1.589	0.0849	0.1923	0.1939	0.1816	0.4113	0.4148
1.877	0.8868	2.0416	2.304	0.09955	0.229	0.2586	0.2121	0.4882	0.5309
2.30	0.91405	1.697	1.9353	0.13388	0.2486	0.2835	0.2181	0.4049	0.46176
3.17	1.1288	2.453	3.2902	0.1814	0.3943	0.5288	0.2334	0.5073	0.6804
4.60	1.758	3.762	5.182	0.2603	0.557	0.7673	0.2786	0.596	0.82115
Al_2/Cu_*									
1.200	0.8387	1.302	1.25	0.1065	0.165	0.1586	0.1806	0.280	0.269
1.47	1.179	2.249	2.2603	0.1259	0.2375	0.2412	0.2159	0.4074	0.4138
1.80	0.7395	1.498	1.512	0.1053	0.2134	0.2154	0.1997	0.4048	0.40814
2.48	0.9762	2.402	2.51	0.1997	0.4914	0.513	0.2236	0.55	0.574
3.60	0.9231	1.625	1.815	0.418	0.735	0.821	0.352	0.6196	0.692
Al_3/Cu_*									
1.125	0.995	1.821	1.679	0.1326	0.243	0.224	0.206	0.377	0.3477
1.552	2.535	3.968	4.823	0.3905	0.611	0.743	0.4108	0.643	0.7813
2.25	1.754	3.174	3.66	0.2101	0.3802	0.4385	0.3534	0.6394	0.7375
Al_4/Cu_*									
0.673	1.127	1.766	1.785	0.0913	0.143	0.1445	0.1326	0.2078	0.21
0.825	1.42	2.31	2.52	0.1612	0.262	0.2854	0.1387	0.226	0.246
1.138	1.256	2.193	2.073	0.175	0.305	0.288	0.185	0.322	0.305
1.65	1.346	2.44	2.52	0.147	0.267	0.276	0.2024	0.367	0.379
Al_5/Cu_*									
0.612	0.705	1.46	1.32	0.0615	0.127	0.115	0.083	0.171	0.155
0.75	0.826	1.375	2.36	0.076	0.126	0.216	0.117	0.194	0.333
1.034	1.285	2.53	2.65	0.166	0.327	0.342	0.1455	0.287	0.300
1.5	1.05	2.13	1.98	0.1353	0.275	0.254	0.1712	0.347	0.322

Table (5.22); Intensity and Thickness Ratios of Aluminium-Copper Specimens at 500kv.

Thickness ratios t_{Al}/t_{Cu}	Intensity ratio (I_{Al}/I_{Cu})								
	I_{111}/I_{200}	I_{111}/I_{220}	I_{111}/I_{311}	I_{220}/I_{200}	I_{220}/I_{220}	I_{220}/I_{311}	I_{311}/I_{200}	I_{311}/I_{220}	I_{311}/I_{311}
Al_1/Cu_*									
1.533	1.202	2.606	2.484	0.1468	0.3182	0.3033	-	-	-
1.877	1.758	4.187	5.1425	0.1795	0.4274	0.525	-	-	-
2.30	1.806	5.875	5.8026	0.1184	0.3853	0.381	-	-	-
3.17	2.323	5.138	5.946	0.2805	0.6206	0.7181	0.2851	0.6306	0.7297
4.6	2.149	4.3456	6.198	0.21953	0.444	0.70693	0.6232	1.2602	2.007
Al_2/Cu_*									
1.20	1.2487	3.3871	3.2398	0.05505	0.14931	0.1428	-	-	-
1.47	1.081	3.49	3.9175	0.08949	0.28893	0.32432	-	-	-
1.80	1.5556	4.425	4.9781	0.10875	0.30933	0.348	-	-	-
2.48	1.9237	4.212	5.3633	0.196214	0.42962	0.54706	0.41886	0.91712	1.16782
3.60	4.6277	7.2857	10.6298	0.4343	0.683753	0.9976	0.71	1.1178	1.63087
Al_3/Cu_*									
1.125	1.3306	3.5724	3.3455	0.0689	0.1851	0.1733	-	-	-
1.552	1.299	3.5374	3.453	0.24565	0.6688	0.653	0.1919	0.5225	0.5099
2.25	1.456	4.8732	5.2715	0.11176	0.37404	0.4046	-	-	-
Al_4/Cu_*									
0.673	0.8206	1.535	1.6484	0.0648	0.12125	0.1302	0.1060	0.1983	0.213
0.825	0.9531	2.4818	2.5797	0.0747	0.1944	0.20211	0.1552	0.404	0.4199
1.138	1.0861	2.5353	2.513	0.1043	0.2435	0.2414	0.12853	0.3000	0.2974
1.65	1.338	3.3226	3.238	0.11986	0.29769	0.29012	0.1769	0.4393	0.4281
Al_5/Cu_*									
0.612	0.8553	1.7677	1.692	0.0326	0.0673	0.0644	-	-	-
0.75	0.7786	1.6646	1.5713	0.0452	0.0966	0.0912	-	-	-
1.034	1.146	2.765	2.811	0.0827	0.2004	0.2037	-	-	-
1.50	1.253	2.963	3.2051	0.806	0.1905	0.2060	0.1117	0.2641	0.2857

Table (5.23); Intensity and Thickness Ratios of Aluminium-Copper Specimens at 1000kv.

Thickness ratios t_{Al}/t_{Cu}	Intensity ratio (I_{Al}/I_{Cu})								
	I_{111}/I_{200}	I_{111}/I_{220}	I_{111}/I_{311}	I_{220}/I_{200}	I_{220}/I_{220}	I_{220}/I_{311}	I_{311}/I_{200}	I_{311}/I_{220}	I_{311}/I_{311}
Al_1/Cu_*									
1.533	0.1284	0.3616	0.318	0.0767	0.216	0.19	0.1735	0.489	0.4299
2.30	1.113	2.487	2.715	0.114	0.2542	0.2774	0.221	0.493	0.538
3.17	1.478	3.89	4.194	0.1468	0.3864	0.4165	0.281	0.7386	0.796
4.60	1.254	3.45	3.365	0.2973	0.8169	0.797	0.2031	0.558	0.545
Al_2/Cu_*									
1.20	1.191	2.789	2.607	0.1057	0.2476	0.2315	-	-	-
1.47	1.10	2.749	2.567	0.1299	0.3247	0.3031	0.1834	0.458	0.4278
1.80	0.9735	2.981	3.16	0.1114	0.3413	0.3618	0.1607	0.4922	0.5218
2.48	1.4225	4.155	4.377	0.1734	0.5063	0.5334	0.2043	0.5967	0.6287
Al_3/Cu_*									
1.125	1.0434	2.571	2.551	0.1053	0.2594	0.2574	0.1667	0.4108	0.4076
1.552	1.5594	3.206	3.159	0.3193	0.6564	0.6469	0.2443	0.5023	0.495
2.25	1.356	3.834	4.223	0.1528	0.432	0.4758	0.184	0.5202	0.573
Al_4/Cu_*									
0.673	0.989	2.553	2.2324	0.0435	0.1123	0.09822	-	-	-
0.825	1.176	2.817	-	-	-	-	-	-	-
1.138	1.546	4.89	5.433	0.0679	0.2151	0.2388	-	-	-
1.65	1.2599	3.816	3.973	0.0963	0.2916	0.3036	-	-	-
Al_5/Cu_*									
0.612	0.8373	2.195	2.067	-	-	-	-	-	-
0.75	1.061	2.598	2.446	0.0311	0.0761	0.0717	-	-	-
1.034	2.29	5.323	6.823	-	-	-	-	-	-
1.5	0.975	3.14	3.195	-	-	-	-	-	-

5.6.2 The Intensity Ratio of Aluminium and Nickel Combination.

In this combination, aluminium and nickel were the materials forming the double-layered specimen. The aluminium was at the top of the specimen, and the intensity ratio was aluminium intensity to nickel intensity at 80kv, 100kv, 400kv, 600kv, 800kv and 1000kv. The measurable diffraction rings for aluminium were (111) and (220), and for nickel were (200) and (311). Then the intensity ratio was for (111/200), (111/311), (220/200) and (220/311) for different specimens' thickness.

The following tables (5.24) through (5.29) give the intensity ratio of aluminium-nickel specimens at 80kv, 100kv, 400kv, 600kv, 800kv and 1000kv respectively, and the thickness ratio of the specimens.

Table (5.24); The Intensity and Thickness Ratios of Aluminium-Nickel Specimens at 80kv.

Thickness ratio t_{Al}/t_{Ni}		Intensity ratio (I_{Al}/I_{Ni})			
		I_{111}/I_{200}	I_{111}/I_{311}	I_{220}/I_{200}	I_{220}/I_{311}
Al_1/Ni*	1.227	0.919	2.82	0.100	0.307
	2.025	1.706	4.128	0.322	0.780
	3.613	1.843	5.356	0.226	0.657
	4.05	2.313	7.056	0.474	1.446
	6.75	2.682	6.375	0.628	1.493
Al_2/Ni*	0.773	0.822	2.200	0.076	0.202
	1.275	1.187	2.713	0.188	0.430
	1.645	1.173	3.421	0.160	0.467
	4.25	4.579	9.889	0.714	1.541
Al_3/Ni*	0.6212	1.063	2.605	0.130	0.318
	1.025	1.319	-	0.225	-
	1.325	1.456	2.96	0.275	0.56
	2.05	2.527	4.733	0.481	0.9004
	3.417	2.873	5.693	0.464	0.919
Al_4/Ni*	0.530	0.620	1.707	0.102	0.282
	0.875	1.104	2.902	0.142	0.374
	1.13	1.251	3.128	0.168	0.420
	1.75	1.703	4.372	0.259	0.662
	2.917	2.012	6.296	0.313	0.978
Al_5/Ni*	0.379	0.789	2.378	0.0329	0.099
	0.625	0.977	2.020	0.131	0.270
	0.806	1.095	2.783	0.160	0.407
	1.25	-	4.367	-	0.455
	2.083	1.658	5.435	0.263	0.862

Table (5.25); The Intensity and Thickness Ratios of Aluminium-Nickel Specimens at 100kv.

Thickness ratio t_{Al}/t_{Ni}		Intensity ratio (I_{Al}/I_{Ni})			
		I_{111}/I_{200}	I_{111}/I_{311}	I_{220}/I_{200}	I_{220}/I_{311}
Al_1/Ni_*	1.227	0.919	3.225	0.115	0.404
	2.025	1.433	5.306	0.204	0.754
	2.613	1.626	6.599	0.307	1.244
	4.05	3.92	16.010	0.685	2.800
	6.75	3.427	11.040	0.891	2.869
Al_2/Ni_*	0.773	0.814	2.748	0.084	0.284
	1.275	1.886	7.378	0.297	1.16
	1.645	1.295	6.146	0.231	1.098
	4.25	3.387	10.719	0.488	1.544
Al_3/Ni_*	0.6212	0.777	1.862	0.0835	0.200
	1.025	1.283	3.406	0.149	0.397
	1.323	1.847	5.487	0.181	0.536
	2.05	2.775	6.768	0.355	0.866
	3.417	2.158	5.926	0.406	1.114
Al_4/Ni_*	0.530	0.923	2.133	-	-
	0.875	1.257	3.855	0.131	0.402
	1.13	0.761	2.154	0.162	0.458
	1.75	2.227	6.127	0.26	0.715
	2.917	2.797	8.006	0.349	0.998
Al_5/Ni_*	0.625	1.349	3.361	0.123	0.308
	0.806	1.324	4.013	0.141	0.428
	1.25	1.58	4.829	0.186	0.568
	2.08	2.055	5.996	0.263	0.767

Table (5.26); The Intensity and Thickness Ratios of Aluminium-Nickel Specimens at 400kv.

Thickness ratio t_{Al}/t_{Ni}		Intensity ratio (I_{Al}/I_{Ni})			
		I_{111}/I_{200}	I_{111}/I_{311}	I_{220}/I_{200}	I_{220}/I_{311}
Al_1/Ni_*	1.227	1.281	2.934	0.132	0.302
	2.025	1.65	4.25	0.334	0.861
	2.613	2.25	5.4	0.482	1.16
	4.05	3.05	10.02	0.705	2.32
	6.75	4.61	14.06	0.815	2.49
Al_2/Ni_*	0.773	1.09	2.087	0.102	0.196
	1.275	1.35	3.99	0.16	0.474
	1.645	1.364	3.39	0.162	0.404
	4.25	4.33	10.24	0.487	1.15
Al_3/Ni_*	0.6212	1.55	3.63	-	-
	1.025	1.55	3.33	0.161	0.345
	1.323	1.95	3.98	0.117	0.24
	2.05	2.79	9.01	0.394	1.27
	3.417	2.75	7.74	0.373	1.05
Al_4/Ni_*	0.530	0.831	1.77	-	-
	0.875	1.25	2.68	0.129	0.278
	1.13	1.49	3.28	0.172	0.38
	1.75	1.99	4.075	0.309	0.63
	2.917	2.85	6.74	0.298	0.706
Al_5/Ni_*	0.379	0.881	1.87	0.066	0.14
	0.625	1.14	2.49	0.074	0.161
	0.0806	2.03	3.41	0.16	0.268
	1.25	1.72	3.9	0.235	0.534

Table (5.27); The Intensity and Thickness Ratios of Aluminium-Nickel Specimens at 600kv.

Thickness ratio t_{Al}/t_{Ni}		Intensity ratio (I_{Al}/I_{Ni})			
		I_{111}/I_{200}	I_{111}/I_{311}	I_{220}/I_{200}	I_{220}/I_{311}
Al_1/Ni_*	1.227	0.7925	2.52	0.1786	0.568
	2.025	0.9954	2.702	0.2544	0.6907
	2.613	1.286	2.959	0.485	1.115
	4.05	2.82	9.044	0.759	2.434
	6.75	3.04	9.57	0.912	2.87
Al_2/Ni_*	0.773	0.829	2.02	0.112	0.274
	1.275	1.15	2.87	0.195	0.487
	1.645	1.50	4.33	0.26	0.75
	4.25	3.30	13.11	0.547	2.17
Al_3/Ni_*	0.6212	0.992	2.71	0.16	0.436
	1.025	1.40	3.46	0.233	0.575
	1.323	1.43	3.02	0.251	0.533
	2.05	2.29	6.14	0.46	1.23
	3.417	2.41	8.65	0.391	1.4
Al_4/Ni_*	0.530	0.712	1.39	0.09	0.172
	0.875	1.22	2.78	0.185	0.42
	1.13	1.174	2.65	0.158	0.36
	1.75	1.28	3.37	0.242	0.636
	2.917	1.09	3.28	0.206	0.621
Al_5/Ni_*	0.379	0.584	1.34	0.096	0.22
	0.625	0.975	2.58	0.157	0.416
	0.806	1.59	4.25	0.209	0.556
	1.25	2.464	4.73	0.356	0.682
	2.083	1.91	6.42	0.301	1.011

Table (5.28); The Intensity and Thickness Ratios of Aluminium-Nickel Specimens at 800kv.

Thickness ratio		Intensity ratio (I_{Al}/I_{Ni})			
	t_{Al}/t_{Ni}	I_{111}/I_{200}	I_{111}/I_{311}	I_{220}/I_{200}	I_{220}/I_{311}
Al_1/Ni_*	1.227	0.767	2.495	0.0622	0.2023
	2.025	1.932	5.73	0.421	1.247
	2.613	1.819	6.081	0.436	1.458
Al_2/Ni_*	0.773	0.678	2.600	0.0432	0.1654
	1.275	1.113	3.803	0.158	0.539
	1.645	1.404	4.056	0.2062	0.596
	4.25	3.313	-	0.469	-
Al_3/Ni_*	0.6212	1.043	2.659	-	-
	1.025	1.462	2.686	0.219	0.4023
	1.323	2.046	6.462	0.268	0.845
	2.05	1.522	5.198	0.318	1.085
	3.417	4.822	16.64	0.5455	1.883
Al_4/Ni_*	0.530	0.779	1.736	0.105	0.2333
	0.875	0.909	2.719	0.134	0.4011
	1.13	1.403	4.109	0.2013	0.5896
	1.75	2.282	5.659	0.261	0.647
	2.917	1.628	6.305	0.253	0.98
Al_5/Ni_*	0.379	0.742	1.929	-	-
	0.625	1.237	3.994	-	-

Table (5.29); The Intensity and Thickness Ratios of Aluminium-Nickel Specimens at 1000kv.

Thickness ratio t_{Al}/t_{Ni}		Intensity ratio (I_{Al}/I_{Ni})			
		I_{111}/I_{200}	I_{111}/I_{311}	I_{220}/I_{200}	I_{220}/I_{311}
Al_1/Ni_*	1.227	0.852	3.7	0.0752	0.327
	2.025	1.72	6.128	0.178	0.633
	2.613	1.23	3.801	0.145	0.449
	4.05	4.177	15.833	0.783	2.967
	6.75	0.672	2.361	0.0505	0.178
Al_2/Ni_*	1.275	1.31	3.539	0.1696	0.459
	1.645	1.521	4.44	0.179	0.523
	4.25	3.06	10.66	0.4176	1.455
Al_3/Ni_*	0.6212	0.728	2.286	0.0651	0.2044
	1.025	1.659	4.06	0.148	0.362
	1.323	1.953	4.387	0.2092	0.47
	2.05	1.373	4.005	0.217	0.632
	3.417	2.003	6.32	0.305	0.962
Al_4/Ni_*	0.530	1.02	2.985	0.0965	0.283
	0.875	1.014	3.475	0.1076	0.3687
	1.13	1.322	3.728	0.1357	0.3826
	1.75	2.132	8.22	0.2014	0.777
	2.917	2.061	7.047	0.204	0.698
Al_5/Ni_*	0.379	0.827	2.56	0.05	0.154
	0.625	0.9621	2.595	0.1124	0.3032
	0.806	1.341	3.84	0.1395	0.399
	1.25	1.781	4.993	0.188	0.527

5.6.3 The Intensity Ratio of Silver and Copper Combination.

In this combination, silver and copper were the materials forming the double-layered specimen. The silver was at the top of the specimen, and the intensity ratio was silver intensity to copper intensity at 400kv, 600kv and 800kv. The measurable diffraction rings for silver were (111) and (220) and for copper were (200) and (311). Then the intensity ratio was for (111/200), (111/311), (220/200) and (220/311) for different specimens thickness.

The following tables (5.30) through (5.32) give the intensity ratio for silver-copper specimens at 400kv, 600kv and 800kv respectively, and the thickness ratio of the specimen.

Table (5.30); Intensity and Thickness Ratios of Silver-Copper Specimens of 400kv.

Thickness ratio t_{Ag}/t_{Cu}	Intensity ratio (I_{Ag}/I_{Cu})			
	I_{111}/I_{200}	I_{111}/I_{311}	I_{220}/I_{200}	I_{220}/I_{311}
Ag_2/Cu_*				
0.546	5.56	34.27	1.142	7.036
0.814	4.44	33.42	1.13	8.486
Ag_3/Cu_*				
0.4091	4.04	8.86	0.765	1.677
0.6102	-	22.93	-	3.348
0.837	4.505	14.896	1.44	4.749
Ag_4/Cu_*				
0.3295	3.305	14.861	0.5201	2.339
0.492	3.961	15.625	0.539	2.125
0.674	2.749	12.86	0.368	1.72
0.879	-	23.197	-	4.905
1.21	-	57.155	-	12.718
Ag_5/Cu_*				
0.25	3.177	7.336	0.418	0.965
0.373	4.063	7.2	0.661	1.171
0.512	3.023	16.586	0.336	1.844
0.667	-	27.576	-	4.04

Table (5.31); Intensity and Thickness Ratios of Silver-Copper Specimens at 600kv.

Thickness ratio t_{Ag}/t_{Cu}		Intensity ratio (I_{Ag}/I_{Cu})			
		I_{111}/I_{200}	I_{111}/I_{311}	I_{220}/I_{200}	I_{220}/I_{311}
Ag_1/Cu_*	0.716	6.372	12.213	1.38	2.644
Ag_2/Cu_*	0.546	4.079	9.996	0.743	1.82
	0.814	6.856	18.92	0.892	2.461
	1.1163	7.084	28.29	1.401	5.596
	1.455	7.793	28.34	1.29	4.68
	2.00	-	56.60	-	12.83
Ag_3/Cu_*	0.4091	4.22	16.41	0.674	2.62
	0.6102	4.82	16.58	0.988	3.399
	0.837	4.72	22.70	0.675	3.25
	1.50	-	33.204	-	6.468
Ag_4/Cu_*	0.329	4.189	11.298	0.6167	1.663
	0.492	4.225	10.586	0.9304	2.331
	0.674	3.5388	7.0731	0.5467	1.0926
	0.879	7.31	15.726	1.6013	3.445
Ag_5/Cu_*	0.25	2.775	8.173	0.274	0.8065
	0.373	-	10.0904	-	1.225
	0.512	3.228	5.989	0.3109	0.5767
	0.667	4.5161	9.7222	0.536	1.154

Table (5.32); Intensity and Thickness Ratios of Silver-Copper Specimens at 800kv.

Thickness ratio t_{Ag}/t_{Cu}		Intensity ratio (I_{Ag}/I_{Cu})			
		I_{111}/I_{200}	I_{111}/I_{311}	I_{220}/I_{200}	I_{220}/I_{311}
Ag_1/Cu_*	0.716	-	8.028	-	2.03
	1.068	-	15.45	-	3.2325
	1.91	2.083	8.761	0.423	1.778
Ag_4/Cu_*	0.3295	3.8123	5.231	0.9593	1.316
	0.492	4.19	6.986	0.67	1.117
	0.674	3.084	6.31	0.733	1.5
	0.879	5.736	8.766	0.9614	1.47
	1.21	-	17.84	-	3.631
Ag_5/Cu_*	0.25	2.083	3.704	0.463	0.8227
	0.373	4.147	8.372	0.797	1.609
	0.512	2.660	4.730	0.6125	1.089
	0.667	2.863	5.511	0.794	1.528
	0.917	-	11.94	-	2.88

5.7 Summary

This Chapter has been divided into six sections which give all the experimental results determined throughout this work. In the intensity ratio section, some intensity ratios were missing for some specimens and that is due to the diffraction for such rings or specimens was not very good, so the microdensitometer could not trace them.

These results should be analysed for both single and composite specimens, Chapter Six presents the analysis of these results.

- CHAPTER SIX -

ANALYSIS OF THE RESULTS

6.1 Introduction.

For the analysis of the results of single specimens obtained in Chapter Five, equation (2.22) has been used to find (n)

$$\text{Log}\left[\frac{I_1}{I_2}\times\frac{d_2^2P_2}{d_1^2P_1}\right] = n\ \text{Log}\left[\frac{F_{e1}\bar{e}^{D}1}{F_{e2}\bar{e}^{D}2}\right] \qquad (6.1)$$

Where the subscript (1) relates to the (hkl) of the strongest line which was always (111) line, and the subscript (2) is for all the other possible (hkl) maxima in the electron diffraction pattern of the specimen which were (200), (220), (311) and (422). The last line (422), was only for silver and copper in the (silver-copper) combination.

For the double-layered specimens, equation (2.11) has been used first in order to find the k's ratio:

$$\frac{(I'_{hkl})_1}{(I'_{hkl})_2} = \frac{(k'_{hkl})_1}{(k'_{hkl})_2}\cdot\frac{t_1}{t_2} \qquad (6.2)$$

Equation (2.25) could be written as follows:

$$\text{Log}\left[\frac{(I'_{hkl})_1/(I'_{hkl})_2}{t_1/t_2}\times\frac{d_2P_2}{d_1P_1}\right] = n\ \text{Log}\left[\frac{F_{e1}\bar{e}^{D}1\ v_2}{F_{e2}\bar{e}^{D}2\ v_1}\right] \qquad (6.3)$$

Equation (6.3) was then used in order to find (n) which relates to which theory was operating. In the last two equations (6.2) and (6.3), the subscript (1) relates to the material at the top of the composite specimen, and the subscript (2) is for the material at the bottom of the specimen; all the symbols have the same meaning as mentioned in Chapter Two.

6.2 Analysis of Single Specimens.

This section presents the analysis of aluminium and copper in the (aluminium-copper) combination; aluminium and nickel in the (aluminium-nickel) combination; silver and copper in the (silver-copper) combination.

The $(F_e\, e^{-D})_{111}/(F_e\, e^{-D})_{hkl}$ ratio has been determined for all the materials, aluminium, copper, nickel and silver as shown in table (6.1).

Table (6.1); The Structure Factor and Debye-Waller Temperature Ratio.

Material	$\frac{(F_e e^{-D})_{111}}{(F_e e^{-D})_{200}}$	$\frac{(F_e e^{-D})_{111}}{(F_e e^{-D})_{220}}$	$\frac{(F_e e^{-D})_{111}}{(F_e e^{-D})_{311}}$	$\frac{(F_e e^{-D})_{111}}{(F_e e^{-D})_{422}}$
Al	1.230	2.030	2.600	-
Cu	1.143	1.640	1.980	3.754
Ni	1.150	1.660	2.070	-
Ag	1.124	1.610	1.975	3.876

To find which theory, dynamic or kinematic, was operating, (n) in equation (6.1) should be determined for each specimen in each combination at all voltages. To do so, a graph of $\log\left[\frac{I_1}{I_2}x\frac{d_2^2P_2}{d_1^2P_1}\right]$ versus $\log\left[\frac{F_{e1}e^{-D}1}{F_{e2}e^{-D}2}\right]$ should be drawn. The resultant graph should be a straight line of slope (n) whose value determines which of the two theories is operating, as has been explained in section (2.6) of Chapter Two.

The value of $\left[\frac{I_1}{I_2}x\frac{d_2^2P_2}{d_1^2P_2}\right]$ has been determined for each specimen in the three combinations of different voltages.

6.2.1 $\frac{I_{111}}{I_{hkl}}x\frac{(d^2P)_{hkl}}{(d^2P)_{111}}$ For Aluminium and for Copper in the (Aluminium-Copper) Combination.

This section presents four tables (6.2) through (6.5) showing the intensity ratio times d-spacing and the multiplicity ratio for aluminium and for copper at 80kv, 100kv, 500kv and 1000kv respectively.

Table (6.2); The Intensity Ratio Times d-spacing and the Multiplicity Ratio for Aluminium and for Copper at 80kv.

Specimen	Thickness	$\frac{I_{111}}{I_{200}} \times \frac{(d^2P)_{200}}{(d^2P)_{111}}$	$\frac{I_{111}}{I_{220}} \times \frac{(d^2P)_{220}}{(d^2P)_{111}}$	$\frac{I_{111}}{I_{311}} \times \frac{(d^2P)_{311}}{(d^2P)_{111}}$
Cu_1	600	1.495	2.158	4.170
Cu_2	490	1.181	2.057	2.820
Cu_3	400	1.181	1.940	2.800
Cu_4	290	1.245	2.330	3.098
Cu_5	200	1.21	2.260	3.36
Al_1	920	1.495	2.500	2.63
Al_2	720	1.06	1.910	2.69
Al_3	450	1.15	2.73	3.49
Al_4	330	1.24	2.92	4.96

Table (6.3); The Intensity Ratio Times d-spacing and the Multiplicity Ratio for Aluminium and for Copper at 100kv.

Specimen	Thickness	$\frac{I_{111}}{I_{200}} \times \frac{(d^2P)_{200}}{(d^2P)_{111}}$	$\frac{I_{111}}{I_{220}} \times \frac{(d^2P)_{220}}{(d^2P)_{111}}$	$\frac{I_{111}}{I_{311}} \times \frac{(d^2P)_{311}}{(d^2P)_{111}}$
Cu_1	600	0.993	2.890	5.73
Cu_2	490	1.210	2.220	3.395
Cu_3	400	1.390	2.470	4.096
Cu_4	290	1.530	2.650	4.540
Cu_5	200	1.27	2.410	4.611
Al_1	920	1.489	1.930	2.797
Al_2	720	1.460	2.690	4.53
Al_3	450	1.460	2.690	6.090
Al_4	330	2.100	5.35	9.26

Table (6.4); The Intensity Ratio Times d-spacing and the Multiplicity Ratio for Aluminium and for Copper at 500kv.

Specimen	Thickness	$\frac{I_{111}}{I_{200}} \times \frac{(d^2P)_{200}}{(d^2P)_{111}}$	$\frac{I_{111}}{I_{220}} \times \frac{(d^2P)_{220}}{(d^2P)_{111}}$	$\frac{I_{111}}{I_{311}} \times \frac{(d^2P)_{311}}{(d^2P)_{111}}$
Cu_1	600	1.164	2.65	4.11
Cu_2	490	0.994	2.23	2.73
Cu_3	400	0.965	2.37	3.24
Cu_4	290	1.144	2.63	3.74
Cu_5	200	0.935	2.57	4.598
Al_1	920	0.826	3.56	3.58
Al_2	720	1.11	3.46	4.43
Al_3	450	1.25	3.25	4.70
Al_4	330	1.53	4.58	5.82

Table (6.5); The Intensity Ratio Times d-spacing and the Multiplicity Ratio for Copper at 1000kv.

Specimen	Thickness	$\frac{I_{111}}{I_{200}} \times \frac{(d^2P)_{200}}{(d^2P)_{111}}$	$\frac{I_{111}}{I_{220}} \times \frac{(d^2P)_{220}}{(d^2P)_{111}}$	$\frac{I_{111}}{I_{311}} \times \frac{(d^2P)_{311}}{(d^2P)_{111}}$
Cu_1	600	1.38	2.35	4.68
Cu_2	490	1.27	2.03	3.49
Cu_3	400	1.24	2.36	2.96
Cu_5	200	1.22	3.22	5.65

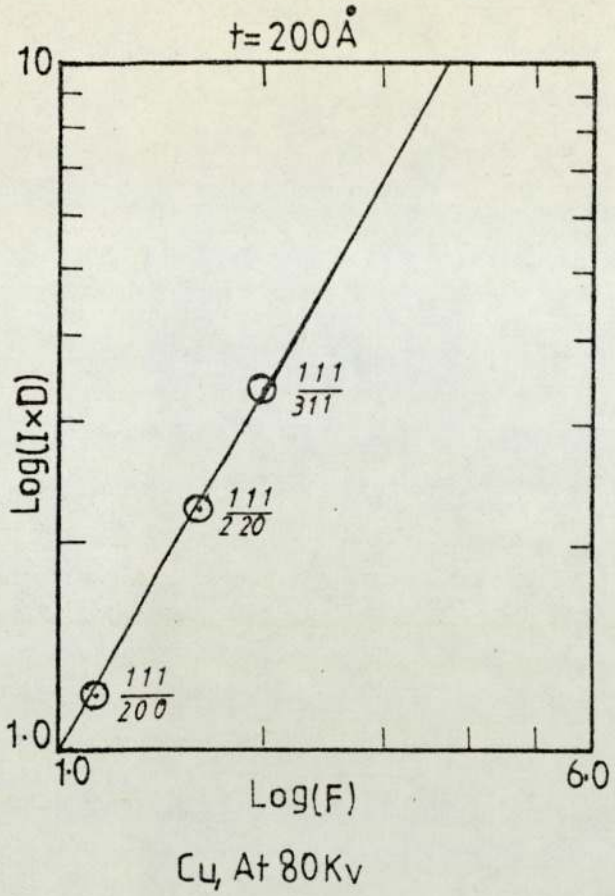

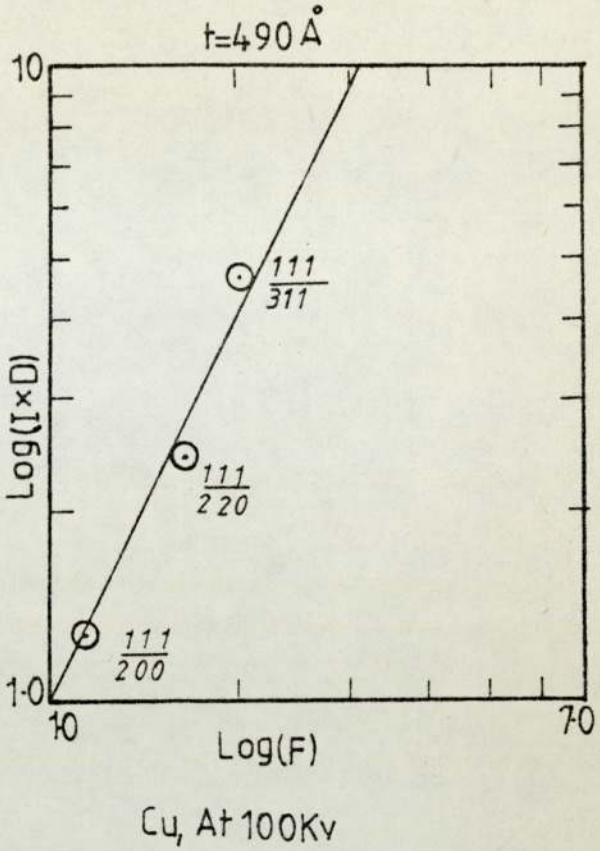

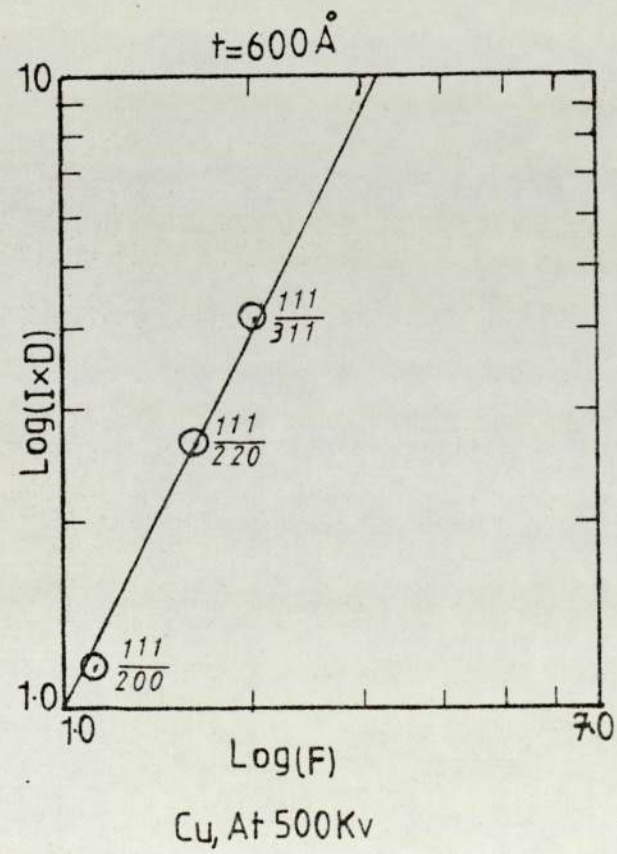

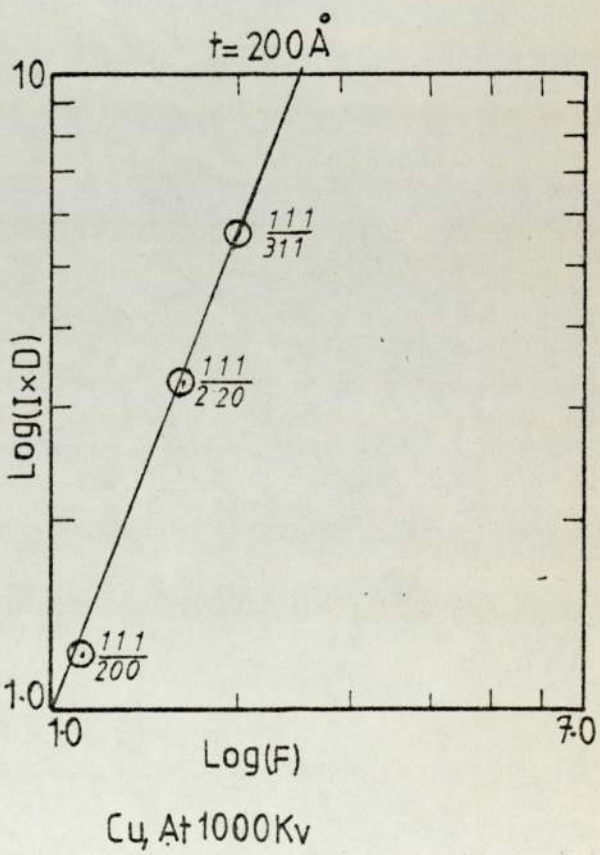

Fig. (6.1) Logarithmic plot of the intensity ratio times the interplanar spacing - the multiplicity ratio versus structure factor - Debye Waller temperature ratio for various thicknesses and voltages, for copper, (Aluminium-Copper).

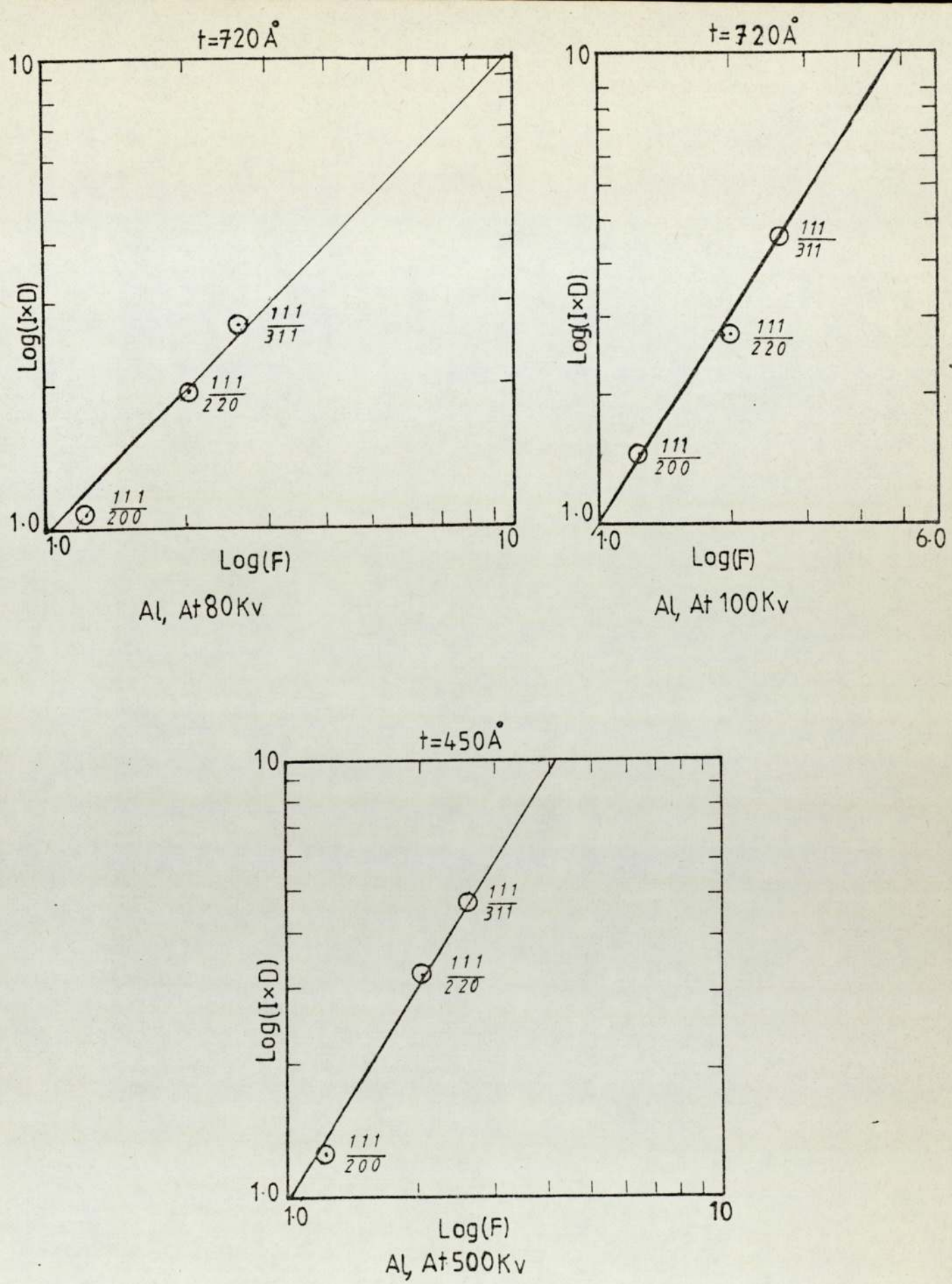

Fig. (6.2) Logarithmic plot of the intensity ratio times the interplanar spacing - the multiplicity ratio versus structure factor - Debye Waller temperature ratio for various thicknesses and voltages, for aluminium, (Aluminium-Copper).

From the data in table (6.1) and in table (6.2) through (6.5), graphs of log $\left[\frac{I_{111}}{I_{hkl}} \times \frac{(d^2P)_{hkl}}{(d^2P)_{111}}\right]$ versus log $\left[\frac{(F_e e^{-D})_{111}}{(F_e e^{-D})_{hkl}}\right]$ were drawn for all different specimens of aluminium and copper at different voltages. Figures (6.1) and (6.2) shows samples only of such graphs, where [I.D] represents $\left[\frac{I_{111}}{I_{hkl}} \times \frac{(d^2P)_{hkl}}{(d^2P)_{111}}\right]$ and (F) represents $\left[\frac{(F_e e^{-D})_{111}}{(F_e e^{-D})_{hkl}}\right]$. The slope of the resulting straight lines of all the graphs are listed in table (6.6).

Table (6.6); The Values of (n) for Aluminium and for Copper in (Aluminium-Copper) Combination at 80kv, 100kv, 500kv and 1000kv.

Specimen	n			
	80kv	100kv	500kv	1000kv
Cu_1	1.45	2.96	2.10	1.8
Cu_2	1.54	2.0	1.94	1.5
Cu_3	1.43	1.73	2.3	1.6
Cu_4	1.65	1.7	2.14	-
Cu_5	1.80	2.05	2.75	2.4
Al_1	0.824	0.73	2.34	-
Al_2	1.10	1.46	1.96	-
Al_3	1.63	1.6	1.62	-
Al_4	1.76	1.93	1.9	-

(6.2.2) $\frac{I_{111}}{I_{hkl}} \times \frac{(d^2P)_{hkl}}{(d^2P)_{111}}$ for Aluminium and for Nickel in the (Aluminium-Nickel) Combination.

This section presents tables (6.7) through (6.11) giving the values of the [I.D] ratio for aluminium and for nickel for different thicknesses at 80kv, 100kv, 400kv, 600kv and 800kv respectively.

Table (6.7); The [I.D] Ratio for Aluminium and for Nickel at 80kv.

Specimen	Thickness	$\frac{I_{111}}{I_{200}} \times \frac{(d^2P)_{200}}{(d^2P)_{111}}$	$\frac{I_{111}}{I_{220}} \times \frac{(d^2P)_{220}}{(d^2P)_{111}}$	$\frac{I_{111}}{I_{311}} \times \frac{(d^2P)_{311}}{(d^2P)_{111}}$
Ni_1	660	1.494	4.087	5.46
Al_1	810	0.901	2.554	3.33
Al_5	250	1.17	2.34	4.165

Table (6.8); The [I.D] Ratio for Aluminium and for Nickel at 100kv.

Specimen	Thickness	$\frac{I_{111}}{I_{200}} \times \frac{(d^2P)_{200}}{(d^2P)_{111}}$	$\frac{I_{111}}{I_{220}} \times \frac{(d^2P)_{220}}{(d^2P)_{111}}$	$\frac{I_{111}}{I_{311}} \times \frac{(d^2P)_{311}}{(d^2P)_{111}}$
Ni_1	660	1.55	4.3	5.24
Ni_2	400	1.44	4.99	6.85
Ni_3	310	1.77	5.22	6.67
Ni_4	200	1.83	4.72	7.43
Ni_5	120	1.7	4.93	6.8
Al_1	810	1.2	3.34	5.53
Al_1	510	1.57	3.55	6.34;
Al_2	410	1.64	3.72	5.73
Al_3	350	1.75	5.74	7.44
Al_4	250	1.09	3.03	5.34
Al_5				

Table (6.9); The [I.D] Ratio for Aluminium and for Nickel at 400kv.

Specimen	Thickness	$\frac{I_{111}}{I_{200}} \times \frac{(d^2P)_{200}}{(d^2P)_{111}}$	$\frac{I_{111}}{I_{220}} \times \frac{(d^2P)_{220}}{(d^2P)_{111}}$	$\frac{I_{111}}{I_{311}} \times \frac{(d^2P)_{311}}{(d^2P)_{111}}$
Ni_1	660	1.08	2.64	3.55
Ni_2	400	1.53	3.55	4.73
Ni_3	310	1.17	3.05	3.74
Ni_4	200	1.21	3.42	4.22
Ni_5	120	1.34	3.31	3.98
Al_1	810	1.12	2.51	3.4
Al_2	510	1.39	2.4	3.45
Al_3	410	1.62	2.34	3.72
Al_4	350	0.79	2.59	3.1
Al_5	250	1.42	3.33	6.49

Table (6.10); The [I.D] Ratio for Aluminium and for Nickel at 600kv.

Specimen	Thickness	$\frac{I_{111}}{I_{200}} \times \frac{(d^2P)_{200}}{(d^2P)_{111}}$	$\frac{I_{111}}{I_{220}} \times \frac{(d^2P)_{220}}{(d^2P)_{111}}$	$\frac{I_{111}}{I_{311}} \times \frac{(d^2P)_{311}}{(d^2P)_{111}}$
Ni_1	660	1.48	3.01	4.91
Ni_2	400	1.17	3.35	4.56
Ni_3	310	1.26	2.92	4.71
Ni_4	200	1.34	3.24	5.07
Ni_5	120	1.31	3.48	5.13
Al_1	810	1.08	2.23	3.48
Al_2	510	1.40	2.54	4.46
Al_3	410	1.39	2.5	5.12
Al_4	350	1.64	3.27	5.95

Table (6.11); The [I.D] Ratio for Aluminium and for Nickel at 800kv.

Specimen	Thickness	$\frac{I_{111}}{I_{200}} \times \frac{(d^2P)_{200}}{(d^2P)_{111}}$	$\frac{I_{111}}{I_{220}} \times \frac{(d^2P)_{220}}{(d^2P)_{111}}$	$\frac{I_{111}}{I_{311}} \times \frac{(d^2P)_{311}}{(d^2P)_{111}}$
Ni_1	660	1.67	4.39	5.88
Ni_2	400	1.93	4.28	5.43
Ni_3	310	1.91	3.68	5.57
Ni_4	200	1.57	6.10	6.87
Ni_5	120	1.54	3.92	5.56
Al_1	810	0.96	2.25	4.03
Al_2	510	1.30	2.73	3.83

From the data of aluminium and nickel in table (6.1) and in tables (6.7) through (6.11) graphs of log $\left[\frac{I_{111}}{I_{hkl}} \times \frac{(d^2P)_{hkl}}{(d^2P)_{111}}\right]$ versus log $\left[\frac{(F_e e^{-D})_{111}}{(F_e e^{-D})_{hkl}}\right]$ were drawn for all different specimens of aluminium and nickel at different voltages.

Figures (6.3) and (6.4) show samples of such graphs. The slopes of the resulting straight lines of all the graphs are listed in table (6.12).

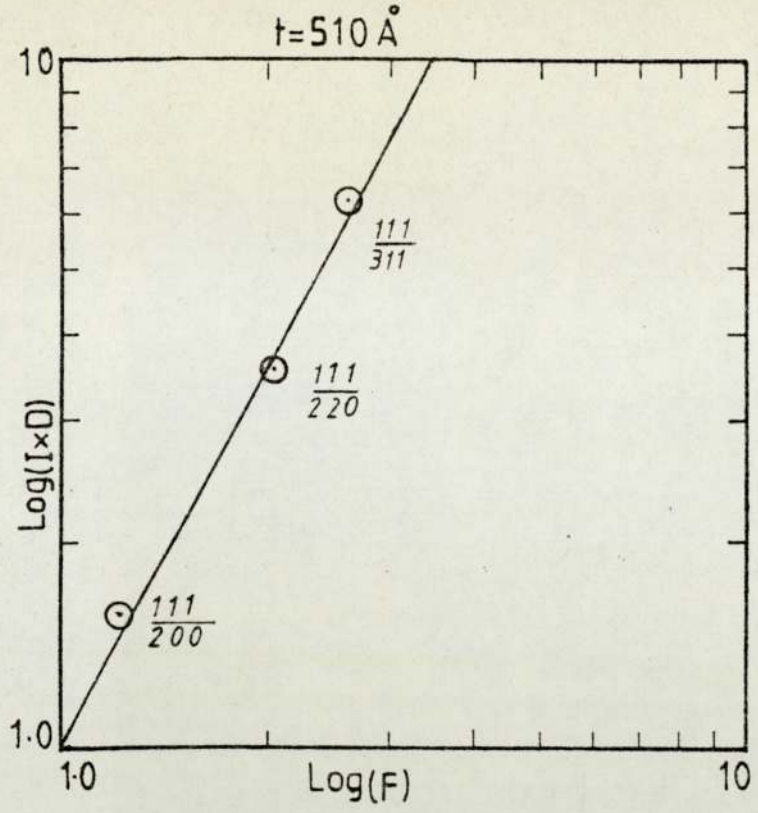

Al, At 100Kv

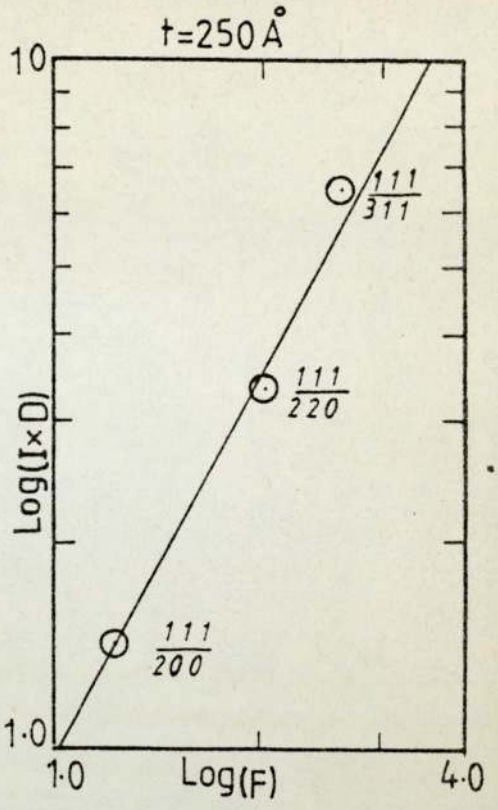

Al, At 400Kv

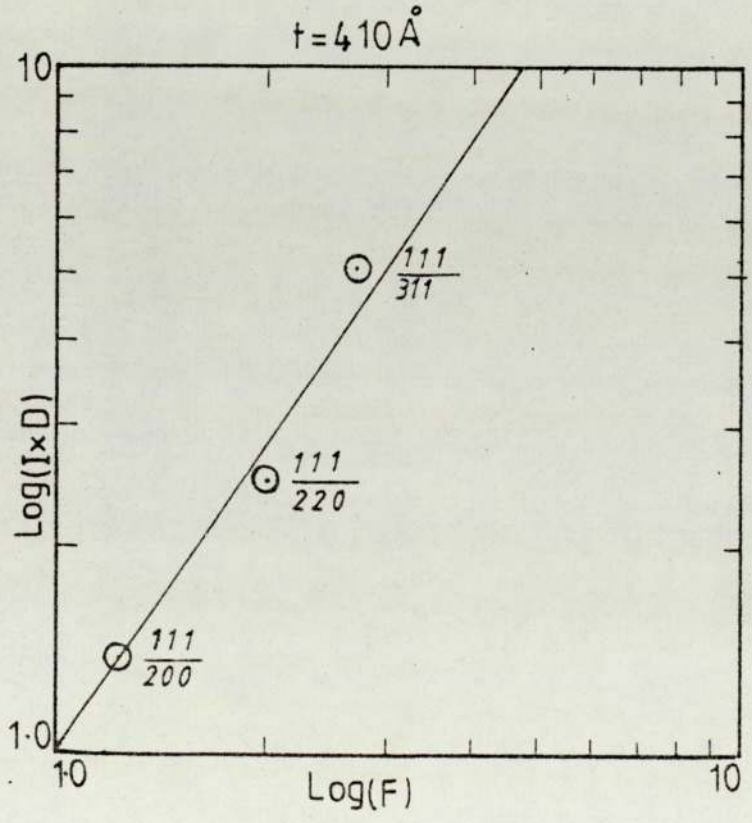

Al, At 600Kv

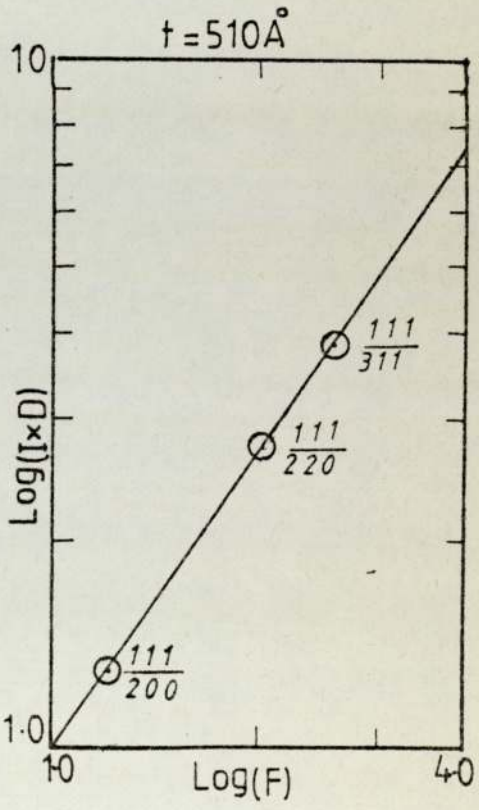

Al, At 800Kv

Fig. (6.3) Logarithmic plot of the intensity ratio times the interplanar spacing - the multiplicity ratio versus structure factor - Debye Waller temperature ratio for various thicknesses and voltages, for aluminium, (Aluminium-Nickel).

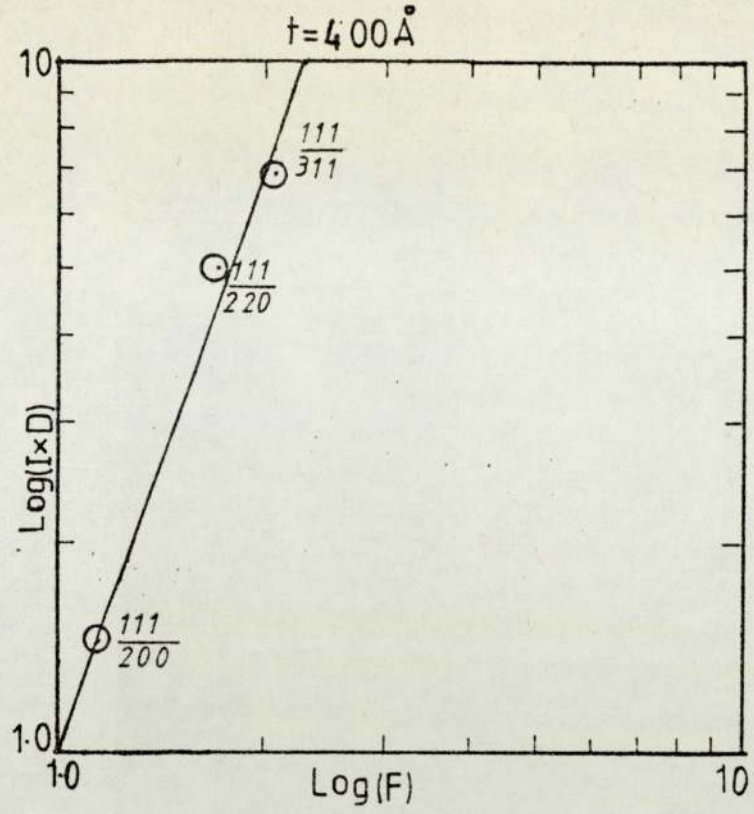

Ni, At 100Kv

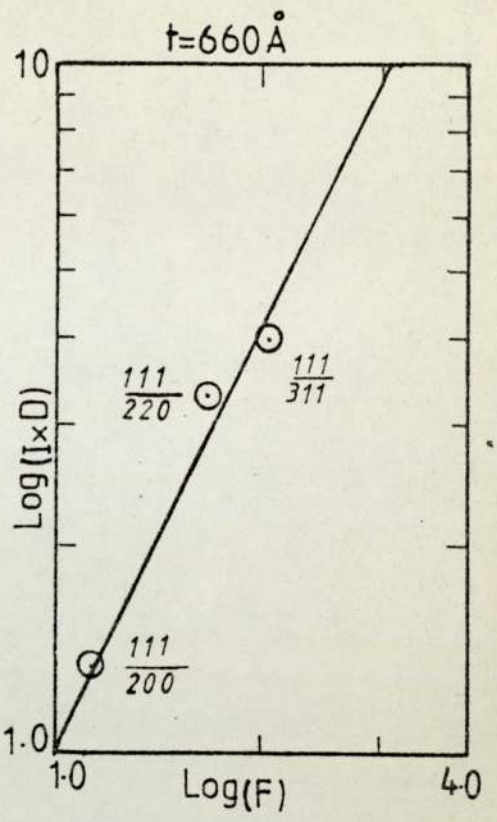

Ni, At 400Kv

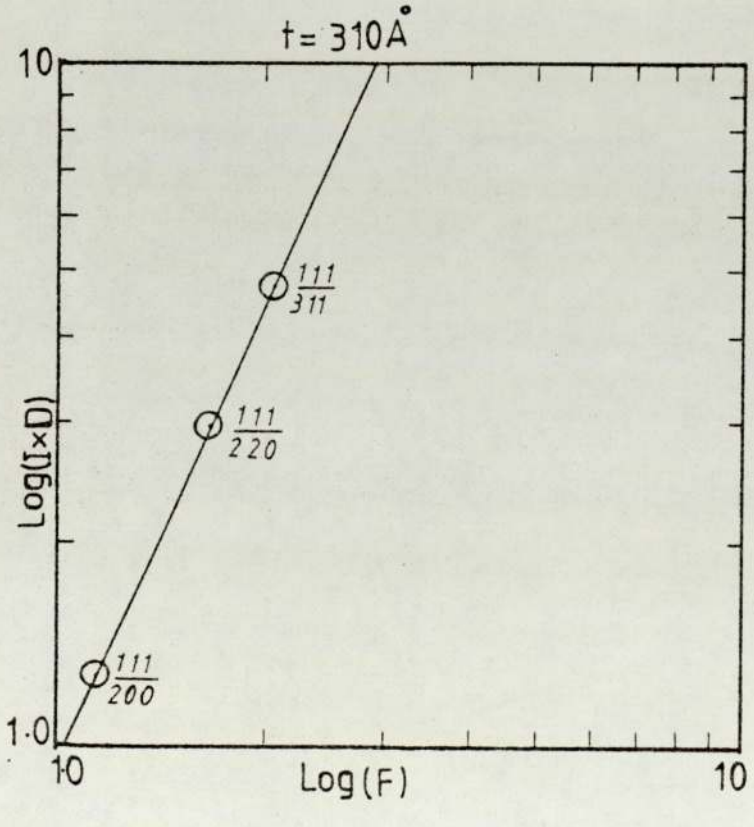

Ni, At 600Kv

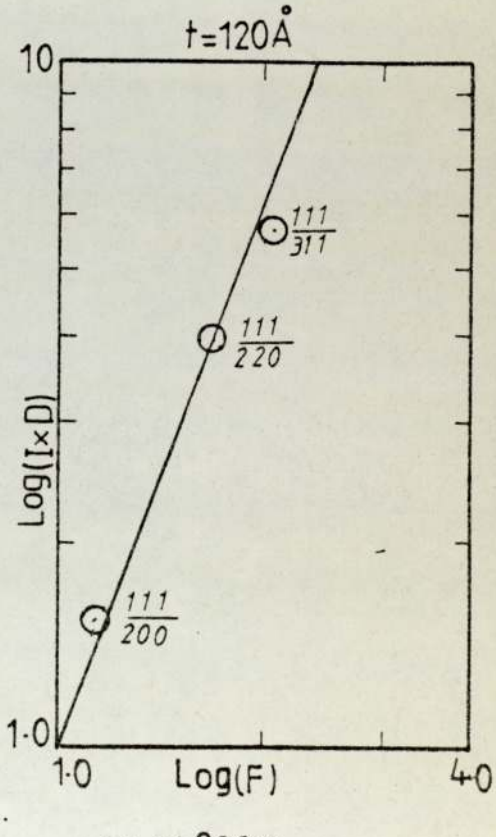

Ni, At 800Kv

Fig. (6.4) Logarithmic plot of the intensity ratio times the interplanar spacing - the multiplicity ratio versus structure factor - Debye Waller temperature ratio for various thicknesses and voltages, for nickel, (Aluminium-Nickel).

Table (6.12); The Values of (n) for Aluminium and for Nickel in the (Aluminium-Nickel) Combination at 80kv, 100kv, 400kv, 600kv and 800kv.

Specimen	n				
	80kv	100kv	400kv	600kv	800kv
Ni_1	2.35	2.14	2.17	2.002	2.32
Ni_2	-	2.8	2.03	2.49	1.88
Ni_3	-	2.44	2.15	2.24	1.83
Ni_4	-	2.43	2.42	2.26	2.85
Ni_5	-	2.56	2.05	2.4	2.600
Al_1	1.85	2.04	1.52	1.5	1.8
Al_2	-	1.8	1.2	1.4	1.86
Al_3	-	1.63	0.964	1.5	-
Al_4	-	2.11	1.97	1.5	-
Al_5	1.5	2.07	1.83	-	-

(6.2.3) $\frac{I_{111}}{I_{hkl}} x \frac{(d^2P)_{hkl}}{(d^2P)_{111}}$ for Silver and for Copper in the (Silver-Copper) Combination.

This section shows three tables (6.13), (6.14) and (6.15) giving the values of the [I.D] Ratios for silver and for copper for different thicknesses at 400kv, 600kv and 800kv respectively.

Table (6.13); The intensity ratio times interplanar spacing-multiplicity ratio for silver and for copper at 600kv.

Specimen	Thickness	$\frac{I_{111}}{I_{200}} \times \frac{(d^2P)_{200}}{(d^2P)_{111}}$	$\frac{I_{111}}{I_{220}} \times \frac{(d^2P)_{220}}{(d^2P)_{111}}$	$\frac{I_{111}}{I_{311}} \times \frac{(d^2P)_{311}}{(d^2P)_{111}}$	$\frac{I_{111}}{I_{422}} \times \frac{(d^2P)_{422}}{(d^2P)_{111}}$
Cu_1	880	1.352	1.996	3.24	-
Cu_2	590	1.08	2.27	2.58	-
Cu_3	430	1.62	3.34	4.17	-
Cu_4	330	1.58	2.89	3.8	-
Cu_5	240	1.68	2.12	3.35	-
Ag_1	630	0.93	1.97	2.97	9.13
Ag_2	480	1.35	3.07	3.06	12.7
Ag_3	360	1.39	2.75	2.85	20.2
Ag_5	220	1.23	2.05	2.76	10.13

Table (6.14); The intensity ratio times interplanar spacing-multiplicity ratio for silver and for copper at 800kv.

Specimen	Thickness	$\frac{I_{111}}{I_{200}} \times \frac{(d^2P)_{200}}{(d^2P)_{111}}$	$\frac{I_{111}}{I_{220}} \times \frac{(d^2P)_{220}}{(d^2P)_{111}}$	$\frac{I_{111}}{I_{311}} \times \frac{(d^2P)_{311}}{(d^2P)_{111}}$	$\frac{I_{111}}{I_{422}} \times \frac{(d^2P)_{422}}{(d^2P)_{111}}$
Cu_1	880	1.224	2.19	3.035	6.63
Cu_2	590	1.56	2.87	4.15	18.6
Cu_3	430	0.94	2.7	2.65	9.26
Cu_4	330	1.47	2.33	3.63	15.92
Ag_1	630	1.11	2.37	2.39	8.54
Ag_2	480	1.36	3.79	3.7	8.72
Ag_3	360	1.03	1.98	2.67	8.69
Ag_4	290	0.645	3.43	2.17	15.35
Ag_5	220	1.28	2.73	3.472	16.11

Table 6.15); The values of (n) for silver and for copper in silver-copper combinations 400kv, 600kv and 800kv.

Specimen	Thickness	$\frac{I_{111}}{I_{200}} \times \frac{(d^2P)_{200}}{(d^2P)_{111}}$	$\frac{I_{111}}{I_{220}} \times \frac{(d^2P)_{220}}{(d^2P)_{111}}$	$\frac{I_{111}}{I_{311}} \times \frac{(d^2P)_{311}}{(d^2P)_{111}}$	$\frac{I_{111}}{I_{422}} \times \frac{(d^2P)_{422}}{(d^2P)_{111}}$
Cu_1	880	1.2	2.8	-	11.14
Cu_2	590	1.21	2.78	-	8.29
Cu_4	330	1.3	4.06	7.82	-
Ag_2	480	0.88	2.37	2.4	-
Ag_3	360	0.88	2.67	2.8	-
Ag_4	290	1.23	2.87	3.41	-

From the data of silver and copper in table (6.1) and tables (6.13) through (6.15), graphs of log $\left[\frac{I_{111}}{I_{hkl}} \times \frac{(d^2P)_{hkl}}{(d^2P)_{111}}\right]$ versus log $\left[\frac{(F_e e^{-D})_{111}}{(F_e e^{-D})_{hkl}}\right]$ were drawn for all different specimens of silver and copper at different voltages.

Figures (6.5) and (6.6) are samples of such graphs. The slopes of the resulting straight lines of all the graphs are listed in table (6.16).

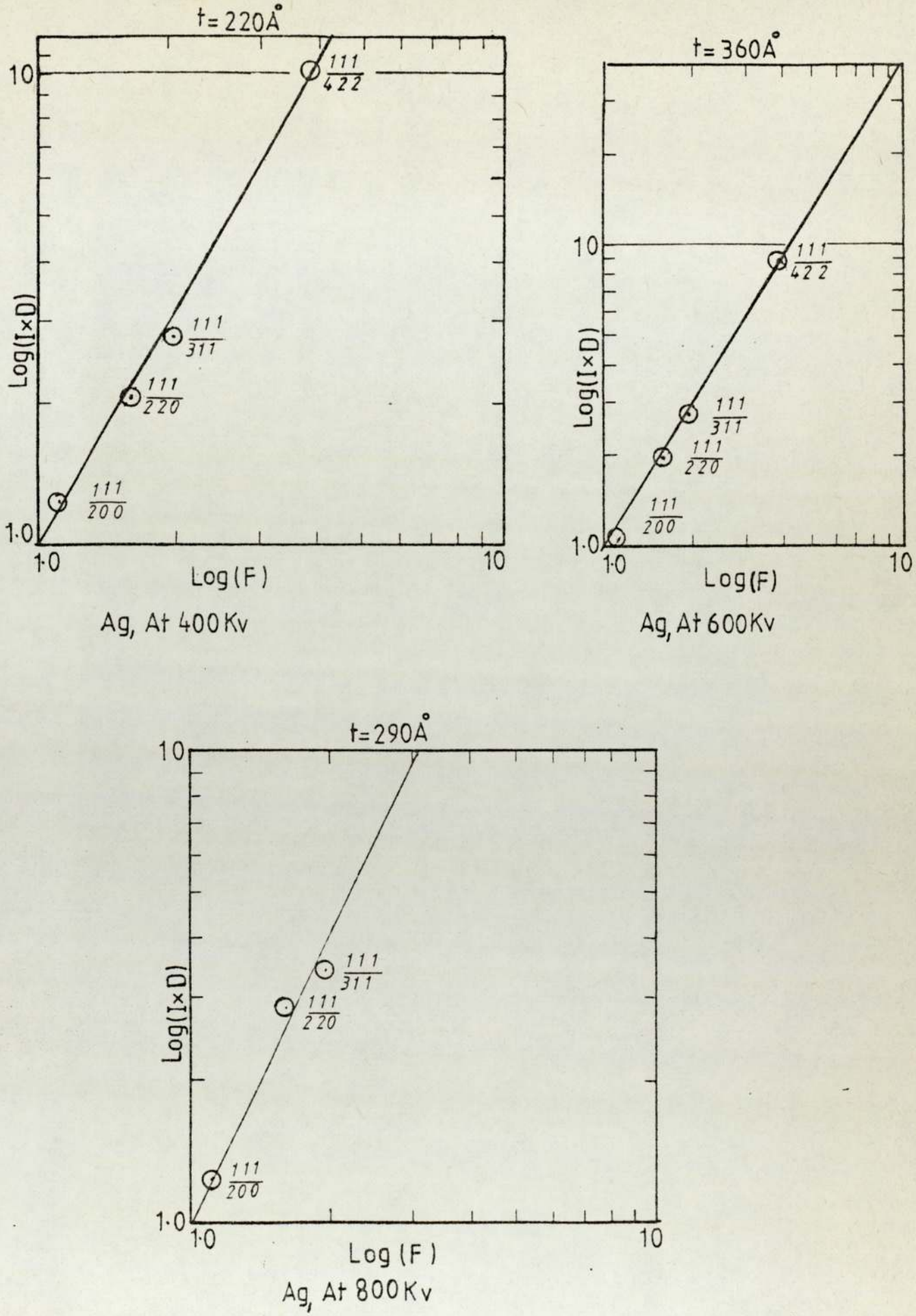

Fig. (6.5) Logarithmic plot of the intensity ratio times the interplanar spacing - the multiplicity ratio versus structure factor - Debye Waller temperature ratio for various thicknesses and voltages, for silver, (Silver-Copper).

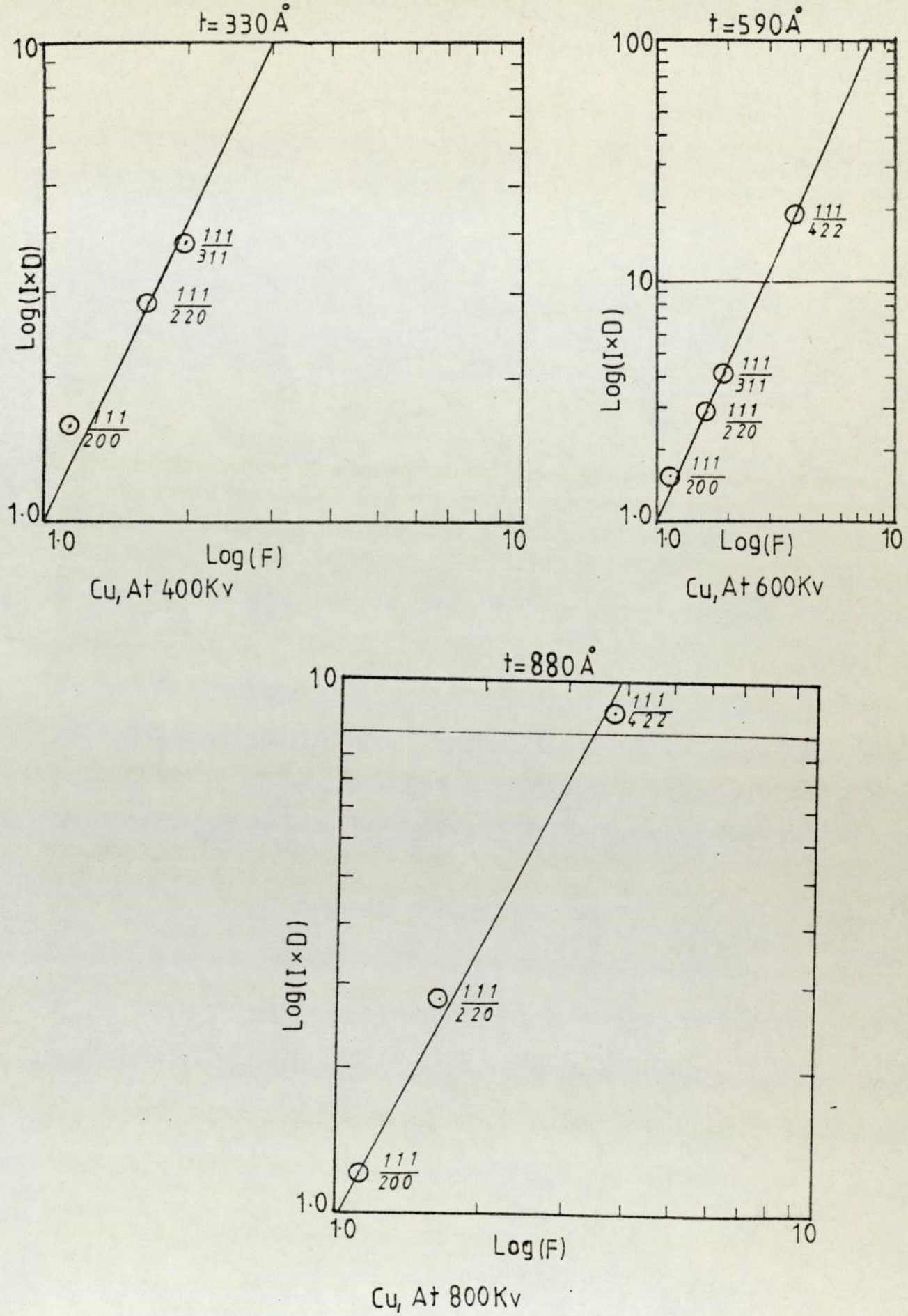

Fig. (6.6) Logarithmic plot of the intensity ratio times the interplanar spacing - the multiplicity ratio versus structure factor - Debye Waller temperature ratio for various thicknesses and voltages, for copper, (Silver-Copper).

Table (6.16); The Values of (n) for Silver and for Copper in the (Silver-Copper) Combination at 400kv, 600kv and 800kv.

Specimen	n		
	400kv	600kv	800kv
Cu_1	1.33	1.4	1.6
Cu_2	1.76	2.2	1.77
Cu_3	1.79	1.88	-
Cu_4	2.06	1.65	3.23
Cu_5	0.987	-	-
Ag_1	1.79	1.64	-
Ag_2	1.84	1.84	2.17
Ag_3	1.89	1.62	2.58
Ag_4	-	2.5	2.06
Ag_5	1.78	2.04	-

6.3 Analysis of Double-Layered Specimens.

The analysis of double-layered specimens with reference to equations (6.2) and (6.3) is presented here for aluminium-Copper specimens of different thickness ratios at 80kv, 100kv, 500kv and 1000kv. Also for aluminium-nickel specimens of different thickness ratios at 80kv, 100kv, 400kv, 600kv, 800kv and 1000kv. And finally for silver-copper specimens of different thickness ratios at 400kv, 600kv and 800kv.

6.3.1 Analysis of Double-Layered Specimens of Aluminium and Copper.

In equations (6.2) and (6.3), the subscripts (1) and (2) stand for aluminium and copper respectively.

In this combination, as mentioned in Chapter Five, the crystallographic orientations which gave measurable diffraction pattern intensities, were Al_{111}, Al_{220}, Al_{311}, Cu_{200}, Cu_{220} and Cu_{311}; so that the ratio of the relative integrated intensities of aluminium to that of copper were taken for (111/200), (111/220), (111/311), (220/200), (220/220), (220/311), (311/200), (311/220) and (311/311).

By using equation (6.2) each of these ratios was plotted against the thickness ratio, (t_1/t_2), of the films in the specimen of 80kv, 100kv, 500kv and 1000kv. The best straight line was drawn through the points in order to find the slope $(k'_{hkl})_{Al}/(k'_{hkl})_{Cu}$ as shown in the sample figures (6.7) through (6.10).

The slope of each line represents the term $[(I'_{hkl})_{Al}/(I'_{hkl})_{Cu}]/(t_{Al}/t_{Cu})$ in equation (6.3). This was then multiplied by $(d_{hkl}.P_{hkl})_{Cu}/(d_{hkl}.P_{hkl})_{Al}$ and the values of $\{[F_e\bar{e}^{D})_{hkl}]_{Al}.v_{Cu}\}/\{[F_e\bar{e}^{D})_{hkl}]_{Cu}.v_{Al}\} = A$ and $\{\frac{(I'_{hkl})_{Al}/(I'_{hkl})_{Cu}}{t_{Al}/t_{Cu}} x \frac{(d_{hkl}P_{hkl})_{Cu}}{(d_{hkl}P_{hkl})_{Al}}\}$ = SB of equation (6.3) were listed in table (6.17) for voltages 80kv, 100kv, 500kv and 1000kv and for the above mentioned ratios.

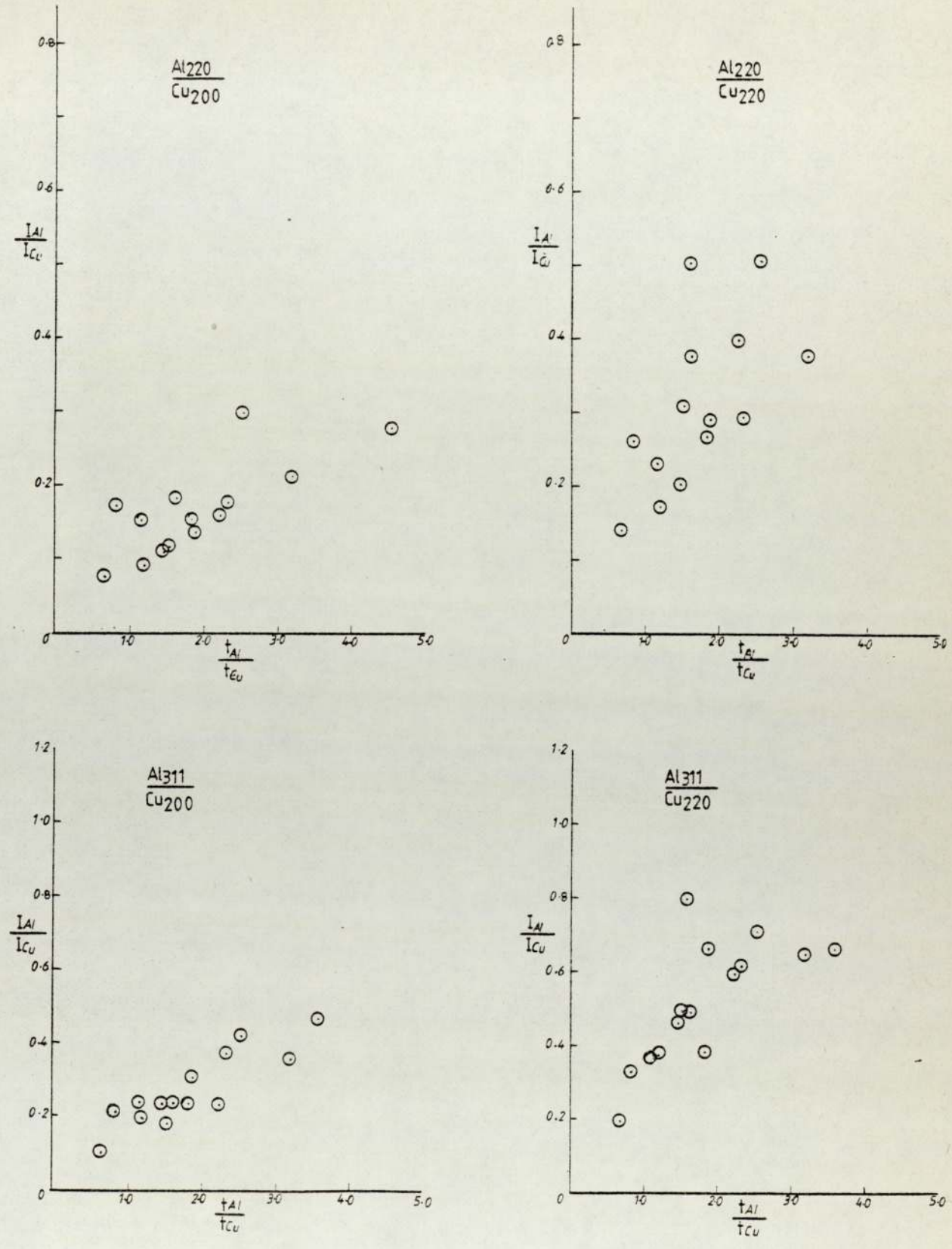

Fig. (6.7) Intensity ratio versus thickness ratio for aluminium-copper combination at 80kv.

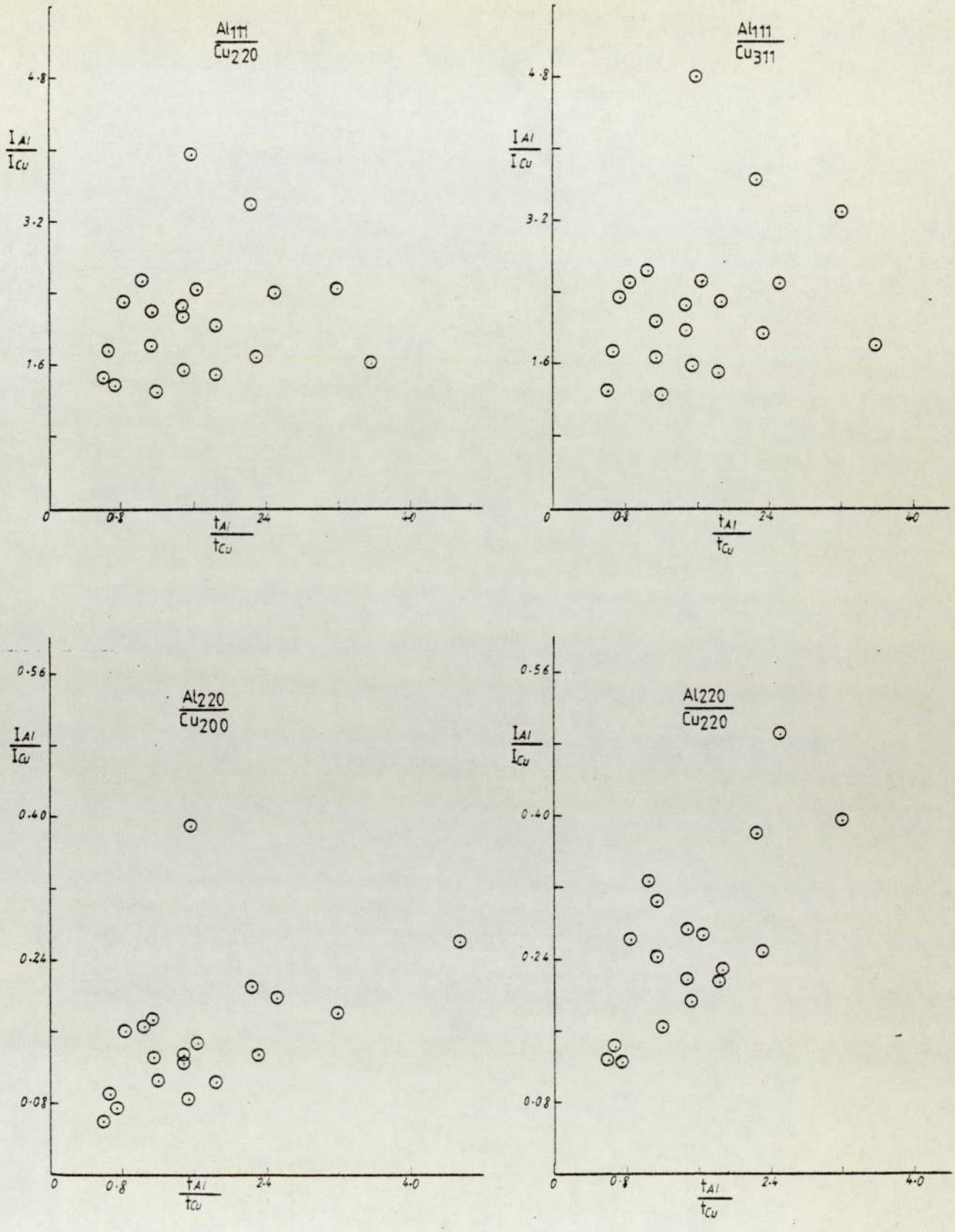

Fig. (6.8) Intensity ratio versus thickness ratio for aluminium-copper combination at 100kv.

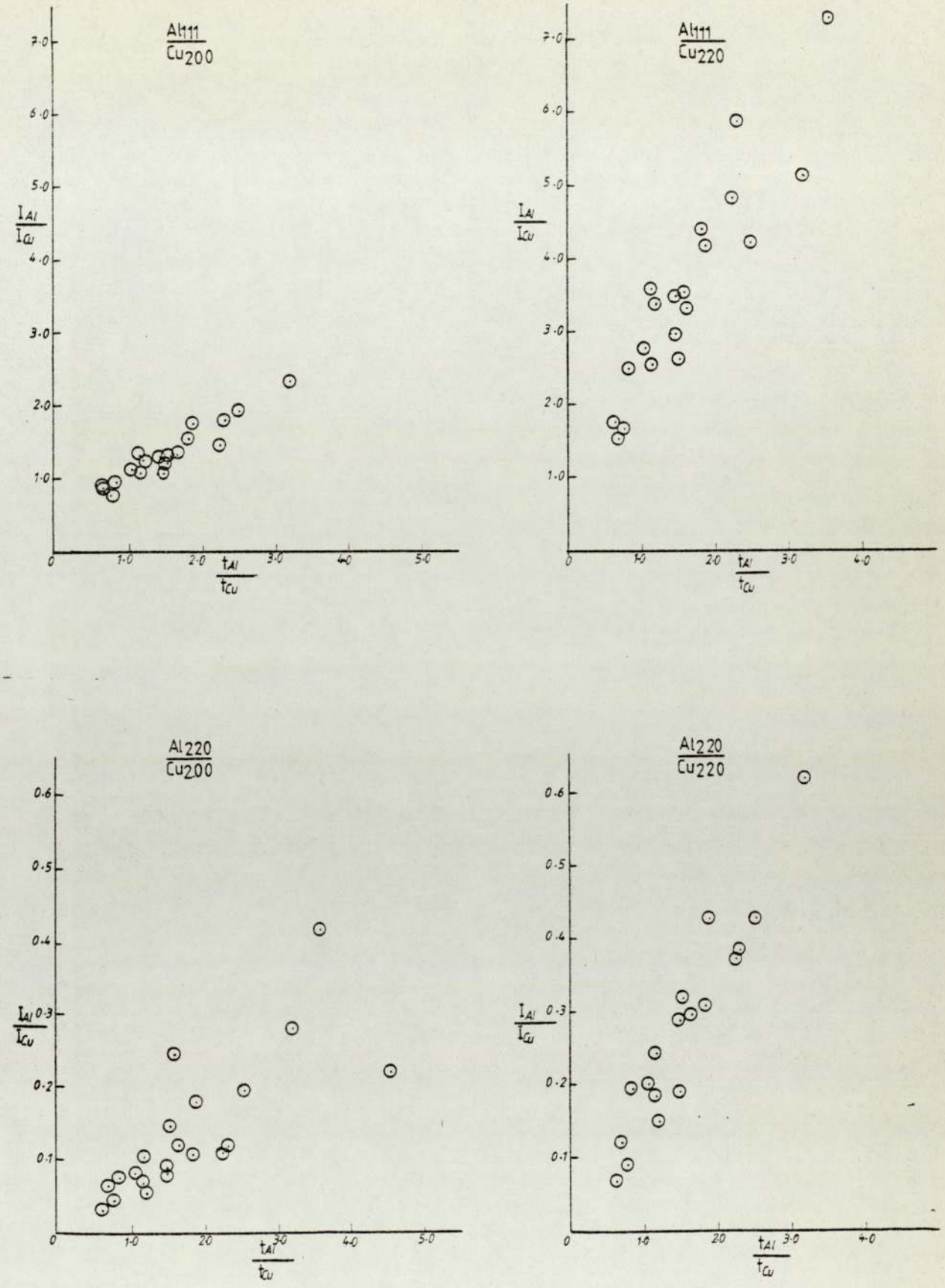

Fig. (6.9) Intensity ratio versus thickness ratio for aluminium-copper combination at 500kv.

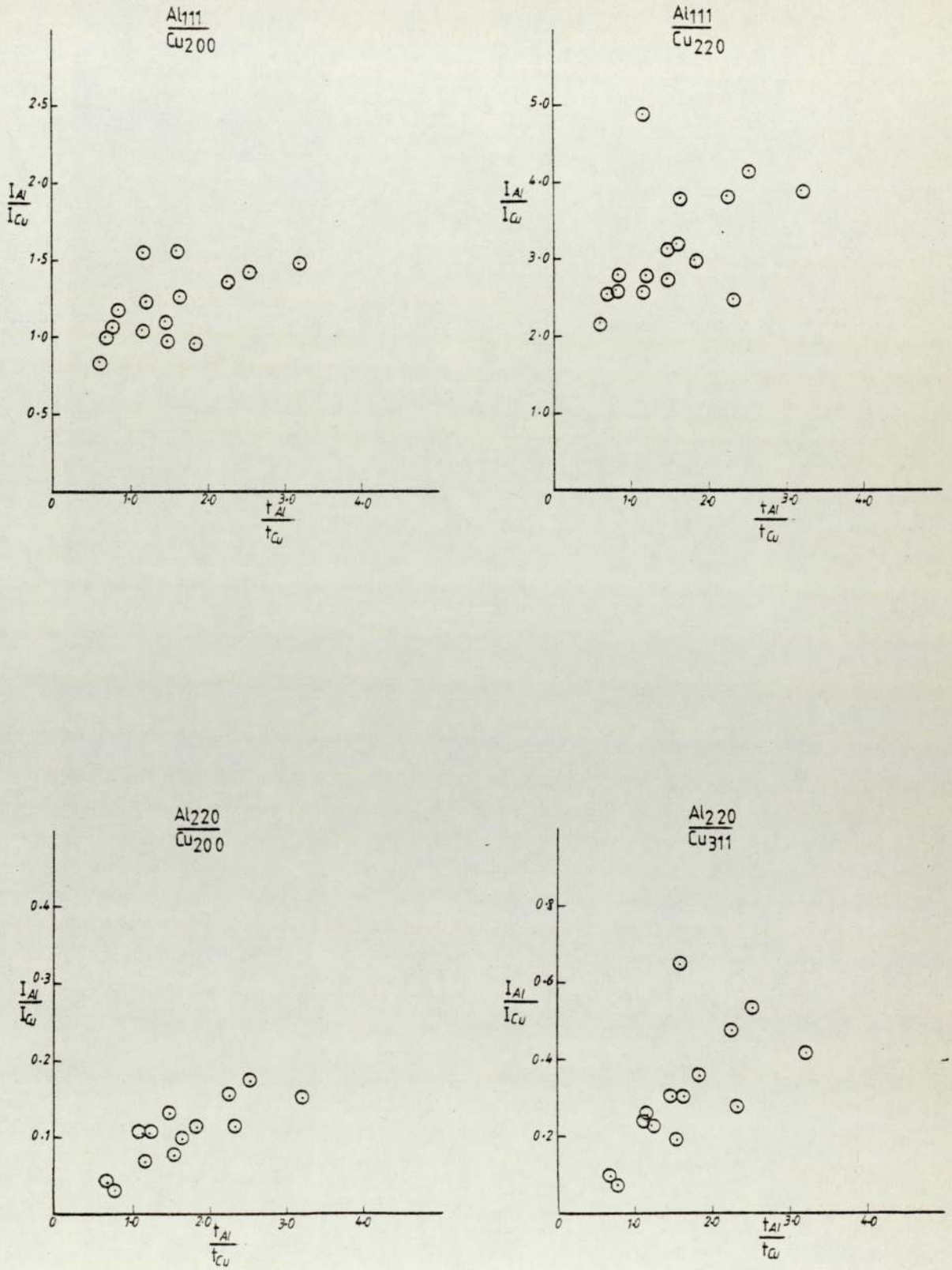

Fig. (6.10) Intensity ratio versus thickness ratio for aluminium-copper combination at 1000kv.

Table (6.17); The (A) and (SxB) Values for Aluminium-Copper Combination at different voltages.

Al_{hkl}/Cu_{hkl}	A	S x B			
		80kv	100kv	500kv	1000kv
111/200	0.576	0.4414	0.479	0.539	0.528
111/220	0.830	1.146	1.237	1.842	1.933
111/311	0.999	2.116	2.299	3.341	3.32
220/200	0.283	0.064	0.066	0.048	0.047
220/220	0.408	0.169	0.171	0.164	0.169
220/311	0.492	0.306	0.318	0.304	0.288
311/200	0.221	0.056	0.051	0.0501	0.038
311/220	0.318	0.149	0.129	0.155	0.137
311/311	0.383	0.271	0.244	0.308	0.235

The values of (SxB) and (A) as given in table (6.17) were plotted as graphs for all (Al_{hkl}/Cu_{hkl}) ratios and voltages. The resulting graphs are shown in figure (6.11). These are striaght lines whose slope (n) was calculated for each case and its values are found to be 2.4, 2.6, 3.00 and 3.07 corresponding to 80kv, 100kv, 500kv and 1000kv respectively. The average value of (n) was found to be = 2.77 ∓ 0.265.

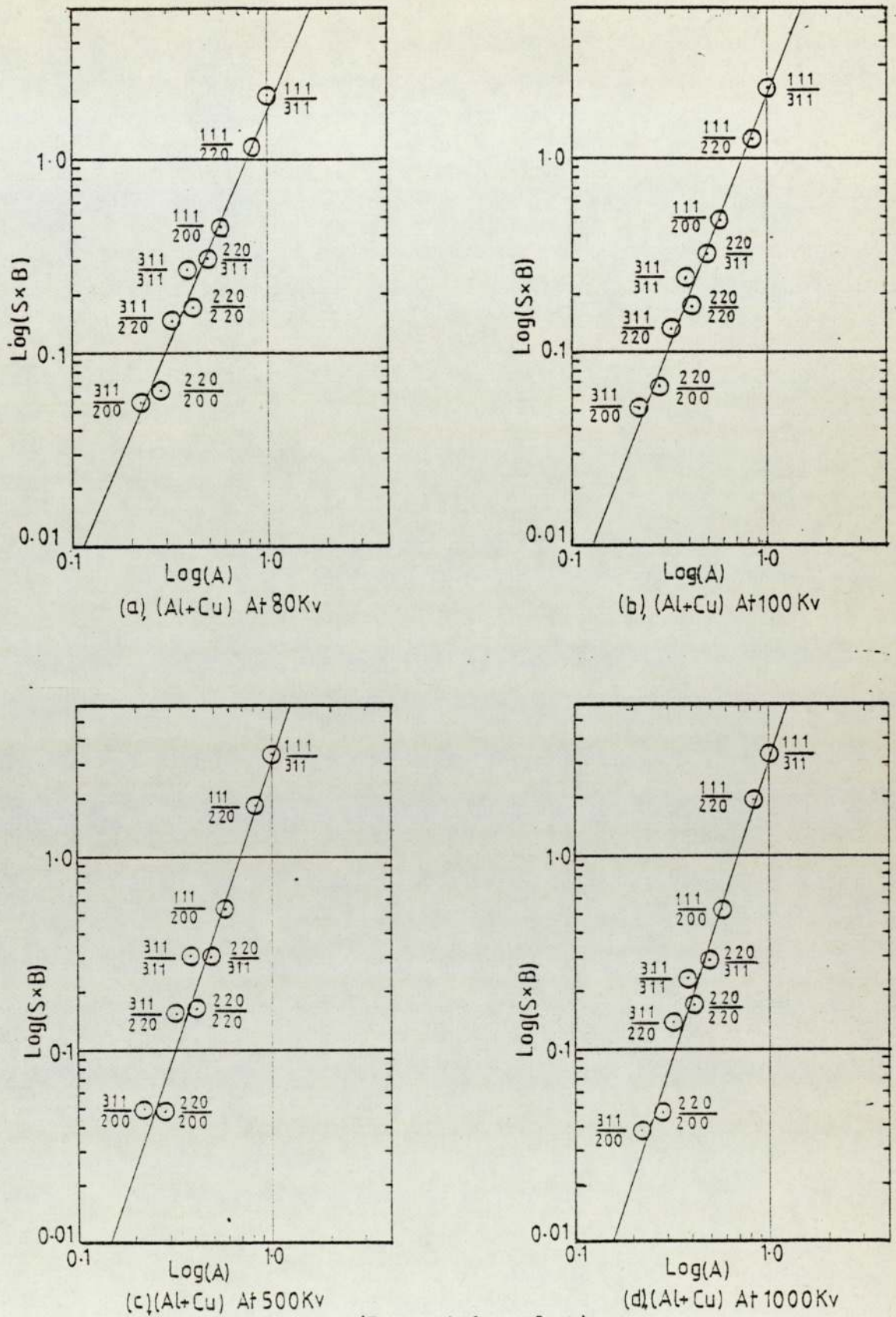

(Logarithm plot)

Fig. (6.11) $\left\{\frac{(I'_{hkl})_{Al}/(I'_{hkl})_{Cu}}{t_{Al}/t_{Cu}} \times \frac{(d_{hkl}P_{hkl})_{Cu}}{(d_{hkl}P_{hkl})_{Al}}\right\} = \frac{\left[(F_e e^{-D})_{hkl}\right]_{Al} \cdot v_{Cu}}{\left[(F_e e^{-D})_{hkl}\right]_{Cu} \cdot v_{Al}}$ = S.B versus A for various voltages.

6.3.2 Analysis of Double-Layered Specimens of Aluminium and Nickel.

In equations (6.2) and (6.3) the subscript (1) stands for aluminium and the subscript (2) stands for nickel.

In this combination, as mentioned in Chapter Five the crystallographic orientation which gave measurable diffraction pattern intensities were, Al_{111}, Al_{220}, Ni_{200} and Ni_{311}, so the ratio of the relative integrated intensities of aluminium to that of nickel were for (111/200), (111/311), (220/200) and (220/311). By using equation (6.2) each of these ratios was plotted against the thickness ratio of the two films in the specimen at 80kv, 100kv, 400kv, 600kv, 800kv and 1000kv. The best straight line was drawn through the points in order to find the slope $(k'_{hkl})_{Al}/(k'_{hkl})_{Ni}$ as shown in the sample figures (6.12) and (6.13).

The same procedure was then followed as in section (6.3.1) to plot (SxB) versus (A), listed in table (6.18), as shown in the graphs of figures (6.14) and (6.15).

Table (6.18); The (A) and (SxB) Values for Aluminium-Nickel Combination at different voltages.

$\frac{Al_{hkl}}{Ni_{hkl}}$	$\frac{[(F_e e^{-D})_{hkl}]_{Al} v_{Ni}}{[(F_e e^{-D})_{hkl}]_{Ni} v_{Al}}$	$\frac{(I'_{hkl})_{Al}/(I'_{hkl})_{Ni}}{t_{Al}/t_{Ni}} \times \frac{(d_{hkl}P_{hkl})_{Ni}}{(d_{hkl}P_{hkl})_{Al}} = (SxB)$					
		80kv	100kv	400kv	600kv	800kv	1000kv
111/200	0.545	0.578	0.63	0.752	0.593	0.6376	0.625
111/311	0.978	3.67	4.63	4.17	3.71	4.7	4.597
220/200	0.268	0.092	0.087	0.091	0.11	0.0899	0.0725
220/311	0.480	0.541	0.67	0.515	0.699	0.6503	0.5362

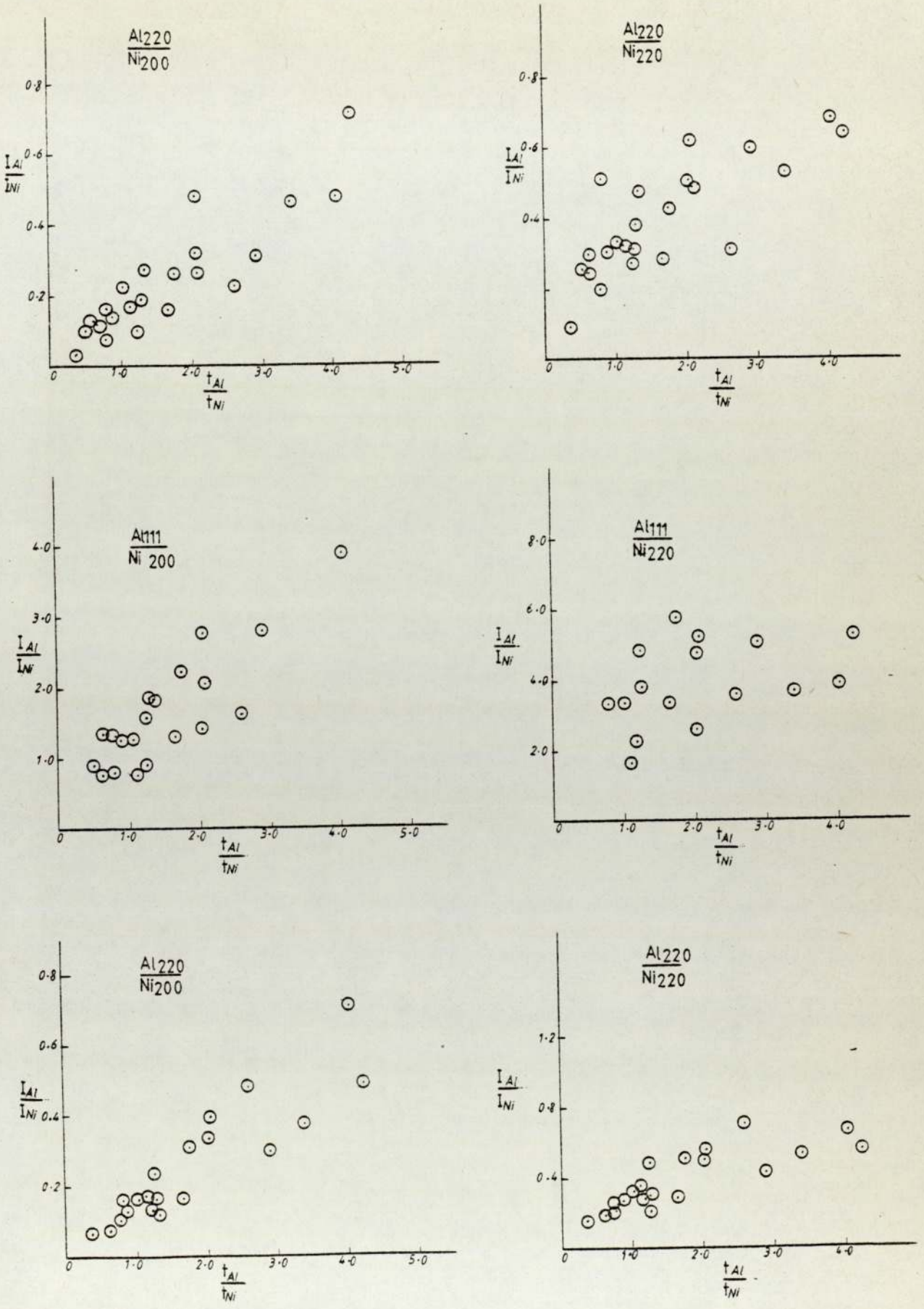

Fig. (6.12) Intensity ratio versus thickness ratio for aluminium-nickel combination at 80kv, 100kv and 400kv.

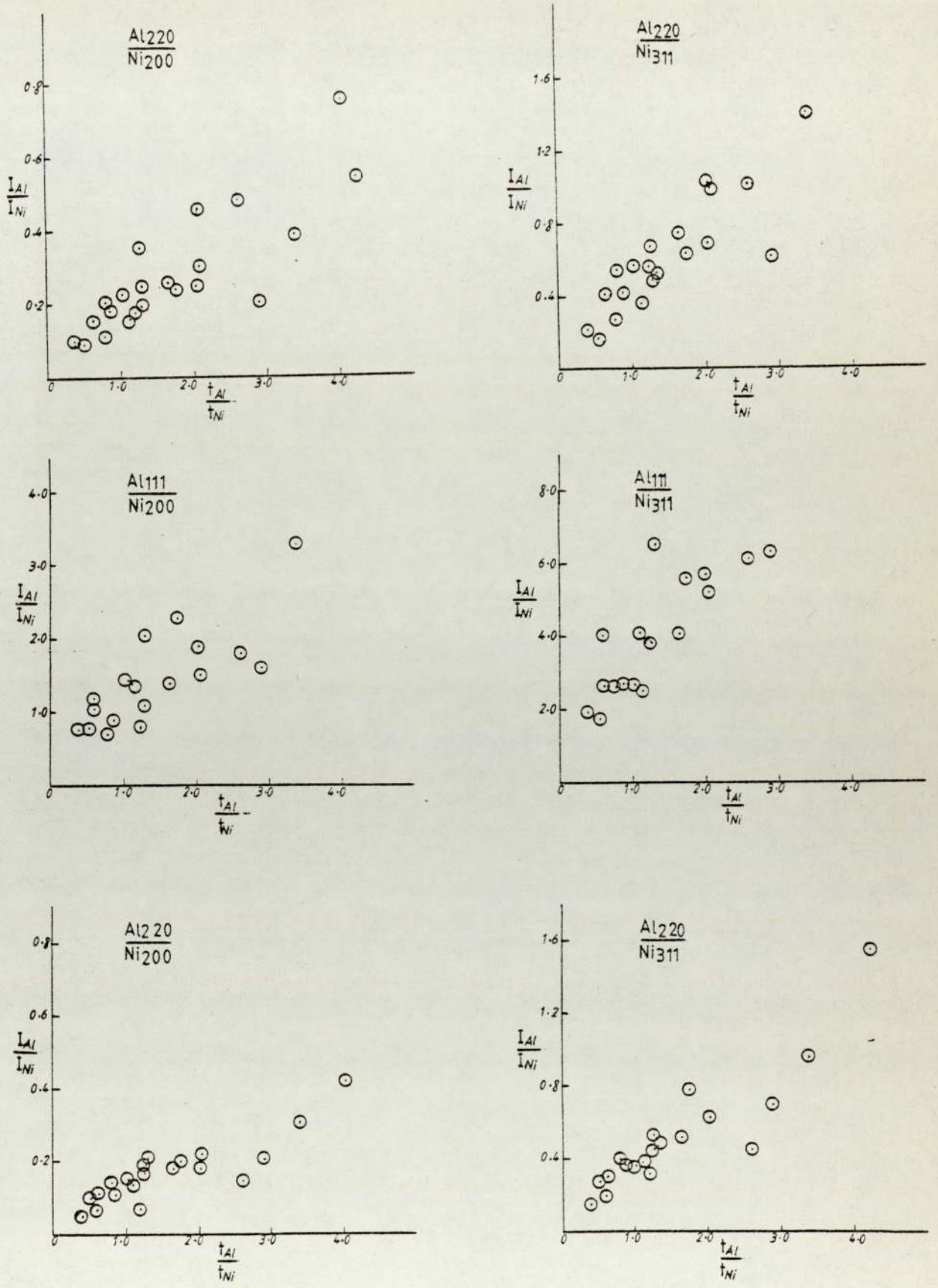

Fig (6.13) Intensity ratio versus thickness ratio for aluminium-nickel combination at 600kv, 800kv and 1000kv.

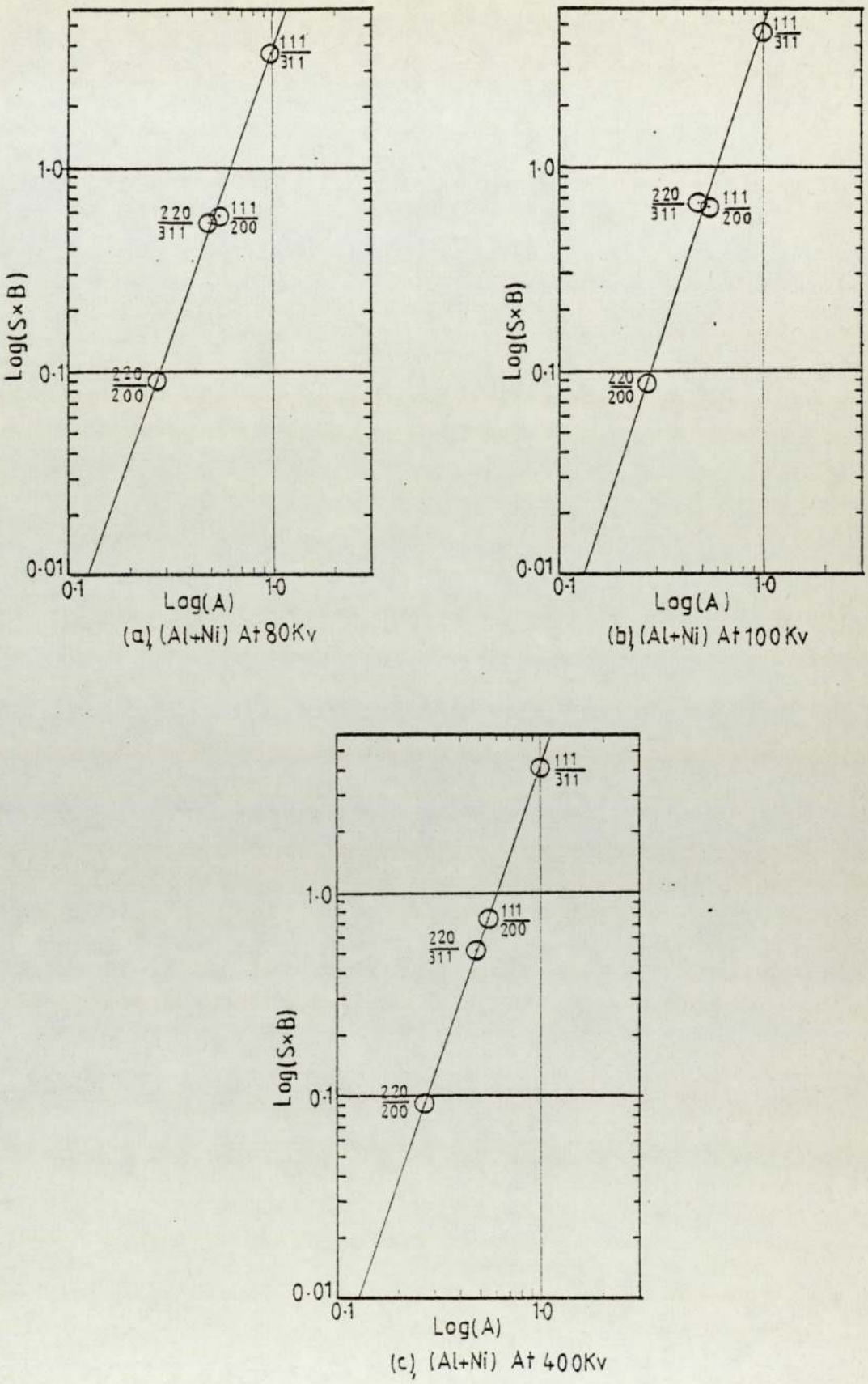

Fig. (6.14) Logarithm plot of (S.B) versus (A) for aluminium-nickel combination at 80kv, 100kv and 400kv.

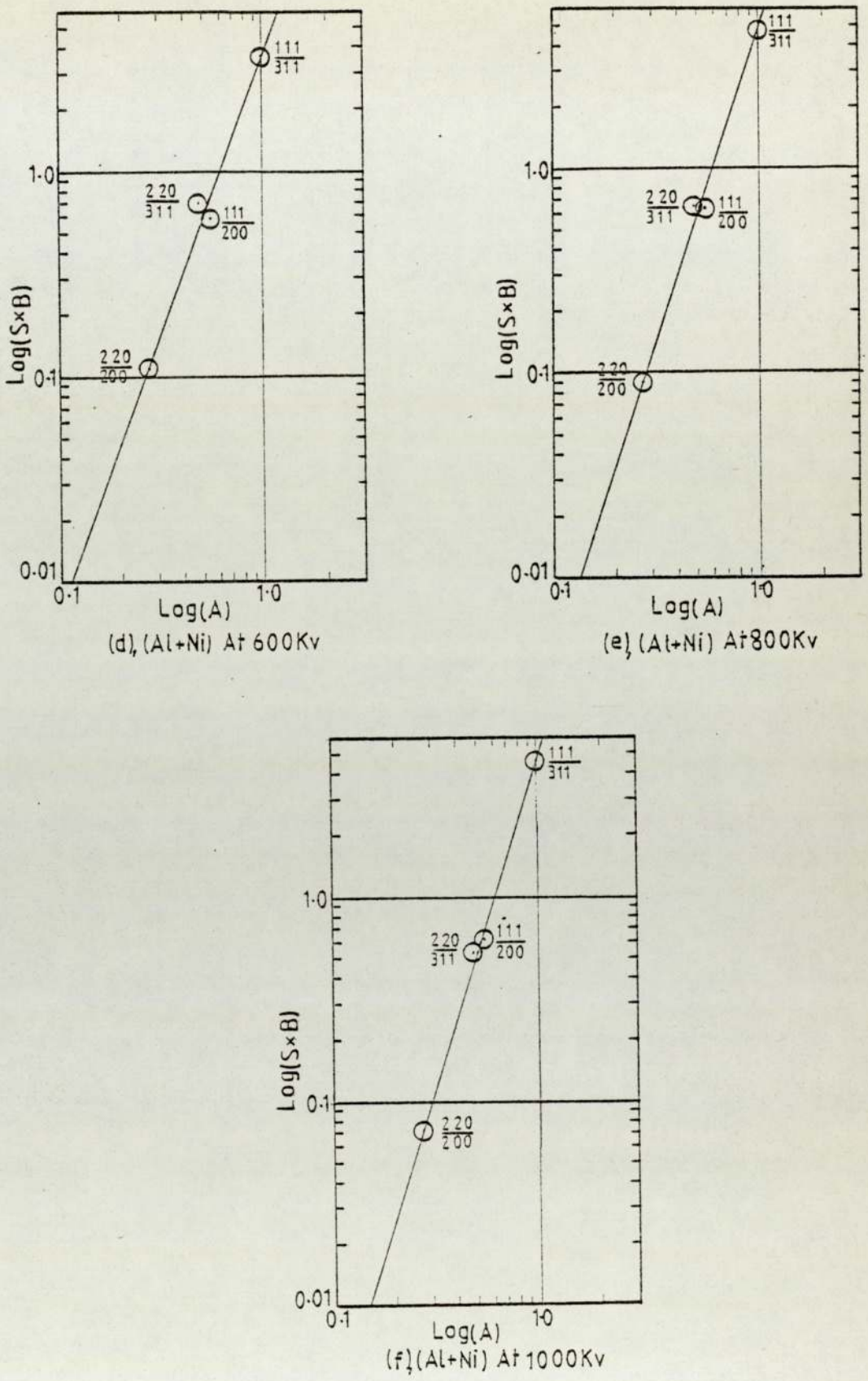

Fig. (6.15) Logarithm plot of (S.B) versus (A) for aluminium-nickel combination at 600kv, 800kv and 1000kv.

The resulting graphs are straight lines whose slope (n) was calculated and its values were found to be 2.8, 3.05, 2.9, 2.69, 3.05 and 3.17 at 80kv, 100kv, 400kv, 600kv, 800kv and 1000kv respectively. The average value for (n) was therefore = 2.95 $\pm$ 0.15.

6.3.3 Analysis of Double-Layered Specimens of Silver and Copper.

In equations (6.2) and (6.3) the subscript (1) stands for silver, and the subscript (2) stands for copper. In this combination the crystallographic orientation which gave measurable diffraction pattern intensities were Ag_{111}, Ag_{220}, Cu_{200} and Cu_{311}, so the ratio of the relative integrated intensities of silver to that of copper were for (111/200), (111/311), (220/200) and (220/311). By using equation (6.2), each of these ratios was plotted against the thickness ratio of the two films in the specimen at 400kv, 600kv and 800kv in order to find the slope $(k'_{hkl})_{Ag}/(k'_{hkl})_{Cu}$, as shown in the sample figure (6.16).

As before [section (6.3.1) and (6.3.2)]; plots of (SxB) versus (A) listed in table (6.19) are shown in the graphs of figure (6.17).

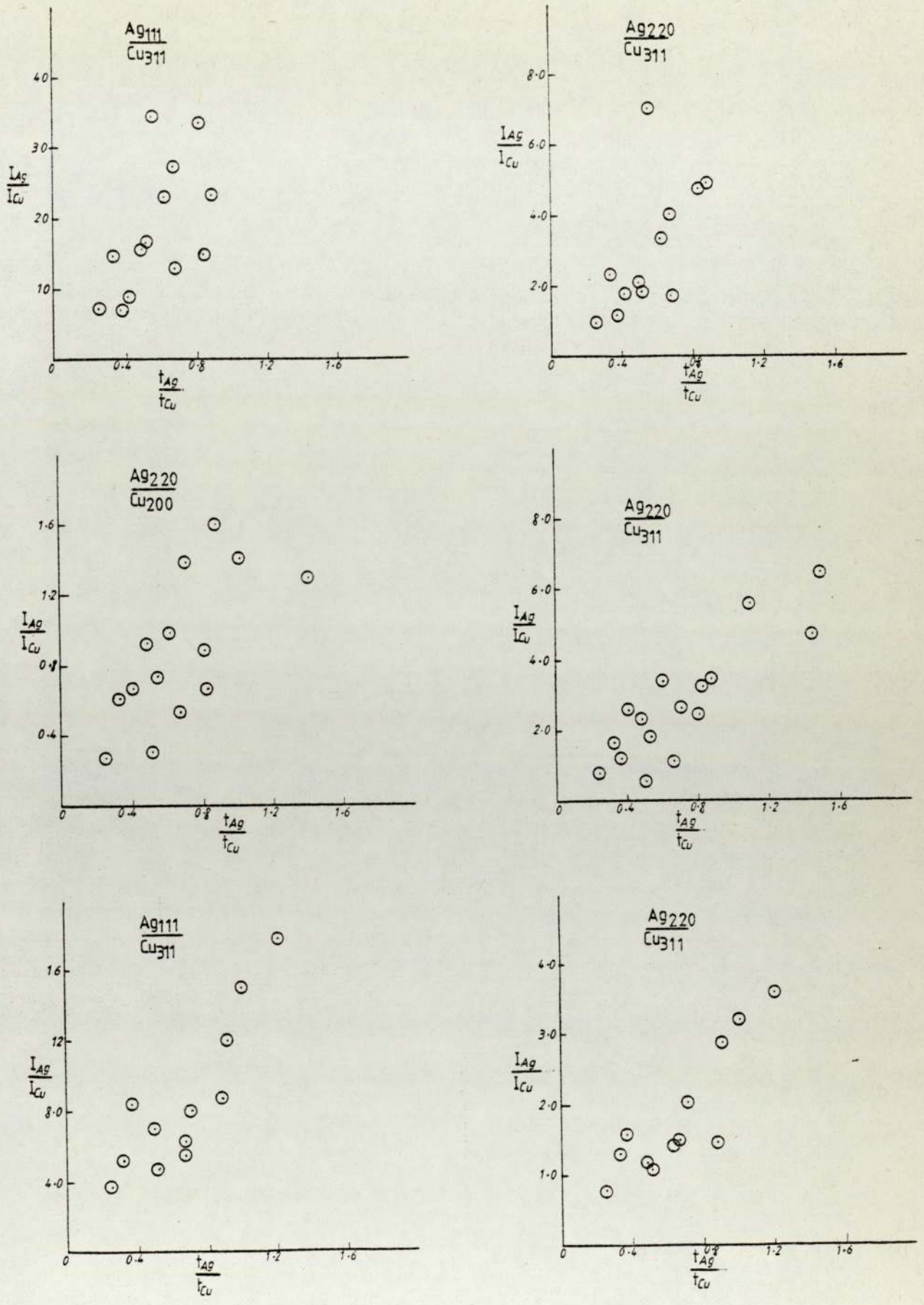

Fig. (6.16) Intensity ratio versus thickness ratio for silver-copper combination at 400kv, 600kv and 800kv.

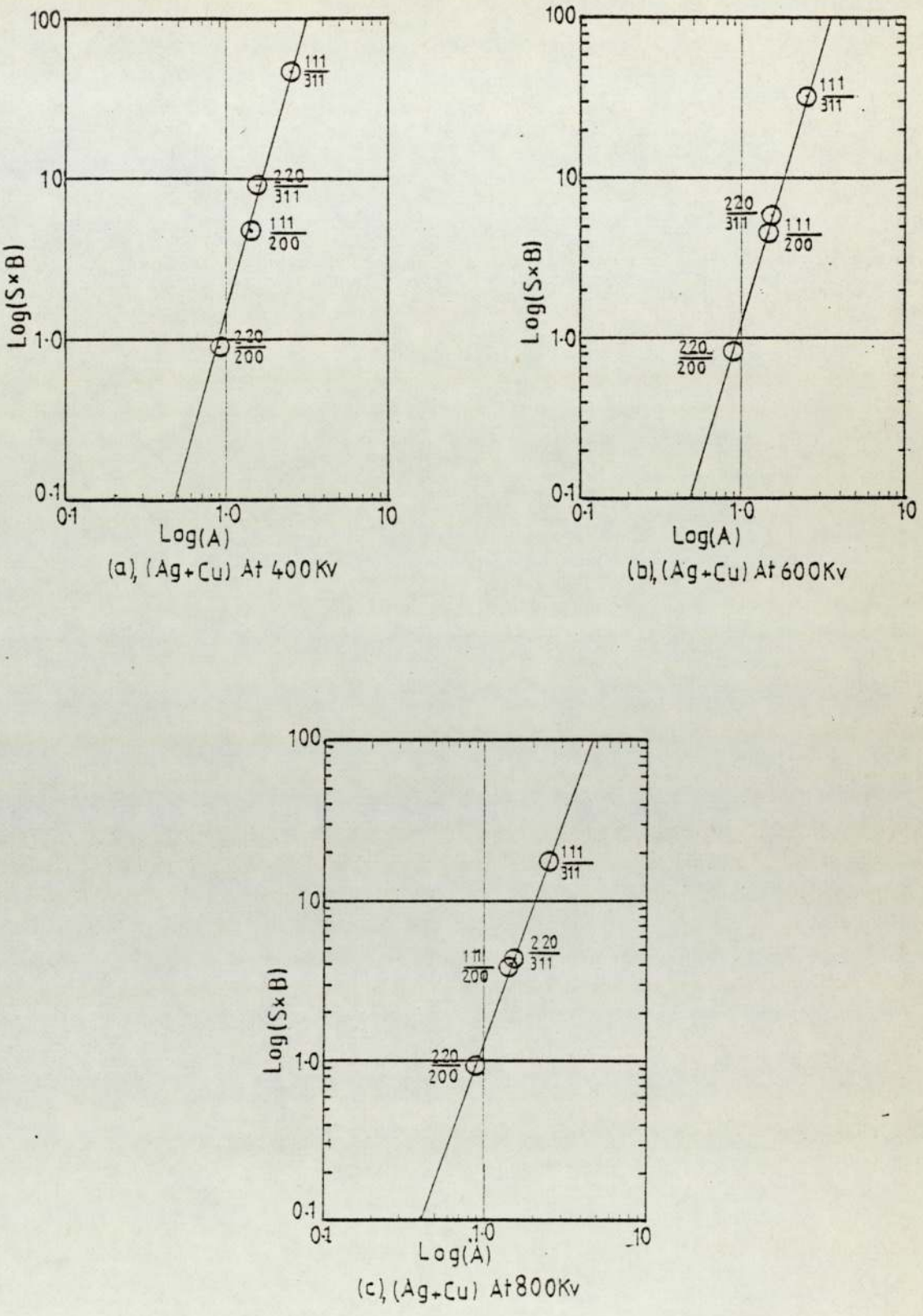

Fig. (6.17) Logarithmic plot of (S.B) versus (A) for silver-copper combination at 400kv, 600kv and 800kv.

Table (6.19); The Value of (A) and (SxB) for Silver-Copper) Combination at different voltages.

$\frac{Ag_{hkl}}{Cu_{hkl}}$	$\frac{[(F_e e^{-D})_{hkl}]_{Ag} v_{Cu}}{[(F_e e^{-D})_{hkl}]_{Cu} v_{Ag}}$	$\frac{(I'_{hkl})_{Ag}/(I'_{hkl})_{Cu}}{t_{Ag}/t_{Cu}} \times \frac{(d_{hkl} P_{hkl})_{Cu}}{(d_{hkl} P_{hkl})_{Ag}} = (SxB)$		
		400kv	600kv	800kv
111/200	1.425	4.75	4.576	3.91
111/311	2.467	46.83	32.24	17.3
220/200	0.886	0.901	0.814	0.907
220/311	1.534	9.19	5.83	4.076

The graphs were straight lines of slope (n) which was equal to (3.2), (3.5) and (2.8) at 400kv, 600kv and 800kv respectively. The average value of n = 3.16 $\pm$ 0.25.

6.4 Summary.

Using equation (6.1), (n) has been determined for all single specimens of aluminium, copper, nickel and silver in the three combinations for different thicknesses and voltages [see tables (6.6), (6.12) and (6.16)].

The procedure followed was to plot log (IxD) against log(F). The slope of the resulting graph is equal to (n).

On the other hand, for composite specimens of (Al+Cu), (Al+Ni) and (Ag+Cu), the procedure followed was firstly to plot the intensity ratio against the thickness ratio [equation (6.2)]. The slope of the graph was then used together with the relavent parameters [equation (6.3)] to

plot log (SxB) against log (A) from which graph the value of (n) was determined.

The values of (n) obtained experimentally were not in full agreement with those from dynamic theory (n=1) or kinematic theory (n=2).

It is clear from equation (6.1) that since $(F_{e_1} \bar{e}^{D}1/F_{e_2} \bar{e}^{D}2)$ and $(d_2^2P_2/d_1^2P_1)$ are both constants for a particular pair of rings, for any material of any thickness and voltage, the intensity ratio (I_1/I_2) must therefore be constant also in order to ensure a constant value of (n).

This condition also holds for composite specimens because in equation (6.3); $(F_{e_1} \bar{e}^{D}1\ v_2)/(F_{e_2} \bar{e}^{D}2\ v_1)$, (d_2P_2/d_1P_1) and the thickness ratio (t_1/t_2) are all constant for any particular pair of rings for the two materials in the double-layered specimen at any voltage.

However, the intensity ratio in both single and composite specimens was not constant due to experimental errors. In the following Chapter a full analysis of these results is presented to explain the discrepancies.

- CHAPTER SEVEN -

DISCUSSION

7.1 Discussion of single specimens

In Chapter Six (section 6.2), the values of (n) were determined for all the materials, Aluminium, Copper, Nickel and Silver in the three combinations (Aluminium-Copper), (Aluminium-Nickel) and (Silver-Copper) for different voltages as can be seen in tables (6.6), (6.12) and (6.16).

These values of (n) showed large scatter around and between the expected values one and two which apply for the dynamic and kinematic theories respectively.

An attempt was made to explain this variation of (n) from the expected values of plotting graphs of (n) versus the thickness (t) as shown in the sample graphs of figure (7.1). However, the results were such that in most cases the variations of (n) were not related to changes in the thickness in any orderly manner.

Another attempt of relating (n) to the voltages also showed disorder as can be seen from graphs of figure (7.2).

It was then decided to draw graphs of (n) against the total scattering number (t/λ_T) for all voltages and thickness of all the materials. The results are shown in figures (7.3), (7.4) and (7.5).

These figures showed the following features.

(i) For aluminium and copper combination, the graph for aluminium - see figure (7.3a) showed that (n)

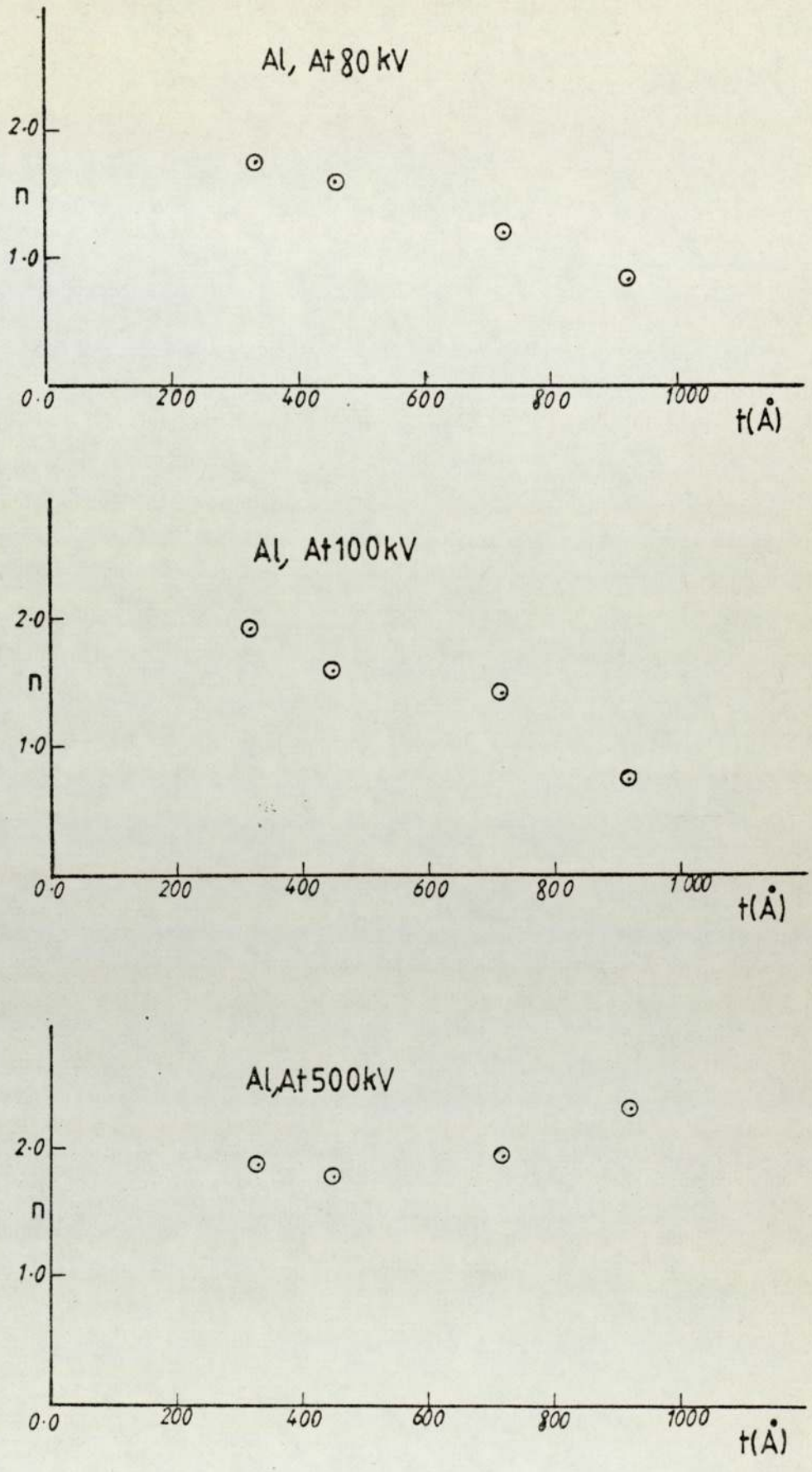

Fig. (7.1) n versus thickness for aluminium at different voltages.

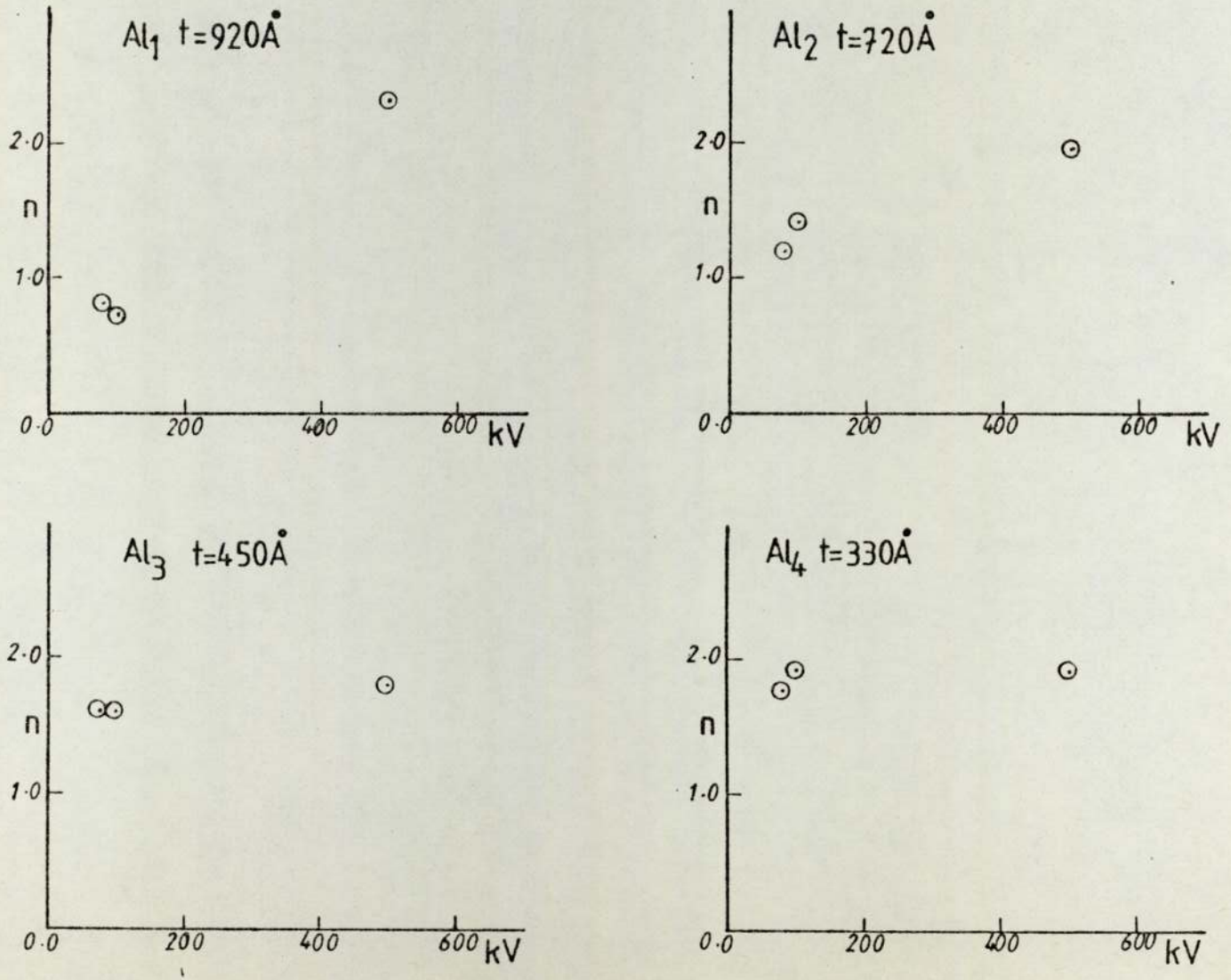

Fig. (7.2) n versus accelerating voltage for different thicknesses of aluminium.

was two at low values of (t/λ_T) the total scattering number, suggesting that the kinematic theory holds for this region. However, for intermediate values of (t/λ_T) the value of (n) to drop from two to one as (t/λ_T) increases which shows a mixed region where both theories apply.

(ii) The same results were obtained for both silver and copper in the silver and copper combination - see figure (7.5).

(iii) For aluminium and nickel combination see figure (7.4), (for both aluminium and nickel) the average value of (n) shown by the dotted line was nearer to two. Similar conclusion could be reached for the copper in the aluminium and copper combination as can be seen from figure (7.3b), although the points on the graph showed more wide scatter.

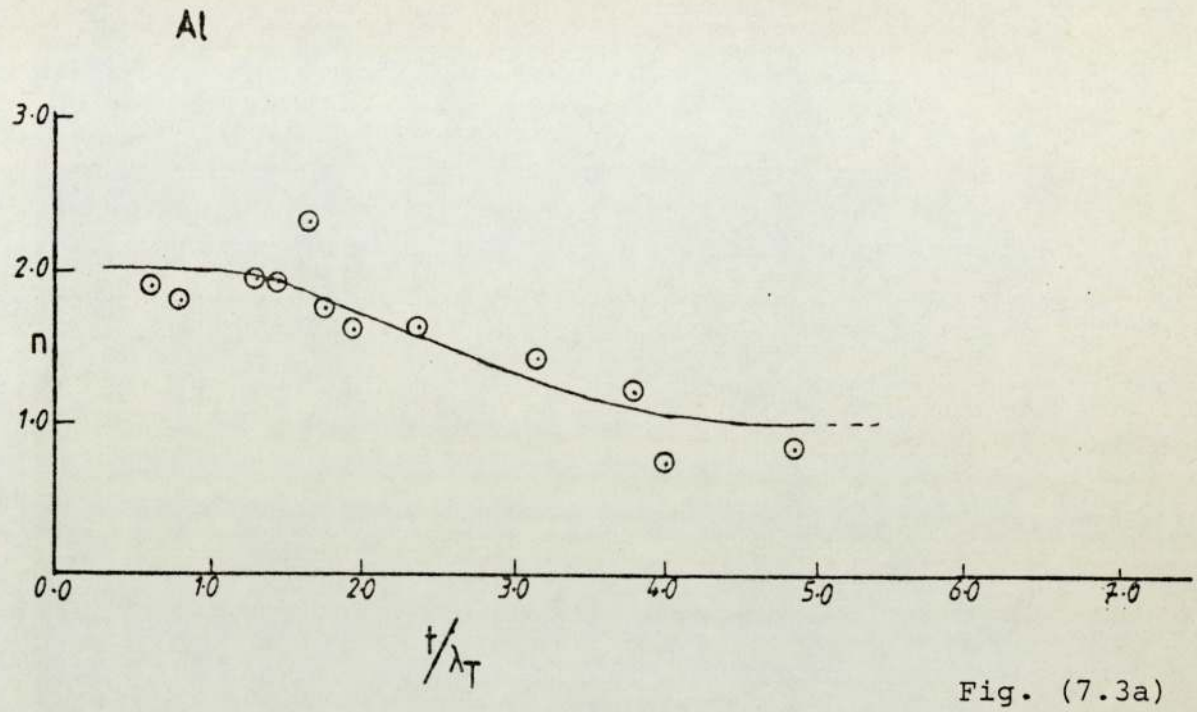

Fig. (7.3a)

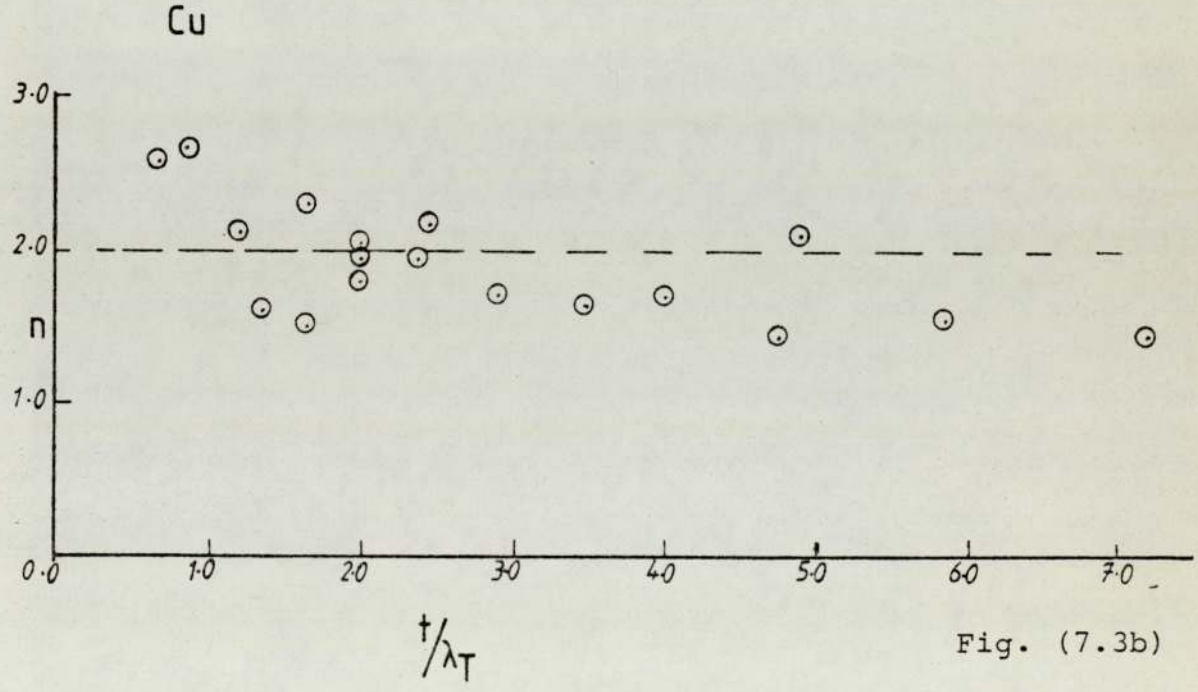

Fig. (7.3b)

Fig. (7.3) n versus the total scattering number for aluminium and for copper, (Aluminium-Copper) combination.

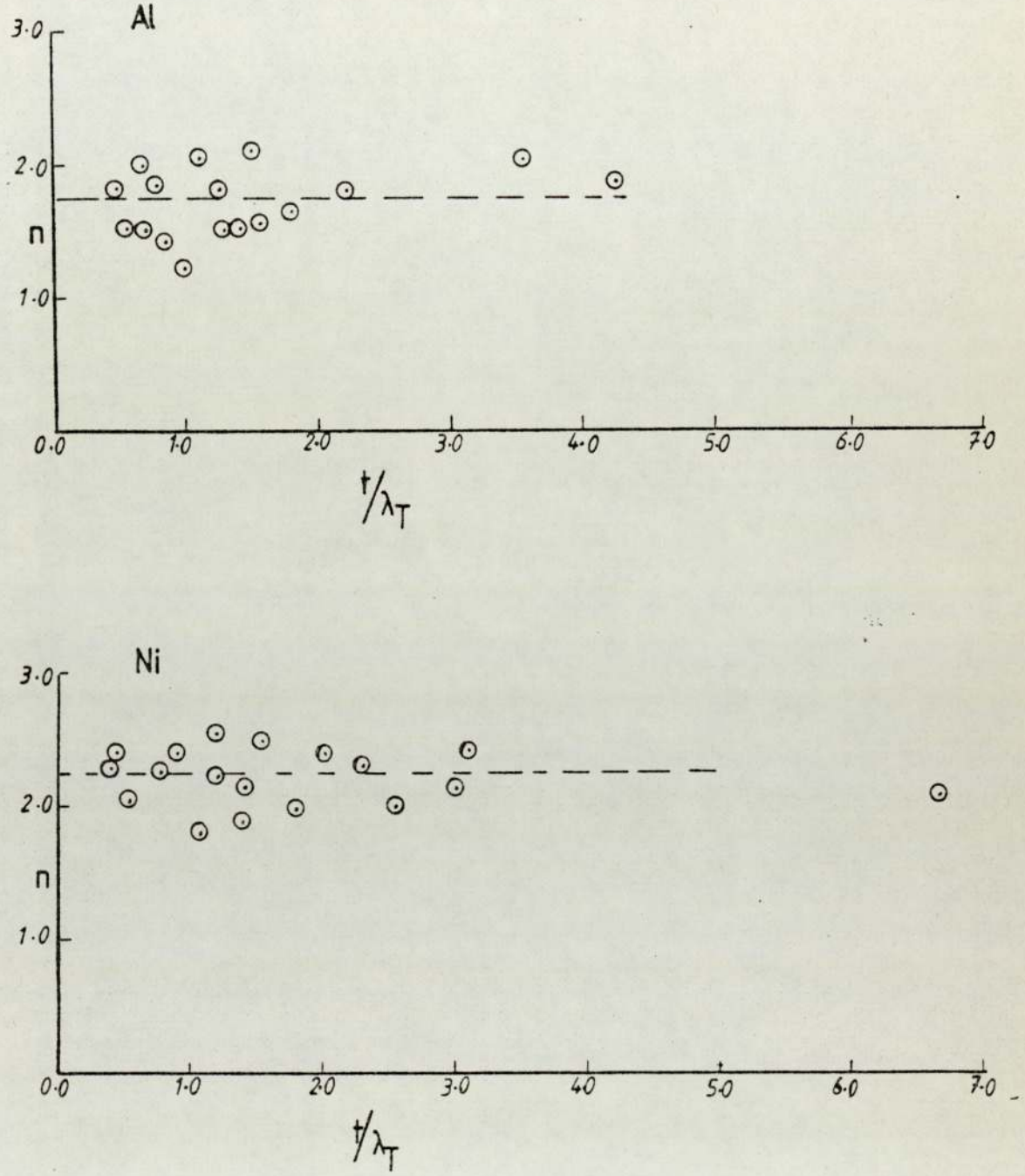

Fig. (7.4) n versus the total scattering number for aluminium and for nickel, (Aluminium-Nickel combination.

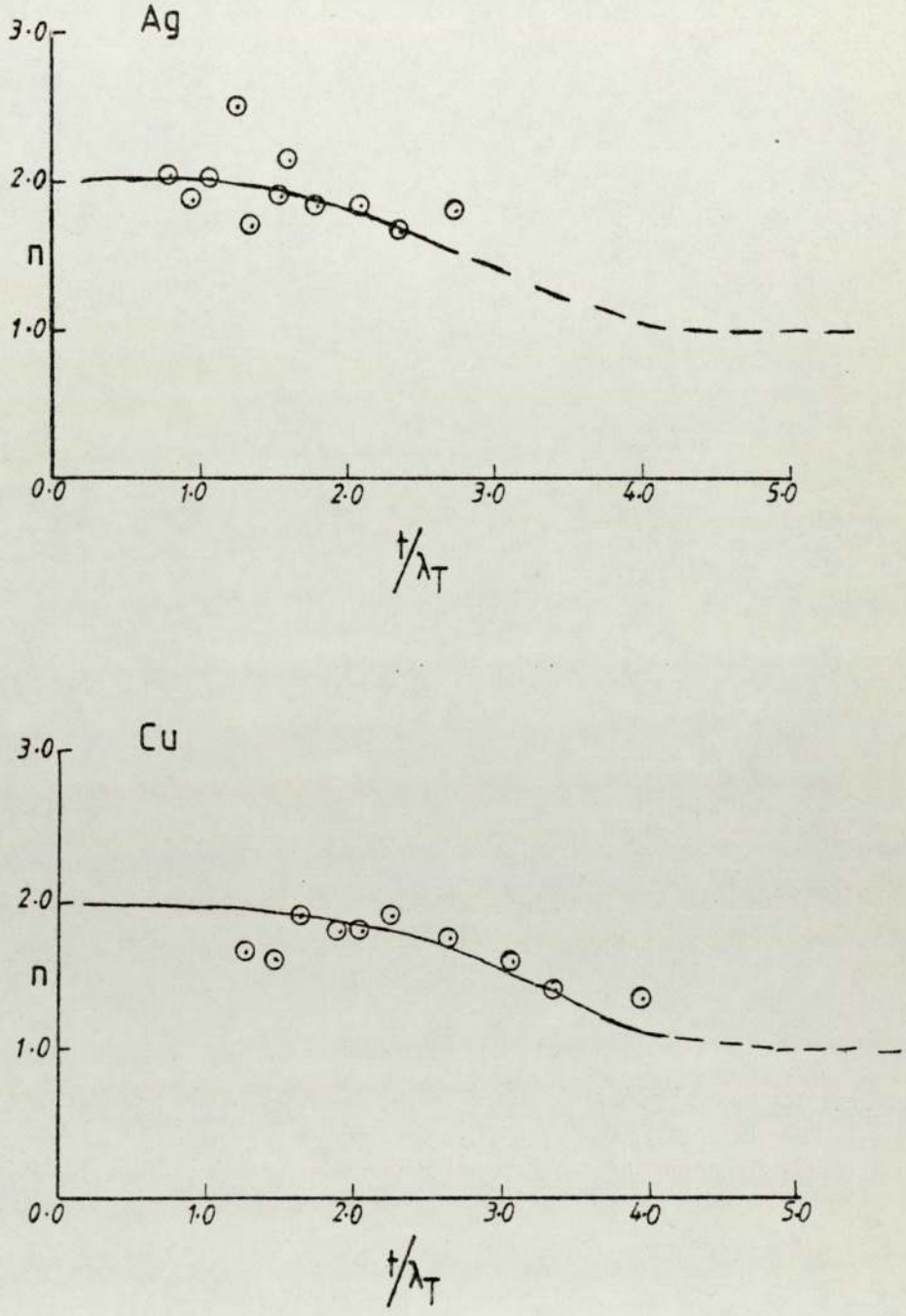

Fig. (7.5) n versus the total scattering number for silver and for copper, (Silver-Copper) combination.

The above results can be summed up in the following illustration [Figure (7.6)].

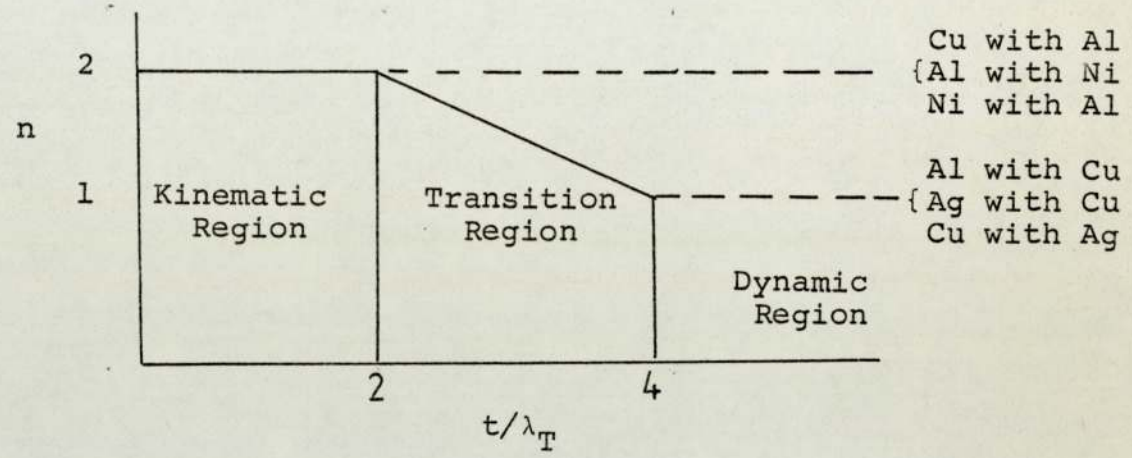

Figure (7.6)

This figure shows that the value of (n) were in general either two or one as expected from kinematic and dynamic theories except for the transitional region.

To relate the above conclusion to the theory of Chapter Two, it is worth remembering that if the relative integrated intensities for the kinematic and dynamic theories are the same then:-

$$\varepsilon = \frac{V_o}{2(F_e)_{hkl}\ \lambda\ e^{-D_{hkl}}} \qquad (7.1)$$

One could call this value of the crystallite size the critical thickness for the dynamic and kinematic theories. For (t) less than this value one could assume that the kinematic theory gives a good approximation to the dynamic theory. For (t) greater than this value it is suggested that the

dynamic theory should operate. A more basic criterion is that the crystallite size of the material should not be greater than the extinction distance (Δ) for using the kinematic theory.

$$\Delta = \frac{\pi V_o}{(F_e)_{hkl} \lambda e^{-D_{hkl}}} \qquad (7.2)$$

If we take this criteria into account, and if we compare the crystallite size of the materials [see Chapter Five table (5.7)] with the extinction distance - see table (7.1), one could find that the crystallite size for almost all the materials was less than the extinction distance, the only exception being that of the thickest aluminium (evaporated with copper). Thus we would expect the kinematic theory to be dominant, as shown by figure (7.6).

Table (7.1); gives the extinction distance (Δ) for Aluminium, Copper, Nickel and Silver.

	Δ							
hkl	80kv	100kv	400kv	500kv	600kv	800kv	1000kv	
111	630	685	1541	1782	2015	2466	2904	Al
200	-	-	-	-	-	-	-	
220	1225	1392	3133	3623	4096	5015	5905	
311	1573	1787	4024	4654	5261	6441	7584	
111	-	-	-	-	-	-	-	Cu
200	347	395	888	1027	1161	1421	1674	
220	499	567	1277	1477	1670	2045	2408	
311	603	685	1542	1784	2017	2469	2907	
111	-	-	-	-	-	-	-	Ni
200	328	373	839	970	1097	1343	1581	
220	-	-	-	-	-	-	-	
311	589	669	1506	1742	1969	2411	2839	
111	-	-	622	-	813	995	-	Ag
200	-	-	-	-	-	-	-	
220	-	-	1000	-	1307	1600	-	
311	-	-	-	-	-	-	-	

7.2 Discussion of Composite Specimens.

In Chapter Six (section 6.3), (n) has been determined for the composite specimens, (Aluminium plus Copper), (Aluminium plus Nickel), and (Silver plus Copper) at different voltages by finding the slope of $\log_{10}(S.B)$ versus $\log(A)$. That (n) was for all the specimens together. To find (n) for each individual specimen the same equation $\log_{10}(S.B) = n\log_{10}(A)$ has been used, from this equation:-

$$n = \frac{\log_{10}S+\log_{10}B}{\log_{10}A}$$, so (n) has been determined for each specimen. Also the total number of scattering $[(t/\lambda_T)_1+(t/\lambda_T)_2]$ for the composite specimen has been determined for each specimen, where (1) stands for the first material and (2) stands for the second material of the composite specimen.

For (Aluminium plus Copper) graphs of (n) versus the total scattering number (N_T) have been drawn - see sample figure (7.7) for each particular pair of rings at different voltages in order to find the variation of (n) with the total scattering number. From these graphs the average of (n) has been determined - see table (7.2).

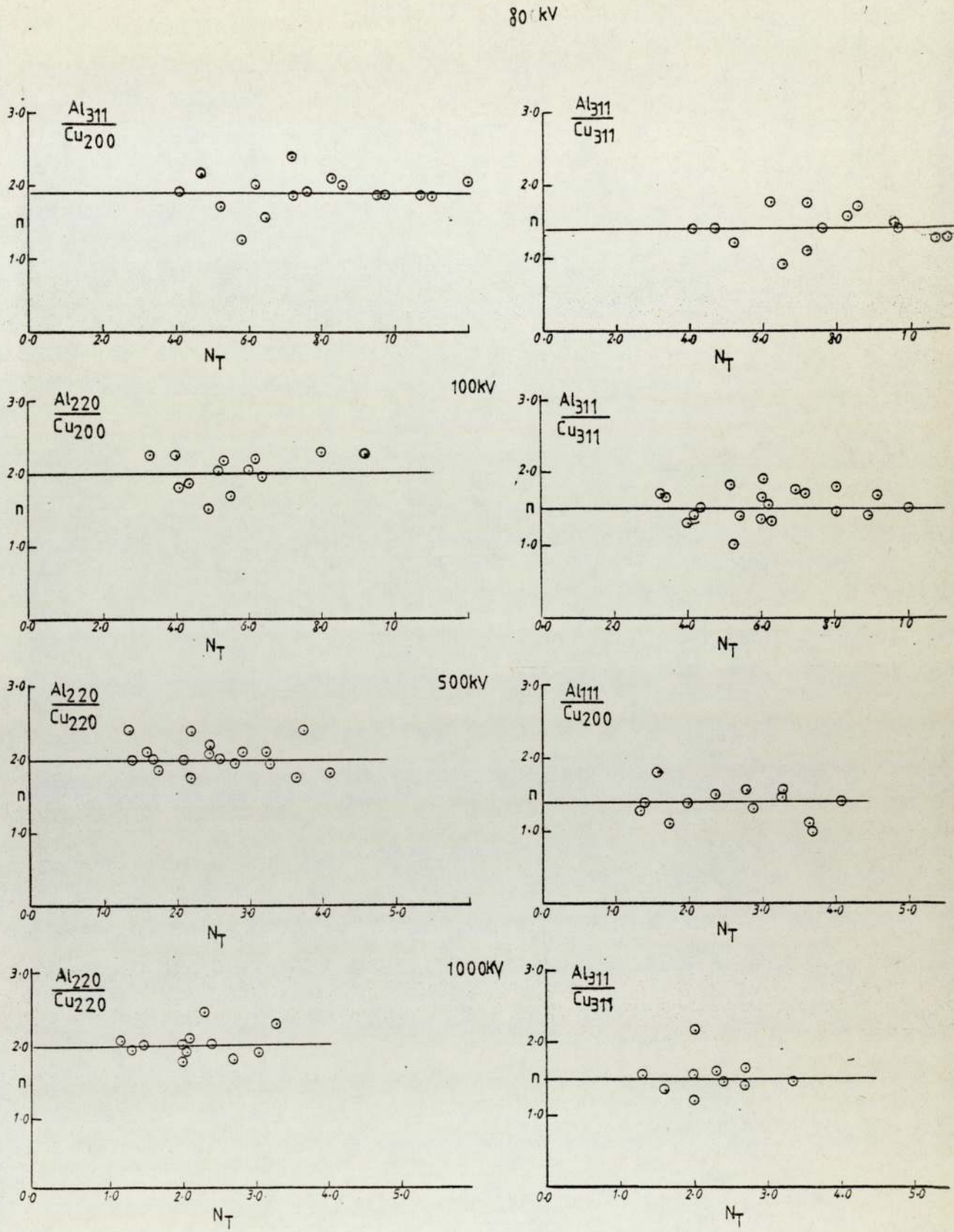

Fig. (7.7) n versus the total scattering number for aluminium plus copper at different voltages.

Table (7.2); Value of (n) at 80kv, 100kv, 500kv and 1000kv from figure (7.7) and the value of the average interplanar spacing ($\bar{d}$).

		n			
Rings	$\bar{d}$	80kv	100kv	500kv	1000kv
111/200	2.073	2.3∓0.3	2.0 ∓0.5	1.4 ∓0.2	1.75∓0.25
111/220	1.81	1.5∓0.5	2.0 ∓0.5		
220/200	1.62	2.2∓0.3	2.0 ∓0.2	2.25∓0.25	2.25
220/220	1.35	2.0∓0.2	2.0 ∓0.4	2.0 ∓0.2	2.0 ∓0.15
220/311	1.26	1.8∓0.2	1.2 ∓0.2	1.75∓0.25	1.8 ∓0.3
311/200	1.515	1.8∓0.2	2.0 ∓0.2	2.0 ∓0.2	2.15∓0.15
311/220	1.25	1.6∓0.2	1.75∓0.2	1.7 ∓0.2	1.75∓0.2
311/311	1.16	1.3∓0.2	1.5 ∓0.2	1.5 ∓0.25	1.5 ∓0.15

It looks as if (n) decreases from two down toward one as the average Bragg angle increases. So from Bragg law $2d\theta \simeq \lambda$ the average Bragg angle $\bar{\theta} = \frac{\theta_1+\theta_2}{2}$ has been determined for each particular pair of rings - see table (7.3).

Table (7.3); The average Bragg angle ($\bar{\theta}$) for (Aluminium plus Copper) at different voltages.

	$\bar{\theta}$			
Rings	80kv	100kv	500kv	1000kv
111/200	0.0103	0.0091	0.00348	0.00214
111/220	0.0127	0.0112	0.0043	0.00264
220/200	0.0315	0.01157	0.00444	0.00273
220/220	0.01555	0.01369	0.00526	0.00323
220/311	0.01692	0.01494	0.00574	0.00352
311/200	0.01441	0.012686	0.00487	0.003
311/220	0.016816	0.014802	0.005685	0.0035
311/311	0.018233	0.01605	0.006164	0.00378

To find the variation of (n) with ($\bar{\theta}$), graphs of (n) versus ($\bar{\theta}$) have been drawn - see figure (7.8), at 80kv, 100kv, 500kv and 1000kv. From these graphs ($\bar{\theta}$) maximum for the kinematic theory $(\bar{\theta}_{kin})_{max}$ has been found for all the voltages. Then these values of $(\bar{\theta}_{kin})_{max}$ have been drawn against the wavelength (λ). The graph was a straight line passing through the origin - see figure (7.9). The slope of the graph was equal to $0.35 = \frac{1}{2\bar{d}_{min}}$, therefore $\bar{d}_{min} = 1.4A^{o}$, which means that ($\bar{d}$) for a particular pair of rings larger than this value ($1.4A^{o}$) then we must apply the kinematic theory, and if ($\bar{d}$) is smaller than ($1.4A^{o}$) then we apply the dynamic theory - see table (7.2).

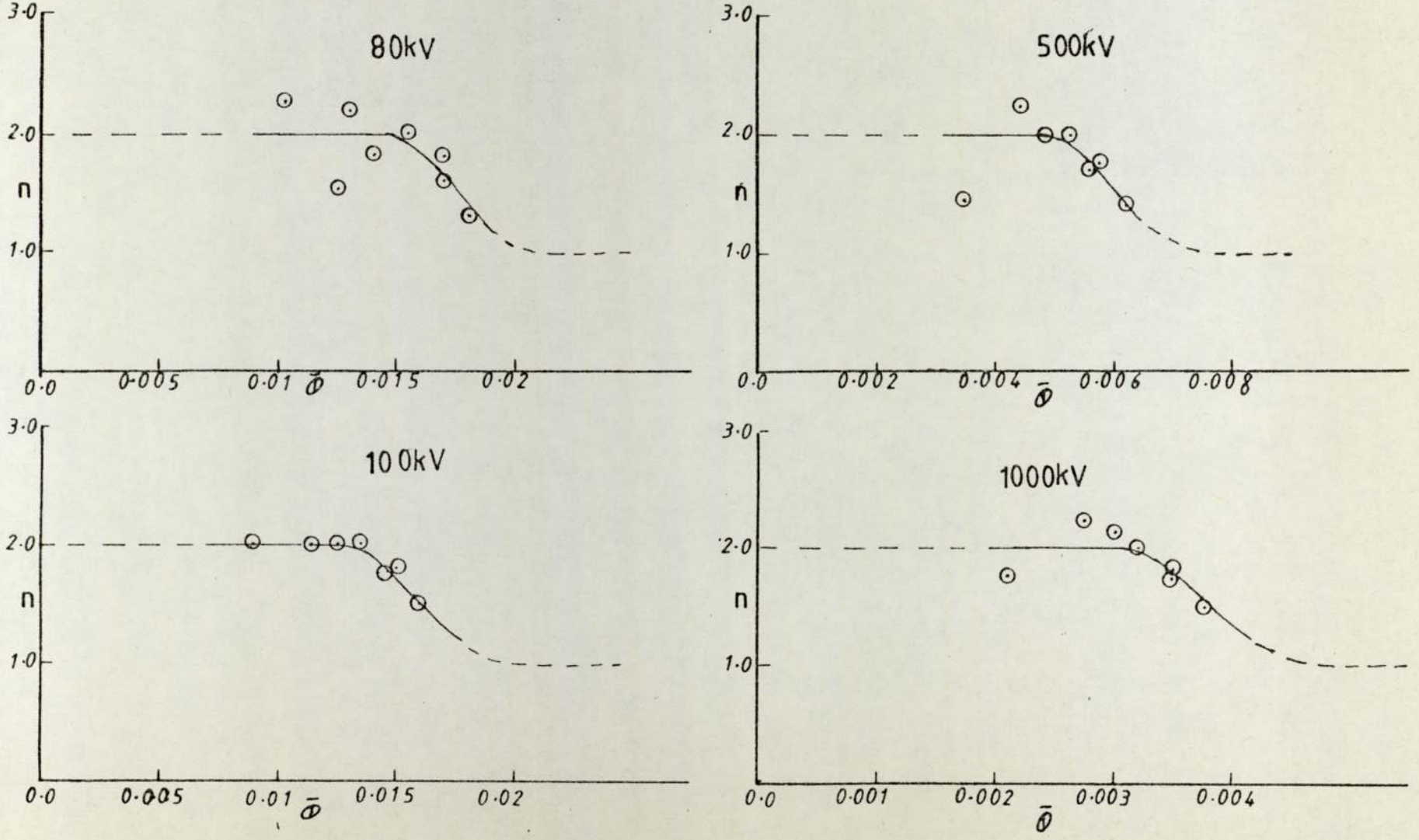

Fig. (7.8) n versus the average Bragg angle for aluminium plus copper at different voltages.

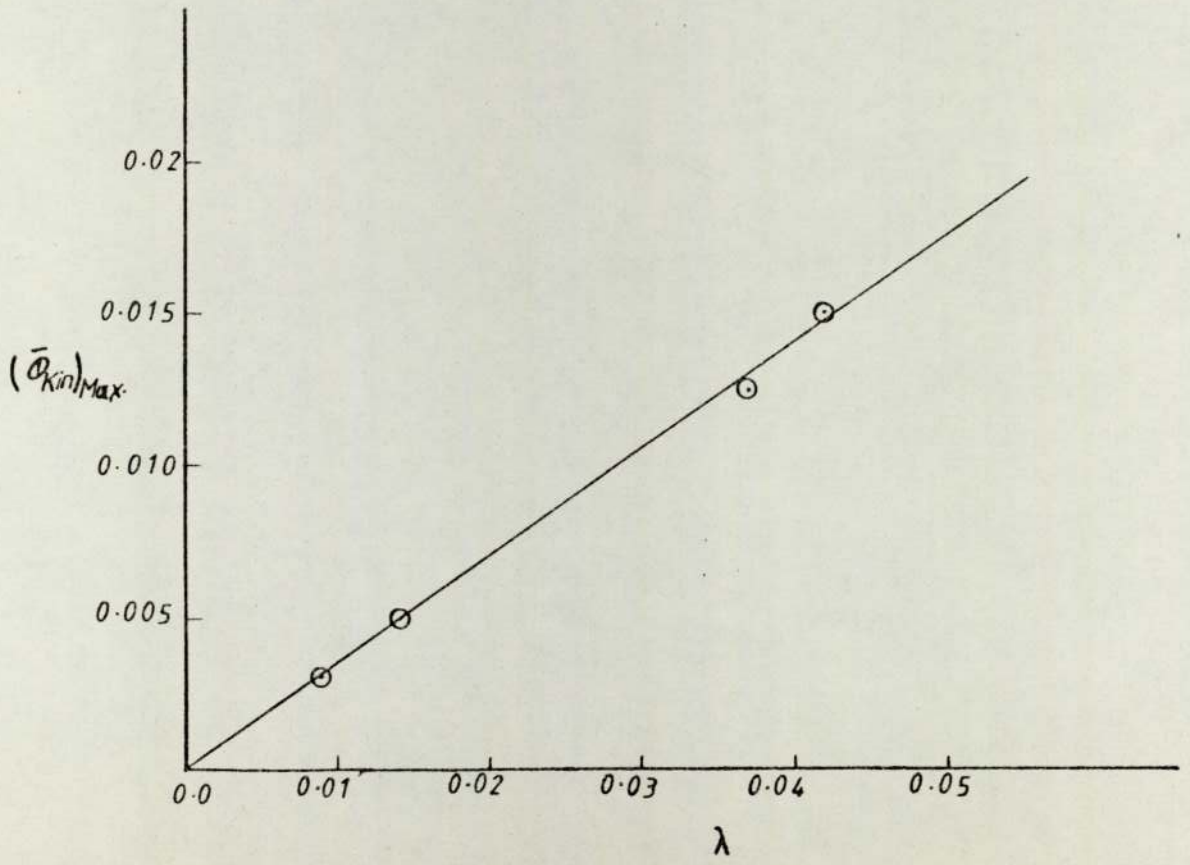

Fig. (7.9) $(\theta_{kin})_{Max}$ versus the wavelength for aluminium plus copper.

For (Aluminium plus Nickel), (n) has been determined for each individual specimen, also (N_T) the total scattering number has been determined for each specimen. Graphs of (n) versus (N_T) have been drawn - see figure (7.10). From these graphs the average of (n) has been determined - see table (7.4).

Table (7.4); The value of (n) at 80kv, 100kv, 400kv, 600kv, 800kv and 1000kv from figure (7.10) and the value for the average interplanar spacing ($\bar{d}$).

	n		
Rings	111/200	220/200	220/311
$\bar{d}$	2.05	1.6	1.25
80kv	1.5 ± 0.2	1.75 ± 0.25	1.25 ± 0.15
100kv	1.5 ± 0.25	1.85 ± 0.15	0.87 ± 0.2
400kv	1.45 ± 0.2	1.75 ± 0.2	1.3 ± 0.25
600kv	1.5 ± 0.3	1.75 ± 0.2	0.88 ± 0.2
800kv	1.45 ± 0.2	1.75 ± 0.2	1.01 ± 15
1000kv	1.45 ± 0.25	1.9 ± 0.2	1.1 ± 0.2

The average Bragg angle ($\bar{\theta}$) has been determined for each particular pair of rings - see table (7.5).

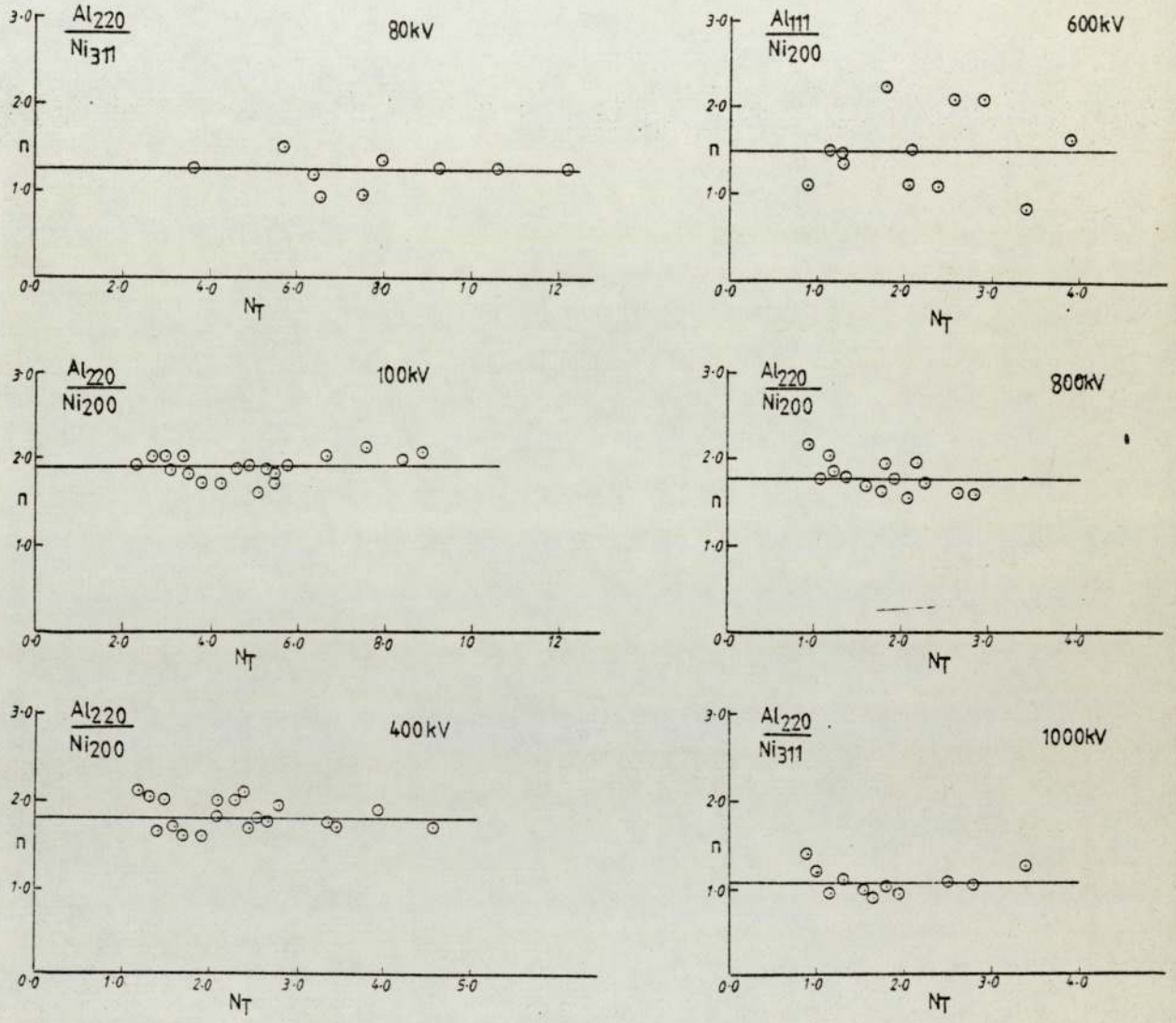

Fig. 7.10) n versus the total scattering number for aluminium plus nickel at different voltages.

Table (7.5); The average Bragg angle ($\bar{\theta}$) for (Aluminium plus Nickel) at different voltages.

	$\bar{\theta}$		
kv	111/200	220/200	220/311
80	0.01045	0.0133	0.017221
100	0.00912	0.0117	0.01516
400	0.0041	0.0052	0.006734
600	0.00313	0.00398	0.00515
800	0.00255	0.00325	0.00421
1000	0.00217	0.00276	0.0036

Graphs of (n) against ($\bar{\theta}$) have been drawn - see figure (7.11). In this case there were only three points and they are not enough to draw a line through them in order to find the variation of (n) with ($\bar{\theta}$), but the idea has been taken from (Aluminium plus Copper) combination. Then $(\bar{\theta}_{kin})_{max}$ has been found and drawn against the wavelength - see figure (7.12). The graph was a straight line passing through the origin of slope equal to 0.25 = $\frac{1}{2\bar{d}_{min}}$. So $\bar{d}_{min}$ = 2.00A^{o} which means if $\bar{d}$ for a particular pair of rings larger than (2.00A^{o}) we can apply the kinematic theory, and if ($\bar{d}$)) is smaller than (2.00A^{o}) we can apply the dynamic theory - see table (7.4).

In (Silver plus Copper) combination, (n) for each specimen was larger than expected value, so it needs more work in future, by taking a large range of voltages.

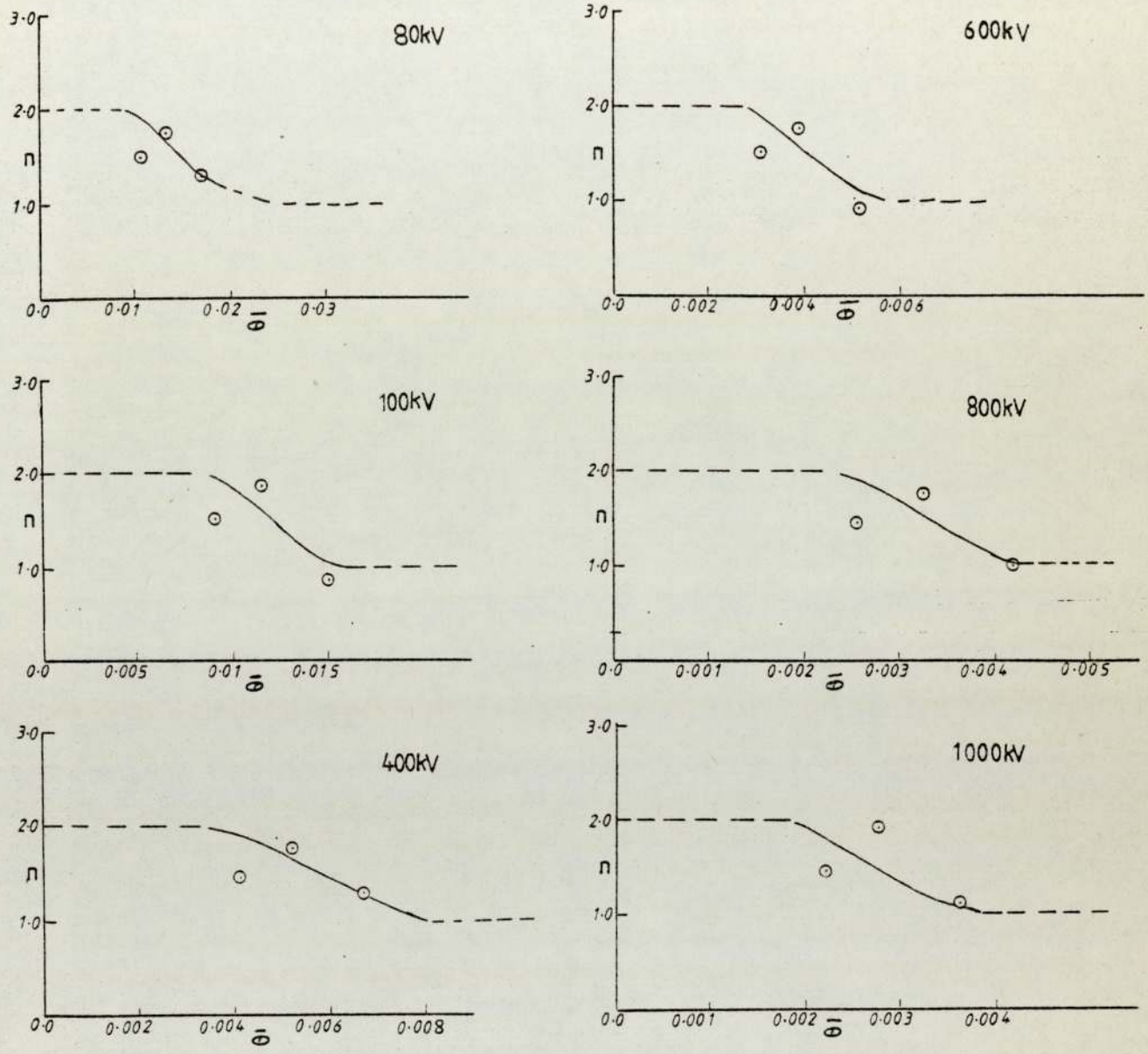

Fig. (7.11) n versus the average Bragg angle for aluminium plus nickel at different voltages.

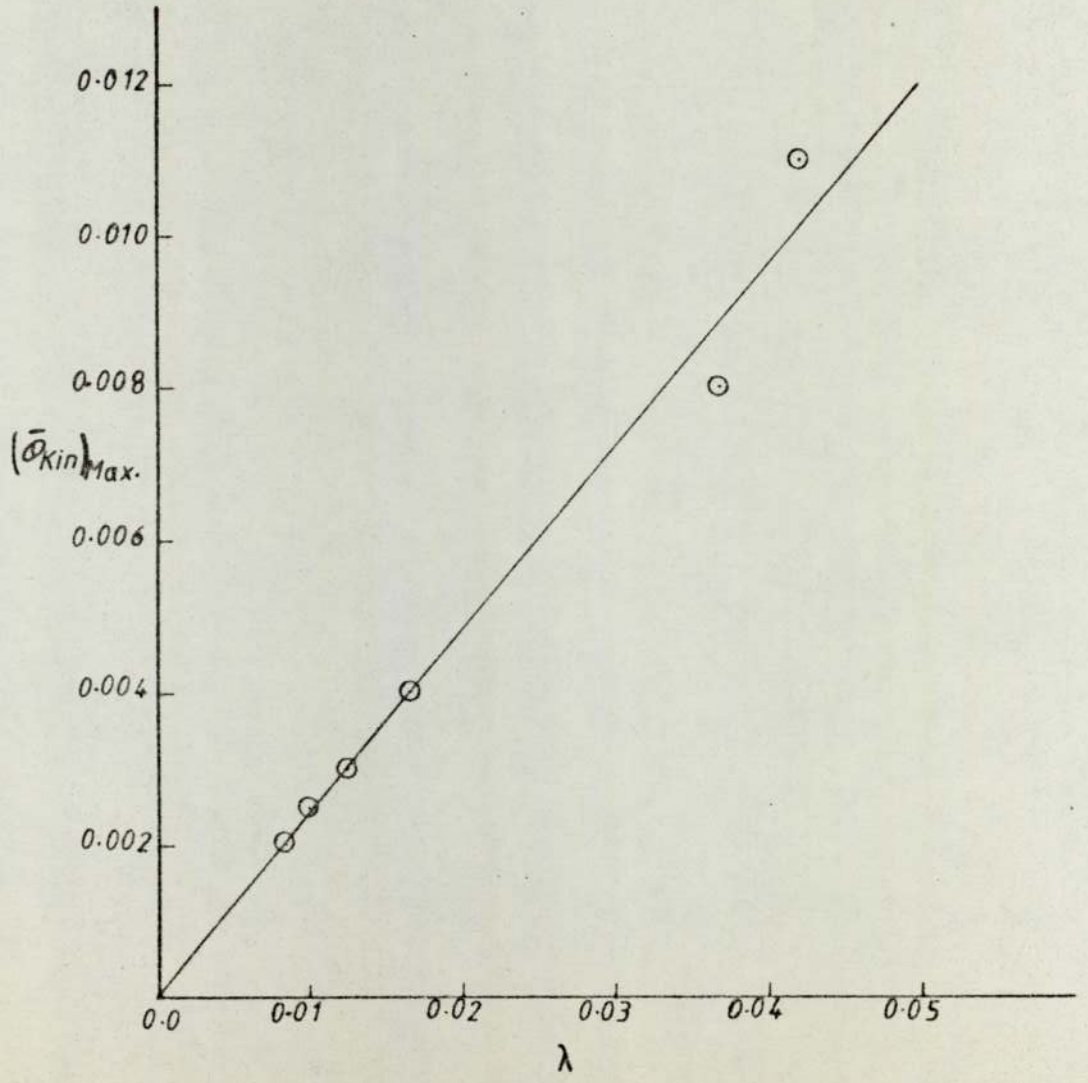

Fig. (7.12) $(\bar{\theta}_{kin})_{Max}$ versus the wavelength for aluminium plus nickel.

- CHAPTER EIGHT -

CONCLUSION

A large range of different thicknesses of single and composite specimens were prepared by thermal evaporation for aluminium-copper, aluminium-nickel and silver-copper combinations. Diffraction patterns have been taken for all specimens using the electron microscope in the selected area mode of operation at different voltages. All the diffraction patterns have been traced using a microdensitometer, and the relative integrated intensities of selected pairs of diffraction maxima have been compared for different thicknesses.

The original aim of the project was to determine the thickness ratio of the two films constituent of the composite specimen. It was hoped to achieve this through the use of a theoretical relationship between the ratio of the relative integrated intensities of the diffraction rings formed by the composite specimen (I'_1/I'_2), and the thickness ratio (t_1/t_2) of the two films of the composite specimen - see equation (1.1).

However, the graphs of intensity ratio against thickness ratio which were obtained experimentally (see Chapter Six, section 6.3) showed a high degree of scatter and it seemed that there was no simple straightforward relationship relating them. But they did show a tendency for the

intensity ratio to increase with an increase in the thickness ratio.

The discrepancy between the theoretical expectations as described by equation (1.1), and the experimentally obtained values was partly due to experimental errors encountered in the measurement of thickness and intensity ratio, but mainly due to the fact that one did not know whether to use the kinematic or the dynamic theory to calculate (k_1'/k_2').

From theory, it can be seen that a linear relationship between the intensity ratio and thickness ratio could only be expected when diffraction is taking place entirely under the condition of the kinematic theory in both layers, or when dynamic conditions are operating throughout, (the crystallite size being constant in both layers).

In measuring the crystallite size it was noted that some of the crystallites were larger than the thickness of the film. This suggests that some of the crystallites grew on the substrate in plate-like form. Thus, measurements in the plane of the specimen would not give a true measure in the direction of the electron beam, and it is this distance which was required for the theoretical calculation of dynamic diffraction parameter.

In the two theories, the diffraction is partly dependent on the crystallite size. The micrograph from the dark field for a specimen showed that the crystallite size varied even for a given layer. It is therefore possible that some

crystallites in a given layer were diffracting under kinematic condition, while the others were diffracting under dynamic theory. These variations in the crystallite size were the primary reason for the discrepancy in the intensity ratio versus thickness ratio plots. In addition to that, the preparation of the specimens was a source of errors since all the composite specimens were prepared by two evaporations, thus causing reheating of the first layer which could affect its crystallite size.

For some materials, it was found (from .n. versus the total scattering number ,t/λ_T,,) that there was a transition from the kinematic to the dynamic theory as the total scattering number increases. For other materials, the kinematic theory was operating.

For composite specimen, it was found from $|(\bar{\theta})_{kin}|_{max}$ versus the wavelength (λ) that $\bar{d}_{min} = 1.4A^{o}$. Thus, for any particular pair of rings, the kinematic theory must be applied when ($\bar{d}$) is larger than $1.4A^{o}$.

The above conclusion was clearly demonstrated for aluminium-copper combination. Therefore in this combination the thickness ratio (t_1/t_2) could be predicted by equation (1.1) provided that:-

(i) (k_1'/k_2') is given by the kinematic theory, and

(ii) the crystallite size (ε) is smaller than the extinction distance (Δ), and finally

(iii) the average interplanar spacing is larger than $1.4A^{o}$.

Aluminium-nickel and silver-copper combinations need more work in future in order to find conditions for predicting (t_1/t_2) from equation (1.1).

For further work it is suggested;

(a) Using low accelerating voltages, thin specimens, and large crystallite size for aluminium-copper and aluminium-nickel combinations in order to examine the validity of the dynamic theory and the mixed region for the two theories.

(b) Materials of high atomic number should be used in order to determine the limit of applicability of kinematic theory.

(c) Other geometries;

1. Mixture, evaporating aluminium and copper at the same time in the same bell-jar with different proportion of aluminium and copper.
2. Columnar model, columns of aluminium in a matrix of copper. The column's length could be equal or smaller to the specimen thickness.

REFERENCES

1. C. Davisson and L.H. Germer, Nature, vol. 119, 558, 1927.
2. G. P. Thomson and A. Reid, Nature, vol. 119, 890, 1927.
3. G. P. Thomson, proc. Roy. Soc. of London, vol. 117, 600, (1927-1928).
4. G. P. Thomson, proc. Roy. Soc. of London, vol. 119, 651, 1928.
5. G. P. Thomson, proc. Roy. Soc. of London, A vol. 125, 352, 1929.
6. T. F. J. Quinn and N. H. Hayes, Proportional Analysis of Composite Polycrystalline Specimen of Copper and Aluminium by Electron Diffraction, (1977).
7. T. B. Rymer, Electron Diffraction, Methuen and Co, London, 1970.
8. T. F. J. Quinn and M. E. Dirwish, A Feasibility Study of the use of Selected Area Electron Diffraction for the Proportional Analysis of Composite Specimens of Lead and Aluminium, (1973) unpublished.
9. T. F. J. Quinn and N. M. Dawe, Proportional Analysis of Composite Specimens of Copper and Aluminium by Electron Diffraction, (1974) unpublished.
10. T. F. J. Quinn and G. Boxley, Proportional Analysis of Composite Polycrystalline Specimens of Copper and Aluminium by Electron Diffraction, (1976) unpublished.
11. T. F. J. Quinn and T. J. Liddicoat, The Proportional Analysis of Composite Polycrystalline Specimens of Copper and Aluminium by Electron Diffraction, (1977) unpublished.

12. T. F. J. Quinn and R. G. Ansell, Proportional Analysis of Composite Polycrystalline Specimens of Aluminium and Nickel by Electron Diffraction, (1977) unpublished.

13. Instruction Manual, for the Hilger and Watts N130, Interferometer, London 1963.

14. Instruction Manual, Joye Microdensitometer Model MLII IC, 1963

15. P. B. Hirsch, Electron Microscopy of Thin Crystal, Butterworths London 1965.

16. G. Thomas, Transmission Electron Microscopy of Metals, John Wiley and Sons, London 1962.

17. M. M. Woolfson, An Introduction to X-ray Crystallography, Cambridge University Press, London 1970.

18. International Table for X-ray Crystallography, Vol.II, table 5.2.2B, The Kynoch Press, Birmingham 1974.

19. A. Guinier, X-ray Diffraction, W. H. Freeman and Company, San Francisco and London 1963.